Thesis for doctoral degree (Ph.D.)
2018

Dynamics of proteinopathies in Alzheimer's disease as measured by PET and CSF biomarkers

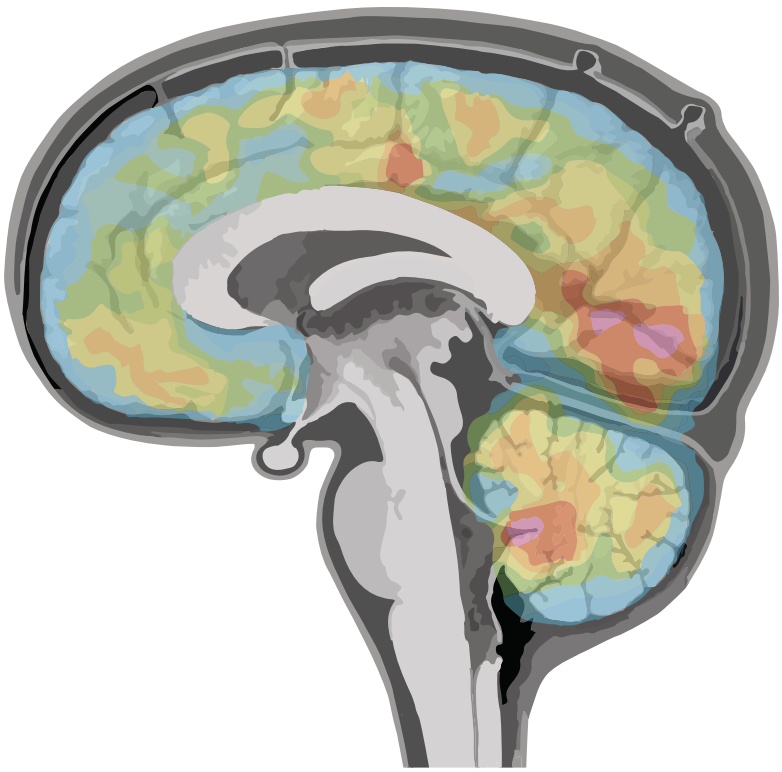

Antoine Leuzy

Karolinska Institutet

From the Division of Clinical Geriatrics
Department of Neurobiology, Care Sciences and Society
Karolinska Institutet, Stockholm, Sweden

DYNAMICS OF PROTEINOPATHIES IN ALZHEIMER'S DISEASE AS MEASURED BY PET AND CSF BIOMARKERS

Antoine Leuzy

Karolinska Institutet

Stockholm 2018

Published by Karolinska Institutet.
Printed by Arkitektkopia AB, 2018

ISBN 978-91-7676-856-3

Dynamics of proteinopathies in Alzheimer's disease as measured by PET and CSF biomarkers

THESIS FOR DOCTORAL DEGREE (Ph.D.)

By

Antoine Leuzy

Principal Supervisor:

Professor Agneta Nordberg
Karolinska Institutet
Department of Neurobiology,
Care Sciences and Society
Division of Clinical Geriatrics

Co-supervisors:

Dr. Elena Rodriguez-Vieitez
Karolinska Institutet
Department of Neurobiology,
Care Sciences and Society
Division of Clinical Geriatrics

Professor Ove Almkvist
Karolinska Institutet
Department of Neurobiology,
Care Sciences and Society
Division of Clinical Geriatrics

Professor Kaj Blennow
University of Gothenburg
Institute of Neuroscience
and Physiology
Department of Psychiatry
and Neurochemistry

Opponent:

Professor Alexander Drzezga
University Hospital of Cologne
Department of Nuclear Medicine

Examination Board:

Professor Lennart Thurfjell
University of Gothenburg
Institute of Neuroscience and Physiology
Department of Clinical Neuroscience

Professor Gitte Moos Knudsen
Copenhagen University Hospital
Department of Neurology and
Neurobiology Research Institute
Rigshospitalet

Professor Irina Alafuzoff
Uppsala University
Department of Immunology,
Genetics and Pathology

To my parents, Vincent and Ingrid.

“An expert is a person who has made all the mistakes
that can be made in a very narrow field.”

– Niels Bohr

ABSTRACT

Alzheimer's disease (AD) is a neurodegenerative disorder characterized by the extracellular aggregation of the amyloid-β (Aβ; amyloid) peptide and the intra-neuronal accumulation of the protein tau. Independently, and in concert, these proteinopathies lead to the loss of synapses and neurons (neurodegeneration). These processes can be measured in living individuals using positron emission tomography (PET) and cerebrospinal fluid (CSF) based measurements (biomarkers). Biomarkers for AD include the retention in the brain of varied PET ligands (e.g. [^{11}C]PIB and [^{18}F]flutemetamol, Aβ; [^{18}F]THK5317, tau; and [^{18}F]FDG, glucose metabolism, a proxy for synaptic integrity), as well as CSF levels of $A\beta_{1\text{-}42}$, and tau phosphorylated at threonine 181 ($p\text{-}tau_{181p}$), and total-tau (t-tau), reflecting Aβ, the formation tau tangle pathology, and axonal damage, respectively. The aim of this thesis, which comprises five studies, was to obtain new insight into how these biomarkers interrelate in AD, and to examine their potential utility from a clinical standpoint. In study I, agreement between dichotomised (i.e. normal/abnormal) [^{11}C]PIB PET and CSF $A\beta_{1\text{-}42}$ in AD and related disorders was found to persist after controlling for potential methodological confounds tied to CSF, suggesting biological underpinnings to biomarker mismatches. Concordance, however, was substantially improved across patient groups when using $A\beta_{1\text{-}42}$ in ratio with $A\beta_{1\text{-}40}$. In study II, the impact of amyloid imaging with [^{18}F]flutemetamol PET was examined in a cohort of diagnostically unclear patients, drawn from a tertiary memory clinic. [^{18}F]Flutemetamol investigations resulted in substantial changes to pre-amyloid PET diagnoses and an incease in the use of cholinesterase inhibitors, with the greatest impact seen among patients with a pre-[^{18}F]flutemetamol diagnosis of MCI. In study III, the relationship between [^{18}F]THK5317 tau PET and CSF tau, including measures derived from assays capturing novel fragments, was shown to vary by isocortical hypometabolism, suggesting that the relationship between tau biomarkers may vary by disease stage. Novel CSF markers better tracked longitudinal PET, as compared to $p\text{-}tau_{181p}$ and t-tau, and improved concordance with [^{18}F]THK5317. Moreover, comparison of cross-sectional and rate of change findings suggest a temporal delay between tau pathology and synaptic impairment. In studies IV and V, perfusion information derived from [^{18}F]THK5317 tau PET scans was shown to strongly correlate with [^{18}F]FDG PET metabolic imaging; though our cross-sectional data support the use of perfusion parameters as a substitute for [^{18}F]FDG, longitudinal findings suggest that the coupling between perfusion and metabolism may vary as a function of disease stage, warranting further studies.

LIST OF PUBLICATIONS

This thesis is based on the following original articles:

I **Leuzy A**, Chiotis K, Hasselbalch SG, Rinne JO, de Mendonça, Otto M, Lleó A, Castelo-Branco M, Santana I, Johansson J, von Arnim CAF, Beer A, Blesa R, Fortea J, Herukka SK, Portelius E, Pannee J, Zetterberg H, Blennow K, Nordberg A. Pittsburgh compound B imaging and cerebrospinal fluid amyloid-beta in a multicentre European memory clinic study. *Brain*. 2016;139(Pt 9):2540-2553.

II **Leuzy A**,[†] Savitcheva I,[†] Chiotis K, Lilja J, Andersen P, Bogdanovic N, Jelic V, Nordberg A. Clinical impact of [^{18}F]flutemetamol PET in memory clinic patients with an uncertain diagnosis. *Manuscript*.

[†] Contributed equally

III **Leuzy A**, Cicognola C, Chiotis K, Saint-Aubert L, Lemoine L, Andreasen N, Zetterberg H, Yei K, Blennow K, Höglund K, Nordberg A. Longitudinal tau and metabolic PET imaging in relation to novel CSF tau measures in Alzheimer's disease. *Manuscript*.

IV Rodriguez-Vieitez E,[†] **Leuzy A**,[†] Chiotis K, Saint-Aubert L, Wall A, Nordberg A. Comparability of [^{18}F]THK5317 and [^{11}C]PIB blood flow proxy images with [^{18}F]FDG positron emission tomography in Alzheimer's disease. *J Cereb Blood Flow Metab*. 2017;37(2):740-749.

[†] Contributed equally

V **Leuzy A**, Rodriguez-Vieitez E, Saint-Aubert L, Chiotis K, Almkvist O, Savitcheva I, Jonasson M, Lubberink M, Wall A, Antoni G, Nordberg A. Longitudinal uncoupling of cerebral perfusion, glucose metabolism, and tau deposition in Alzheimer's disease. *Alzheimers Dement*. 2018;14(5):652-663.

CONTENTS

LIST OF ABBREVIATIONS

Aβ	Amyloid-β
AChEI	Acetylcholinesterase inhibitor
AD	Alzheimer's disease
AIT	Amyloid Imaging Taskforce
AMYPAD	Amyloid imaging to prevent Alzheimer's disease
APOE	Apolipoprotein E
APP	Amyloid precursor protein
AUC	Appropriate Use Criteria
BBB	Blood-brain barrier
BIOMARKAPD	Biomarkers for Alzheimer's and Parkinson's Disease
BP_{ND}	Non-displaceable binding potential
CAA	Cerebral amyloid angiopathy
CBF	Cerebral blood flow
CERAD	Consortium to Establish a Registry for Alzheimer's Disease
CJD	Creutzfeldt-Jakob disease
CRM	Certified reference material
CT	Computed tomography
CU	Cognitively unimpaired
DVR	Distribution volume ratio
EANM	Imaging European Association of Nuclear Medicine
ELISA	Enzyme linked immunosorbent assay
EMA	European Medicines Agency
FDA	US Food and Drug Administration
[^{18}F]FDG	2-deoxy-2-[^{18}F]fluoro-D-glucose
FDR	False discovery rate
FOV	Field-of-view
FTD	Frontotemporal dementia
IDEAS	Imaging Dementia – Evidence for Amyloid Scanning
IWG	International Working Group
keV	Kiloelectron volt
K_1	Tracer delivery rate constant
LC	Liquid chromatography
MAO-A	Monoamine oxidase A
MAO-B	Monoamine oxidase B
MAPT	Microtubule associated protein tau
MCI	Mild cognitive impairment
MMSE	Mini-mental state examination
MNI	Montreal Neurological Institute

MRI	Magnetic resonance imaging
MS	Mass spectrometry
MSD	Meso Scale Discovery
NFT	Neurofibrillary tangle
NIA-AA	National Institute on Aging and the Alzheimer's Association
NINCDS-ADRDA	National Institute of Neurological and Communicative Disorders and Stroke and the Alzheimer's Disease and Related Disorders Association
nM	Nanomolar
OSEM	Ordered subset expectation maximisation
$[O^{15}]H_2O$	Oxygen-15 labelled water
PD	Parkinson's disease
PET	Positron emission tomography
PHF	Paired helical filament
$[^{11}C]$PIB	$[^{11}C]$Pittsburgh Compound-B
PSP	Progressive supranuclear palsy
p-tau	Phosphorylated tau
p-SUVR	Perfusion standardised uptake value ratio
PVE	Partial volume effect
QC	Quality control
RMP	Reference measurement procedure
ROC	Receiver operating characteristic
R_1	Ratio of K_1 in target and reference regions
SCD	Subjective cognitive decline
Simoa	Single-molecule arrays
SNMMI	Society of Nuclear Medicine and Molecular
SPM	Statistical Parametric Mapping
SRM	Selected reaction monitoring
SRTM	Simplified reference tissue model
STAC	Specialized Task Force on Amyloid Imaging in Canada
SUVR	Standardised uptake value ratio
TAC	Time activity curve
TDP-43	TAR-DNA binding protein 43
t-tau	Total-tau
VaD	Vascular dementia
VOI	Volume-of-interest
V_T	Distribution volume
1-TC	One-tissue compartment model
3R	Three repeats of the tau microtubule-binding domain
4R	Four repeats of the tau microtubule-binding domain

1 INTRODUCTION

1.1 FROM NORMAL AGEING TO DEMENTIA

1.1.1 Cognitive changes in ageing

Cognition refers to the mental functions involved in thinking, attention, understanding, learning, remembering, problem solving, and decision making.[1] Cognitive ageing can be defined as a process of change in cognitive functioning that occurs as people get older; this process, however, though gradual and ongoing, is highly variable, both across and within individuals, as well as cognitive domains.[2] Studies attempting to elucidate the mechanisms underlying this phenomenon suggest that it relates to changes in synaptic structure and function, as opposed to neuronal loss.[2] Though cognitive ageing is not a disease per se, distinguishing it from the initial phase of a neurodegenerative disease can prove challenging.

1.1.2 Dementia and the changing demography of ageing

Dementia can be described as the acquired loss of cognitive functioning, sufficient to interfere with independence in everyday activities.[3] Worldwide, an estimated 47 million people currently live with dementia, with this figure projected to reach 82 million by 2030.[4] With increasing age as the greatest risk factor for dementia, a driving factor behind these rising prevalence figures is increased longevity, a factor that has produced a demographic shift resulting in a rapid growth in the number of elderly individuals.[5] Indeed, census bureau projections indicate that there will be more than 2.1 billion people over age 65 by the year 2050.[6] Given the immense social and economic costs tied to the treatment of dementia, and the fact that age is its strongest risk factor, the World Health Organization has recently advocated that dementia be considered as a global public health priority[7,8]

1.1.2.1. Dementia disorders

The term dementia does not refer to a single disease but rather to a variety of clinico-pathological entities, exhibiting both distinct and overlapping characteristics. Alzheimer's disease (AD) is the leading cause of dementia, accounting for between 50 and 70 percent of all cases using current clinical criteria.[5] Other causes of dementia include cerebrovascular disease, frontotemporal lobar degeneration, and Lewy body pathology. Autopsy verified studies suggest that most cases of dementia are due to multiple brain pathologies, including α-synuclein and hyperphosphorylated transactive response DNA-binding protein 43 (TDP-43),[9] with AD and a vascular component the most frequent combination; importantly, mixed pathologies show increased prevalence with advancing age.[10] Finally, additional diseases have been linked to dementia, including traumatic brain injury,[11] Parkinson's disease (PD),[12] Creutzfeldt–Jakob disease,[13] and Down's syndrome,[14] as well as reversible conditions such as normal pressure hydrocephalus, encephalitis, and depression[15] (Figure 1).

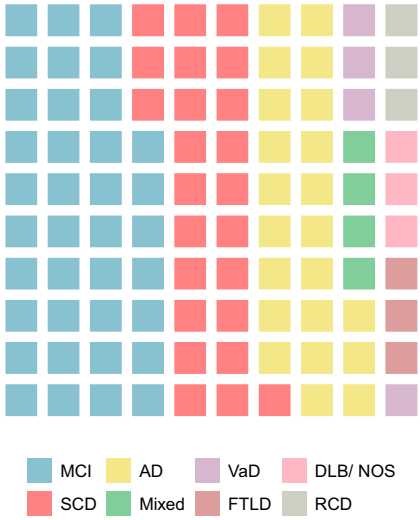

Figure 1. *Waffle plot showing the distribution of diagnostic categories among patients seen due to cognitive complaints at the Clinic for Cognitive Disorders, Theme Aging, Karolinska University Hospital, Stockholm, Sweden (n=580, data from 2017). Each square represents one percent: MCI, mild cognitive impairment (37%); AD, Alzheimer's disease (22%); SCD, subjective cognitive decline (24%), VaD, vascular dementia (4%), FTLD, frontotemporal lobar degeneration (3%); Mixed, mixed dementia (4%); DLB & NOS, dementia with Lewy bodies and dementia not otherwise specified (3%); RCD, reversible cognitive disorder due to other medical condition (3%).*

1.1.3 Subjective cognitive decline

Subjective cognitive decline (SCD), or self-perceived impairment in cognitive function in the absence of objective impairment, has gained growing attention from the scientific community. Though investigators have struggled to achieve a common definition and standardised assessment approach[16,17] since its initial description,[18] the presence of SCD has been shown to be associated with the emergence of objective cognitive impairment and with progression to mild cognitive impairment (MCI and even dementia.[19] Moreover, in comparison to those without SCD, individuals with SCD more often show AD-like biological marker (biomarker) findings (here defined as an objective measure of brain pathology including the accumulation of amyloid-β (Aβ; amyloid) and tau,[20-22] as well as neurodegenerative (decreased glucose metabolism and greater atrophy in AD signature regions)[23-25] and functional (disrupted default mode network connectivity) changes.[26,27] Research criteria for SCD have been put forth[28,29] along with the proposal that SCD may represent late-stage preclinical AD (a protracted period during which AD pathology accumulates in the brain in the absence of symptoms; subtle cognitive decline, i.e. from personal baseline, however, has also been reported as a feature). [41, 534]

1.1.4 Mild cognitive impairment

The concept of MCI was introduced to describe a state of cognitive impairment intermediate between those due to normal ageing and dementia due to AD.[30-32] This diagnosis applies to individuals exhibiting objective cognitive impairment, beyond that expected given their age and education, yet of insufficient severity to meet criteria for dementia. Patients with MCI represent a heterogeneous group, with underlying causes ranging from functional disturbances (e.g. depression, drugs and alcohol) to pathological entities (e.g. AD, vascular disease). When patients with MCI are followed over time, some progress to AD or other forms of dementia (approximately 15% per year), while others remain stable or even recover, reverting to a cognitively unimpaired state.[33,34] Though originally defined as an amnestic syndrome, advances in research on MCI have made apparent the existence of nonamnestic subtypes, as well as the designation of single or multi-domain impairment.[35-37] In light of some of the disadvantages of the concept of MCI,[38,39] the term prodromal AD was introduced in an effort to capture those MCI patients with AD as the underlying pathology, incorporating a specific type of memory loss (impaired free recall that does not normalise with cueing)[40] and supportive biomarker evidence.[41-43] In practice, however, the designation of prodromal AD is often applied in the absence of this specific amnestic profile (i.e. in cases of MCI who show amyloid positivity). Similar to this term is that of MCI due to AD;[44] here, cognitive impairment is not restricted to memory, with the likelihood (high, intermediate, or unlikely) that the syndrome of MCI is due to AD established on the basis of biomarker information.

1.2 ALZHEIMER'S DISEASE

The first set of diagnostic criteria for the clinical diagnosis of AD were put forth in 1984 by a working group established by the National Institute of Neurological and Communicative Disorders and Stroke and the Alzheimer's Disease and Related Disorders Association (NINCDS-ADRDA).[45] According to these criteria, AD could be diagnosed in the presence of a progressive dementia syndrome with an amnestic component, not better accounted for by other neurologic, psychiatric, or systemic disorders; the designation of probable or possible, was also included, depending on the presence of other diseases and typicality of the clinical presentation and course. Importantly, these criteria rested on the notion that a close, one-to-one correspondence existed between clinical symptoms and the underlying AD pathology; as such, those meeting the criteria were assumed to have fully developed pathology, with no recognition of the concept of cognitive impairment in the absence of dementia (i.e. MCI).[46] Further, an only very minor role was ascribed to the use of biological parameters, with these used mainly to exclude other potential causes of dementia.

1.2.1 Neuropathology

AD pathology can broadly be divided into positive lesions due to accumulation (amyloid and hyperphosphorylated tau), negative lesions due to tissue loss (reflecting neurodegenerative changes, including synaptic and neuronal depletion) and reactive processes (neuroinflammation, involving microglial activation and astrocytosis)[47] (Figure 2).

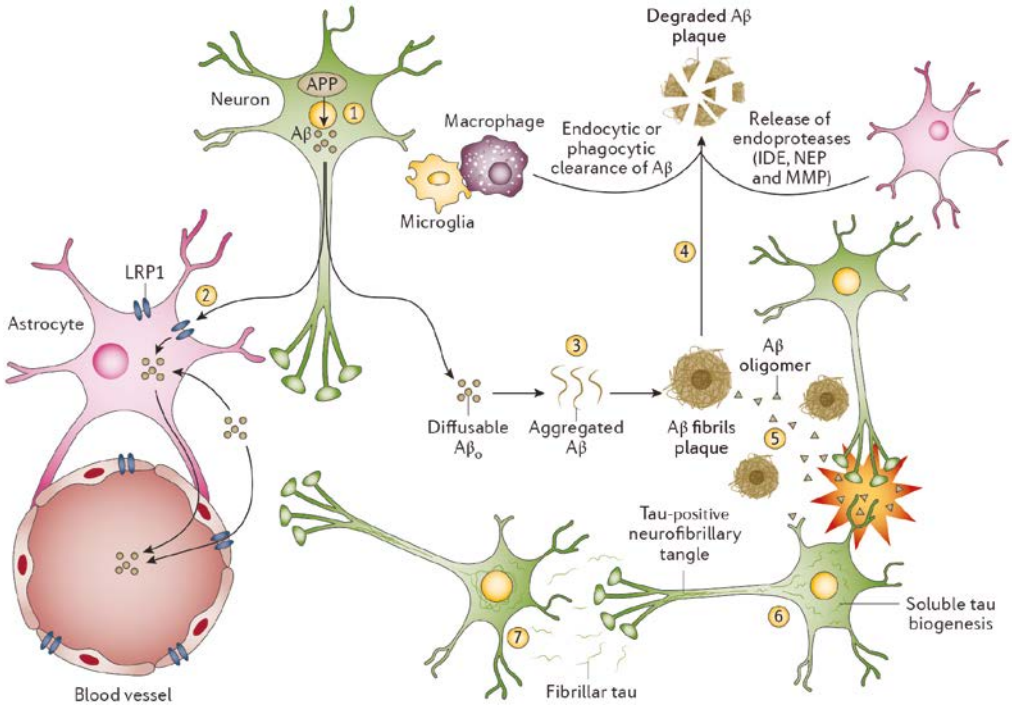

Figure 2. *Overview of plaque and tangle pathology in Alzheimer's disease. Following its cleavage from the amyloid precursor protein (APP; step 1), amyloid-β (Aβ) is released into the extracellular space in the form of diffusible oligomers (Aβo). These can be taken up through APOE related mechanisms or cleared via astrocytes (low-density lipoprotein receptor-related protein 1 (LRP1; step 2). Aggregation of Aβo into fibrillary constructs can also occur in the intercellular space; these, in turn, can amass into plaques (step 3). These can be cleared via macrophages and microglia (endocytic or phagocytic degradation) or by endoproteases from astrocytes (e.g. neprolysin (NEP), insulin-degrading enzyme (IDE), and matrix metalloproteinase (MMP); step 4). Certain oligomers, however, may prove resistant to clearance and exert synaptotoxic effects (step 5) and induce the aggregation of pathological forms of tau. Tau pathology occurs intracellularly, with tau damage mediated by neurofibrillary tangles (step 6). Fibrillary tau species can be secreted by affected neurons and subsequently taken up by healthy ones (step 7). Adapted with permission from Masters CL, Bateman R, Blennow K, Rowe CC, Sperling RA, Cummings JL. Alzheimer's disease. Nat Rev Dis Primers. 2015;1: 15056. Copyright Macmillan Publishers Ltd: Nature, 2015.*

1.2.1.1 Amyloid-β

Though debate surrounds the events critical to the triggering of Aβ pathology,[48] possible explanations include age-related disruption of proteostatic mechanisms[49,50] and impaired clearance.[51,52] Aβ peptides are known to exhibit a propensity to intrinsic self-assembly, producing a range of aggregates referred to as oligomers, protofibrils, or mature amyloid fibrils (Figure 3) on the basis of their appearance by electron microscopy.[53,54] After following a maturation process marked by an increase in the concentration of soluble Aβ, post-translational modifications occur,[55,56] resulting in the accumulation of parenchymal aggregates, primarily in the form diffuse or focal deposits, as well as the deposition of Aβ in the walls of arteries and capillaries (cerebral amyloid angiopathy; CAA).[57]

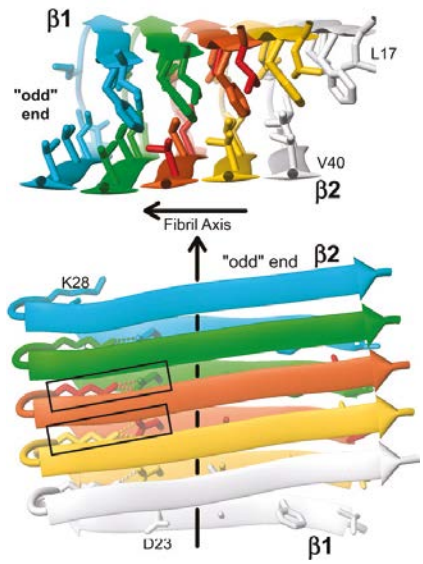

Figure 3. *The 3D structure of an $A\beta_{1-42}$ fibril, obtained using hydrogen-bonding constraints from quenched hydrogen/deuterium-exchange nuclear magnetic resonance. Its structure consists of two in-register intermolecular stacked parallel β-sheets that extend along the fibril axis. Individual molecules are coloured (e.g. end monomer in cyan). Arrows indicate the β-strands, spline curves though C^{α} atom coordinates of the matching residues, the irregular secondary structure. Also shown are the side chain bonds that comprise the core of the protofilament. Dotted lines indicate the intermolecular salt bridge between residues D23 and K28, with the two salt bridges made up by the central Aβ molecule emphasised by rectangles. Adapted with permission from Lührs T, Ritter C, Adrian M, et al. 3D structure of Alzheimer's amyloid-beta (1-42) fibrils. Proc Natl Acad Sci U S A. 2005;102(48):17342-17347. Copyright National Academy of Sciences, 2005.*

Diffuse deposits are convoluted in their contour and exhibit poor immunoreactivity, likely due their having a low content of Aβ peptide. Though they may be crossed by degenerating neurites in advanced AD, this feature is typically absent.[58] Aβ deposits are invariably diffuse in certain brain regions, including in the presubiculum and entorhinal cortex,[59,60] and generally diffuse in the striatum and cerebellum.[47] Focal deposits, by contrast, are spherical in shape, have a high content of 40 and 42 amino acid Aβ isoforms, and can be regrouped into at least three types: compact plaques, comprising a dense central core with no peripheral elements,[58,61] immature plaques, reticular in appearance, possessing no clearly identifiable core,[62] and the so-called classic or neuritic plaque, characterized by a dense amyloid core surrounded by a corona of tau positive processes.[62]

The areal topography of Aβ parenchymal deposits have been shown to follow an ordered pattern of progression, with two neuropathology based staging schemes: according to that proposed by Braak (Figure 4), in which only the cerebral cortex is considered, amyloid deposits are first found in the basal areas of the cortex (stage A), followed by spreading to involve all isocortical areas, save the hippocampus and primary sensorimotor cortices (stage B), and, lastly, all isocortical areas, including those previously spared (stage C).[63] According to Thal et al., amyloid deposition progresses through five phases. Phase 1 involves the isocortex, phase 2 the entorhinal cortex and hippocampus, phase 3 the striatum and diencephalon nuclei, phase 4 certain brainstem nuclei, and, finally, the cerebellum and remaining brainstem nuclei in phase 5.[64]A specific pattern of Aβ progression has also been described for the medial temporal lobe.[65] Though these patterns of progression are based on cross sectional data from different brains (thus amounting to an extrapolation only), recent *in vivo* based staging of amyloid deposition using positron emission tomography (PET) in a large number of individuals across the AD continuum has shown findings consistent with these neuropathologic staging schemes.[66]

1.2.1.2 Tau pathology

The microtubule-associated protein tau (MAPT) is natively unfolded and plays a major role in the assembly and stability of microtubules.[67] In the adult human brain, six isoforms of tau are produced via alternative mRNA splicing of the *MAPT* gene on chromosome 17,[68-70] yielding two functionally distinct groups, possessing either three or four repeats of the microtubule-binding domain (3R and 4R tau, respectively).[71] Equally expressed in the healthy adult brain, 3R and 4R isoforms undergo varying degrees of hyperphosphorylation in neurodegenerative disorders in which the pathological accumulation of tau is seen (tauopathies); while both are equally involved in AD, other disorders are characterized by involvement of predominantly 3R (e.g. Pick's disease) or 4R (e.g. progressive supranuclear palsy; PSP) tau.[71,72]

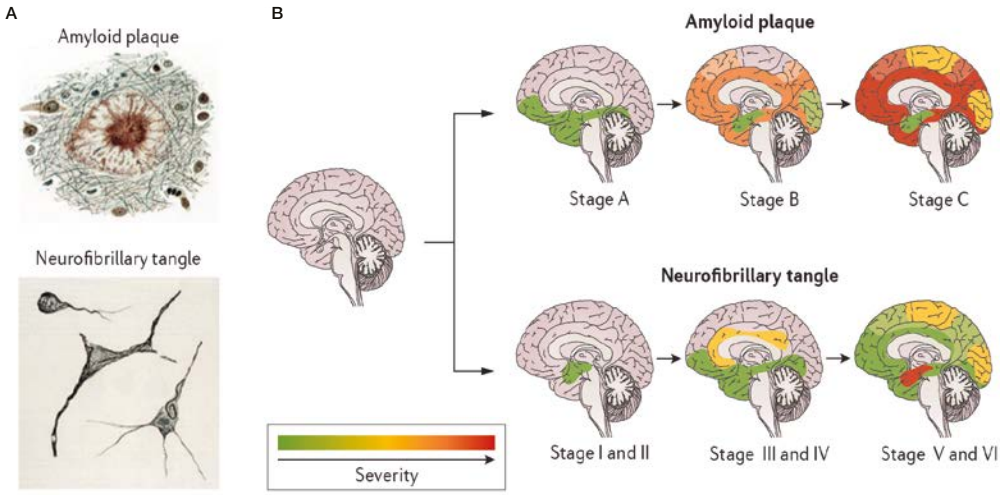

Figure 4. *Evolution of amyloid and tau pathology in Alzheimer's disease Amyloid plaques and neurofibrillary tangles (a) spread through the brain as the disease progresses. Cortical amyloid deposition can be divided into three stages (b): basal neocortex (stage A), adjoining neocortical areas and the hippocampal formation (stage B), and the whole cortex (stage C). For tau pathology, the transentorhinal region followed by the entorhinal region proper are the first areas to be (stage I and II), followed by spreading to include both the hippocampus and the temporal proneocortex and adjoining neocortex (stage III and IV). Eventually, the lesions spread superolaterally, extending into primary neocortical areas (stage V and VI). Adapted with permission from Masters CL, Bateman R, Blennow K, Rowe CC, Sperling RA, Cummings JL. Alzheimer's disease. Nat Rev Dis Primers. 2015; 1:15056. Copyright Macmillan Publishers Ltd: Nat Rev Dis Primers, 2015.*

In contrast to Aβ pathology, tau pathology accumulates intracellularly, within both the somatodendritic and axonal compartments of neurons.[73] Following hyperphosphorylation, tau aggregates into β-sheet paired helical filaments (Figure 5). On the basis of their isoform, tau inclusions adopt differing morphologies.[74,75] In AD, neurofibrillary tangles (NFTs) are found, composed of paired helical filaments (PHFs), and, to a lesser degree, straight filaments.[76,77] As a result of neurofibrillary pathology being only partially cleared from the brain, the density of alterations has been shown to correlate with disease severity and cognitive impairment, allowing for the tracking of disease progression.[47,78]

Though the mechanisms mediating tau pathology are as yet unclear – with possible explanations including age related deficiencies in the proteostatic network[49,50] and faulty clearance mechanisms,[51,52] as for amyloid – its deposition and spread has been shown to follow a characteristic topography, first described by Braak and Braak.[63]

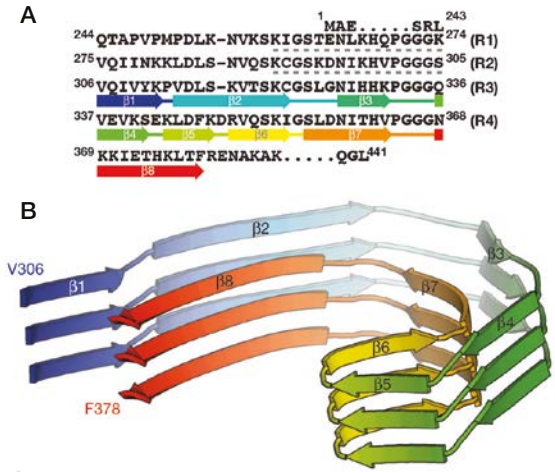

Figure 5. *The 3D structure of the tau protofilament core obtained by cryo-electron microscopy. (a) Sequence alignment of the four microtubule-binding repeats (R1–R4) with the observed eight β-strand regions coloured from blue to red. (b) Rendered view of the secondary structure elements in three successive rungs. Adapted with permission from Fitzpatrick AWP, Falcon B, He S, et al. Cryo-EM structures of tau filaments from Alzheimer's disease. Nature. 2017;547(7662):185-190. Copyright Macmillan Publishers Ltd: Nature, 2017.*

According to their staging system, tau begins in trans-entorhinal and entorhinal regions (stages I/II), followed by limbic (stage III/IV) and neocortical involvement, including primary and secondary fields (stages V/VI) (Figure 4). Convergent findings have also been described by Delacourte et al., save with progression regrouped into 10 stages.[79] Similar to amyloid, however, these studies are based on cross sectional findings from comparatively few cases. Using tau PET, though, several cross-sectional *in vivo* studies have shown patterns of tracer uptake consistent with Braak staging;[80-82] exceptions have been reported, however,[83] including longitudinal findings showing that patterns of accumulation in pathologic tau can differ from those expected based on the Braak model.[84]

1.2.1.3 Neurodegeneration

Two aspects can define synaptic pathology in AD: synaptic involvement in senile plaques[85] and declines in the total number of synapses over time. Pre-synaptic markers such as synaptophysin have been shown to be decreased be decreased arly on in the course of AD,[86] leading to synaptic loss being viewed as the best correlate of cognitive decline.[87,88] Further studies, however, showed that cognitive decline better correlated with tau pathology, relative to the drop in synaptophysin immunoreactivity.[89,90] Levels of synaptic proteins, including the presynaptic vesicle

protein synaptotagmin,[91] the presynaptic membrane protein SNAP-25,[91,92] and the dendritic protein neurogranin,[91,93] have also been shown to be reduced in in the AD brain, reflecting the degeneration and loss of synapses.

Though mixed findings have been documented with respect to the global number of cortical neurons affected in AD,[94] severe neuronal loss has been shown in the entorhinal cortex[95] and hippocampus (CA1 section),[96] as well as in the superior temporal and supramarginal gyri.[97] While the regional and laminar distribution of neuronal loss has been shown to match that of NFTs, he former has been shown to exceed the latter within the same region such that the contribution of neuronal and, presumably, synaptic loss, may exceed that of NFT count with respect to cognitive decline.[95,98] The dissociation between neuronal death and the extent of NFTs suggests that at least two mechanisms may underlie neuronal loss in AD: one targeting tangle-bearing neurons, resulting in the appearance of extracellular NFTs (so-called ghost tangles), and one affecting tangle-free neurons.[99]

1.2.1.4 Neuroinflammation

After a series of classic studies implicating complement factors in the formation of Aβ plaques,[100-103] numerous post-mortem biochemical, immunohistochemical, and molecular findings have confirmed the presence of reactive microglia and astrocytes in the brains of individuals with AD.[104-106] While the relationship between neuroinflammation, Aβ, and tau pathology remains uncertain, glial activation has been shown to play a role in the removal of various forms of Aβ[107-110] and to correlate with the density of neurofibrillary and Aβ deposits and clearance.[111-113] Opposing views have been voiced regarding the significance of these processes in AD, however, with some proposing that they are protective, others, deleterious.[114,115] Possibly, the effects of glial activation may vary by disease stage; specifically, *in vivo* studies using cerebrospinal fluid (CSF) and PET based markers of microglial activation (TREM2 and [^{11}C](R)PK11195, respectively) suggest that microglial activation may shift from an initially protective phenotype during the presymptomatic/MCI stages of AD, to a pro-inflammatory one during the dementia phase.[116-119]

1.2.1.5 Neuropathological criteria for AD

Recommendations for the neuropathological diagnosis of AD were first proposed in 1985, in the form of a specified age-dependent numerical cut-off for senile Aβ plaques.[120] Additional criteria were subsequently proposed, incorporating methodologies for the assessment and staging of NFT pathology.[121,122] The most recent criteria,[123] proposed by the National Institute on Aging and Alzheimer's Association (NIA-AA), incorporate staging schemes for Aβ deposits (Thal),[64] tangle pathology (Braak),[63,124] and neuritic plaque severity (Consortium to Establish a Registry for Alzheimer's Disease; CERAD) (Table 1).[121]

Table 1. Neuropathologic criteria for the diagnosis of AD.

A: Aβ plaque score (Thal phases) †	B: NFT score (Braak stage) ††			C: Neuritic plaque score (CERAD) †††
	B0 or B1 (None or I/II)	B2 (III/IV)	B3 (V/VI)	
A0 (0)	Not	Not	Not	C0 (none)
A1 (1/2)	Low	Low	Low	C0 or C1 (none to sparse)
	Low	Intermediate	Intermediate	C2 or C3 (mod. to freq.)
A2 (3)	Low	Intermediate	Intermediate	Any C
A3 (4/5)	Low	Intermediate	Intermediate	C0 or C1 (none to sparse)
	Low	Intermediate	High	C2 or C3 (mod. to freq.)

AD neuropathologic change is evaluated using an ABC score, derived from three separate 4-point scales: Aβ/amyloid plaques (A) using Thal phases, NFT burden (B) using Braak staging and a neuritic plaque score (C) using the protocol from CERAD. Resulting ABC scores are rated as "Not," "Low," Intermediate," or "High" for AD neuropathologic change, with "Intermediate" or "High" considered sufficient to account for dementia. CERAD, Consortium to Establish a Registry for Alzheimer's disease; mod., moderate; freq., frequent.

†Aβ/amyloid plaque score should be determined according to the method of Thal: Thal DR, Rub U, Orantes M, Braak H. Phases of A beta-deposition in the human brain and its relevance for the development of AD. Neurology. 2002;58(12):1791-1800.

†† NFT stage should be determined by the method of Braak: Braak H, Braak E. Neuropathological stageing of Alzheimer-related changes. Acta Neuropathol. 1991;82(4):239-259; Braak H, Alafuzoff I, Arzberger T, Kretzschmar H, Del Tredici K. Staging of Alzheimer disease-associated neurofibrillary pathology using paraffin sections and immunocytochemistry. Acta Neuropathol. 2006;112(4):389-404;

††† Neuritic plaque score should be determined by the method of CERAD: Mirra SS, Heyman A, McKeel D, et al. The Consortium to Establish a Registry for Alzheimer's Disease (CERAD). Part II. Standardization of the neuropathologic assessment of Alzheimer's disease. Neurology. 1991;41(4):479-486.

Resulting scores are then combined to yield an estimate of AD neuropathologic change (not, low, intermediate or high), with an estimate of intermediate or high required to confirm a clinical diagnosis of AD dementia. These revised guidelines additionally incorporate the reporting of neuropathologic findings tied to common comorbidities, such as Lewy body disease, vascular brain injury, TDP-43 inclusions and argyrophilic grain disease.

1.2.2 Amyloid cascade hypothesis

According to the amyloid cascade hypothesis, AD is caused by the accumulation of Aβ in the brain.[125-128] Originally based on the mapping of the amyloid precursor protein (APP) to chromosome 21,[129-132] the observation of AD neuropathology as an invariable feature in trisomy 21 (Down syndrome),[133] and the linkage of APP mutations to cerebral amyloidosis (hereditary cerebral haemorrhage) and familial AD,[134,135] the amyloid hypothesis has since been revised to include additional lines of evidence suggesting that it is soluble oligomeric Aβ, as opposed to monomers or insoluble Aβ aggregates, that trigger the disease cascade.[136-138] Mechanistically, aggregation of $A\beta_{1-42}$ is thought to lead to tau pathology, neurodegeneration, and clinical symptoms. Alternatively, tau pathology may in fact antecede Aβ, developing in subcortical and medial temporal limbic areas, with Aβ somehow mediating its extratemporal spread.[139,140]

Certain observations, however, have raised doubts about the validity of the amyloid hypothesis. These include the finding of substantial Aβ deposits in asymptomatic individuals,[141] the finding of amyloid and tau pathology in non-Down's syndrome mentally retarded adults,[142] the poor correlation between cognition and the number of Aβ deposits in the brain,[143] the failure of anti-amyloid clinical trials,[144-146] and the recent finding that trisomy of chromosome 21 increases Aβ deposition independently of the additional APP copy.[147] Though alternative hypotheses have been proposed, including those ascribing a primary role to tau and neuroinfammation,[148,149] the amyloid hypothesis thus far possesses the most experimental support and remains the dominant explanatory model of AD.

1.2.3 Cholinergic hypothesis

The cholinergic hypothesis of AD states that the amnestic symptoms seen in AD are tied to the progressive disturbance of cholinergic innervation within limbic and neocortical brain regions.[150] This hypothesis stemmed from three key observations: that presynaptic cholinergic markers are depleted in the brains of people with AD;[151,152] the observation that the nucleus basalis of Meynert, located in the basal forebrain, and the primary source of cholinergic innervation to the cerebral cortex, is heavily affected by neurodegeneration in AD;[153,154] and by the demonstration that memory performance can be impaired by cholinergic antagonists, and restored by cholinergic agonists.[155] This hypothesis received compelling validation following symptomatic improvement in patients with AD after the use of compounds that blocked the breakdown of acetylcholine (acetylcholinesterase inhibitors, AChEIs) (Figure 6).[156] Shown to improve cognition, global function and activities of daily living, as well as some behavioral manifestations in AD,[157,158] the use of this drug class has since become the prevailing standard in the pharmacotherapeutic management of AD.

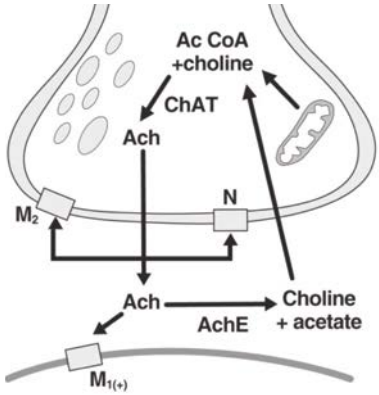

Figure 6. *Physiology of the cholinergic synapse. Choline is the critical substrate for the synthesis of acetylcholine. Acetyl coenzyme A (Ac CoA), which is produced by the breakdown of glucose (carbohydrate) through glycolysis (Krebs cycle), along with the enzyme choline acetyltransferase (ChAT) are critical for the synthesis of the neurotransmitter acetylcholine (Ach). Once the neurotransmitter acetylcholine (Ach) is released into the synapse, it binds (activates) postsynaptic receptors (M1), thus transmitting a signal from one neuron to the other. The excess neurotransmitter in the synaptic cleft is broken down by the enzyme acetyl cholinesterase (AChE) into choline and acetate, which are returned by an uptake mechanism for recycling into Ac CoA. Adapted Hampel H, Mesulam MM, Cuello AC, et al. The cholinergic system in the pathophysiology and treatment of Alzheimer's disease. Brain. 2018;141(7):1917-1933. Copyright Oxford University Press, 2018.*

1.2.4 Neuropsychological assessment

The purpose of neuropsychological testing in the context of a patient presenting with cognitive complaints is to obtain a thorough characterization of the latter. This includes establishing whether the impairment is objective in nature, its distribution across cognitive domains (e.g. episodic memory, language, visuospatial function), and its severity. Often approached in terms of standard deviations below a normative reference group, impairment is generally considered when performance falls 1.5 to 2 units below the reference group mean. In addition to age, norms are often corrected for education; this stems from findings showing that in older individuals with high education, performance may fall in the normal range despite significant cognitive decline.[159] This is assumed to reflect high cognitive reserve, whereby the brain is able to meet the demands imposed by cognitive testing in a more efficient manner.[160-162] Some data suggests, however, that estimation of an individual's premorbid intelligence quotient may better capture cognitive reserve and is thus a more appropriate correction.[163-166]

Neuropsychological testing in AD has played an important role in the detection of early cognitive changes, as well as in the staging and tracking of disease progression. Typically, limbic regions subserving memory are the earliest sites affected in AD, producing a circumscribed deficit in anterograde episodic memory.[63,167-169] As pathology spreads to involve other neocortical regions, additional cognitive domains become affected, including attentional and executive processes, semantic memory, praxis and visuospatial abilities.[170-176] Of note, atypical presentations of AD have been described involving early prominent deficits in non-memory domains, including language and visuospatial perception.[177] Separation of AD from other dementia disorders has been shown possible using cognitive measures;[178-182] neuropsychological testing, however, is most informative early on in the disease course, as the distinctiveness of impairment profiles decreases with clinical progression.[183] Though broad consensus has yet to be reached, a uniform neuropsychological test battery has been proposed for use in the evaluation of dementia disorders.[183,184]

1.3 BIOMARKERS

A biomarker is an objectively measurable physiological, biochemical, or anatomic parameter that can be treated as an indicator of biological processes (normal or pathological) or responses to a treatment.[140,185] In addition to guiding population enrichment and facilitating selection of drug candidates in AD therapeutic trials, biomarkers are increasingly used as diagnostic tools, allowing for earlier and more accurate identification of AD pathology and as aids in the context of treatment decisions.[186] In AD, the most established biomarkers can be divided between those derived from molecular imaging and CSF.

1.4 MOLECULAR IMAGING

A biomedical research discipline, molecular imaging encompasses the visualization, description, and measurement of biological processes of interest, occurring at the cellular and subcellular level, in living subjects.[187] Techniques include positron emission tomography (PET) and magnetic resonance imaging (MRI). While of limited spatial resolution, PET is sensitive to biological processes in the pico-molar (10^{-12}) range; MRI, by contrast, has tremendous spatial resolution (sub-millimetre range) but lower sensitivity (micro-molar; 10^{-6}). In conjunction, these modalities provide critical information on brain physiology and anatomy.

1.5 POSITRON EMISSION TOMOGRAPHY

1.5.1 Fundamentals and quantification

1.5.1.1 PET physics

The key principles underlying PET are summarized in Figure 7. In essence, PET records the spatial distribution of a positron emitting radioactive isotope (radioisotope) in tissue(s) of interest. The initial step preceding and requisite to the PET investigation itself, is the production of a radioisotope. This is generally accomplished using a particle accelerator known as a cyclotron; here, a high-energy beam is used to bombard a stable isotope. In this way, the target nucleus is rendered unstable, yielding the desired radioisotope. The latter is then chemically incorporated into a molecule of interest (specific to the desired biological target), yielding a compound known as a radiopharmaceutical, or PET tracer. Following quality control (QC) procedures, the tracer is then injected into the patient or research subject. As the radioisotope seeks to regain a more stable atomic composition, it undergoes spontaneous decomposition; the product of this process is known as an anti-electron, or positron. Once a positron combines with a surrounding electron, a process known as annihilation occurs, whereby two photons (gamma rays) of 511 kiloelectron volts (keV) each are emitted in approximately opposite directions.

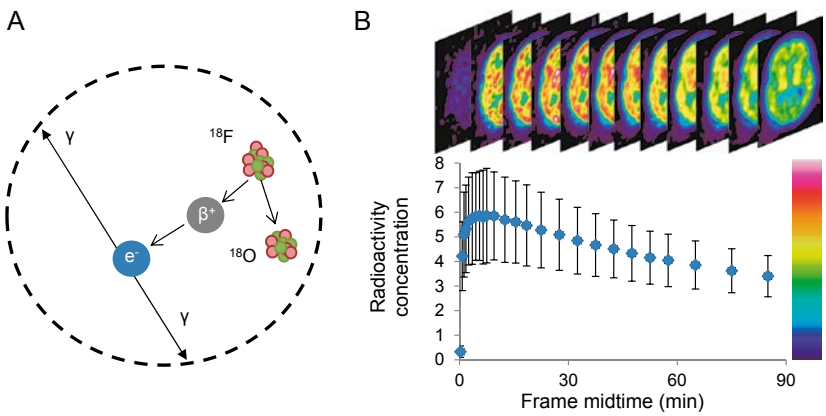

Figure 7. *Schematic representation of a PET detector ring and the two-step emission of γ-rays following the disintegration of an unstable flourine-18 atom, yielding stable oxygen-18 (A). The distance between the fluorine atom and the annihilation is greatly exaggerated. In the rightward panel (B), data is collected in frames during a dynamic PET scan over 90 minutes. The graph shows the time-activity curve for the whole brain uptake, with higher standard deviations early in the scan due to shorter frames. Adapted from Heurling K, Characterization of [^{18}F]flutemetamol binding properties. Doctoral thesis, Uppsala University, 2015.*

A PET scanner comprises a cylindrical assembly of block detectors, in a ring structure, with a depth of several blocks. The depth of this cylinder is known as the field-of-view (FOV), and is the space occupied by a patient or research subject. Detection of 511 keV coincident photons by scintillation detectors within the FOV forms the basis of PET. These detectors, comprised of inorganic crystals, emit flashes of light after photon absorption. Following conversion of this signal to an electrical pulse and amplification by photo-multiplier tubes, the pulse is sorted according to incoming energy and registered as a single event, or count (i.e. a pair of photons detected simultaneously). By means of computer-based algorithms, detected counts can be reconstructed into images showing the spatial distribution of the tracer in units of radioactivity concentration (Bq/mL). These, in turn, can be analysed using mathematical approaches to investigate a range of outcome parameters. A crucial prerequisite to the reconstruction step is correction for several factors, including photon attenuation (due absorption by tissue), random events (two unrelated photons are recorded as an event) and dead time loss (time during which the scanner detection system is unable to record events due a combination of count rate, scintillation decay time, and scanners electronics).

PET acquisition protocols can be divided into dynamic and static approaches. In dynamic scanning, data acquisition is started directly upon injection of the tracer, and collected over time. This can be performed using either pre-specified intervals known as frames (typically of increasing duration), with reconstructed images then showing the events detected at each voxel during the specific time period, or continuously over time (list-mode). In the case of list-mode acquisition, data can then be binned into frames during reconstruction, affording greater flexibility. The radioactivity measured in a voxel or brain region during a dynamic scan can be summarized by a time activity curve (TAC), showing the behaviour of the tracer over time. Static acquisition refers to specifying a single frame over the course of the scan; this provides a single image representing the average amount of radioactivity during the specified interval. Some static protocols, however, incorporate a dynamic component, whereby acquisition is performed over several frames following an uptake period. These frames are typically averaged, however, providing a static image. Though advantages and disadvantages exist for both approaches,[188] head-to-head comparison has shown dynamic scans to provide higher accuracy, reproducibility, and image contrast.[189,190]

In order to be of value in the quantification of targets in the brain, a PET radiotracer must fulfil a range of stringent criteria.[191] These include the ability to readily cross the blood-brain barrier (BBB), a high affinity (nanomolar (nM) range) towards the target, and the absence of radiometabolites passing the BBB that could contaminate the recorded PET signal. Additional criteria include selectivity (i.e. low off-target binding), favourable pharmacokinetics (rapid brain penetrance and wash-out), high specific activity and safe for administration in low doses. Lastly, a PET tracer

should prove amenable to labelling with carbon-11 or fluorine-18; owing to the short half-life of carbon-11 (20 min), several PET studies with different tracers can be performed in a single day, allowing for the collection of complementary information from a disease characterization standpoint.[192] Given the short half-life of carbon-11, however, an on-site cyclotron along with specialized infrastructure and personnel are required. Tracers labelled with the longer-lived fluorine-18 have thus been developed and commercialized for clinical applications as the longer half-life (110 min) allows for centralized production and regional distribution, even to centres lacking access to the full range of resources required for PET.

1.5.1.2 Registration and spatial normalisation

Head movement during PET studies is a common occurrence and can degrade image quality, producing misalignment between emission and attenuation correction data and decreased quantification accuracy.[193-196] As such, approaches for motion correction have been developed that involve the estimation of between-frame realignment parameters (translations and rotations) that minimize the sum of square difference between each frame and a reference image.[197] This process of image realignment is known as registration, and can also be performed between different modality images (co-registration, e.g. PET to MRI) from the same subject. This allows for the delineation of brain structures on high resolution T1-weighted MR images, and their application to PET in order to sample a parameter of interest, such as the non-displaceable binding potential (BP_{ND}), which, for reversibly binding tracers, describes the targets available for tracer binding;[198] moreover, if PET and MR images are co-registered, the PET image can more accurately be mapped onto a template image in stereotaxic space (a process known as spatial normalisation),[199] a step that allows for findings to be reported according to a standard coordinate system.[200-203] Co-registration can also be performed between images stemming from the same modality (e.g. longitudinal studies).

1.5.1.3 Approaches to PET quantification

Compartmental models

Following injection, the tracer distributes throughout the body, assuming a number of states, including a free fraction in the blood pool, a tissue fraction (unbound, specifically bound to the intended target, and non-specifically bound, e.g. to non-target proteins), and a circulating metabolized fraction. The signal recorded by the PET scanner comprises the sum of these physiologically separate tracer pools (known as compartments). In order to isolate the parameter of interest (i.e. tracer specifically bound), kinetic modelling is applied, whereby the dynamics between compartment are described using first order differential equations (compartmental modelling).[198,204] This allows for the estimation of physiological parameters of interest, such as BPND BP_{ND}, (ratio between receptor bound and free ligand)[198,205]

or distribution volume (V_T, volume occupied by tracer/total tissue volume under equilibrium in relation to plasma radioactivity concentration). Requiring arterial blood sampling so as to determine the metabolite corrected arterial input function (i.e. the unchanged radiotracer in arterial plasma), compartmental modelling is regarded as the gold standard in PET quantification.

Reference region models

Due to the invasive and labour-intensive requirements of compartmental modelling, so-called reference tissue models have been developed, whereby arterial plasma is replaced by a reference region as the source of the input function.[204] This class of models assumes that the reference region is free of specific binding (i.e. devoid of the target), with kinetics best described by a 1-tissue compartment (1-TC) model, whereby only tissue uptake and washout are considered.[206-209] These models further assume that free tracer and non-specific binding i.e. ratio of influx/efflux (K_1 and k_2) parameters are the same in both target and reference regions. Commonly used models include the simplified reference tissue model (SRTM),[206] yielding BP_{ND}, k_2 (transfer rate constant for tissue to plasma efflux in the target region) and R_1 (ratio of K_1 in target and reference regions) and reference input Logan,[210] which provides the distribution volume (DVR), defined as ratio of V_T in target and reference regions.

Semi-quantitative approaches

In order to implement compartmental or reference region models, dynamic data acquisition and fairly long scanning durations are required. In contrast, semi-quantitative estimates can be determined using shorter time-windows, on a frame-by-frame basis, or using frame summation, which provides an average image over a given time-window with improved count statistics. A common approach relates the radioactivity concentration in a target region to that within a reference region (assuming the above-mentioned assumptions); this gives a standardised uptake value ratio (SUVR), which provides an estimate of the relative signal from specific (target region) and non-specific (reference region) binding (i.e. activity concentration in target divided by the reference). In addition to the simplified acquisition parameters, SUVR is not affected by potential variability tied to administered radioactivity and body size.[211] Despite its many advantages, SUVR may vary with time if tracer washout varies between target and reference regions;[212] as such, the time window for estimation of SUVR must be validated.

Region and voxel-based approaches

Neuroimaging data can be analysed using region-of-interest (ROI) and voxel-based methods. An ROI (also referred to as volume-of-interest, VOI) broadly refers to a set of voxels that have been grouped together on the basis of a particular characteristic, such as their probability of belonging to a given anatomical brain region.[213-216] A good choice when a strong *a priori* hypothesis exists regarding which brain region(s) are involved, ROI based analyses also provide smoother

TACs (due averaging of voxels within the ROI), resulting in more robust parameter estimates. A drawback, however, is that findings that are constrained to a small area within an ROI, or that lie across ROI borders, will be lost. Voxel-wise analyses, by contrast, require imaging data to be in a standard coordinate space, and use parametric images, whereby a physiological parameter of interest (e.g. DVR), as opposed to radioactivity concentration, is represented by the value of each voxel. Parametric images will often be spatially smoothed with a filter similar in size to the scanner's resolution, removing spurious voxels and increasing data normality and signal-to-noise ratio. While not subject to the limitations of ROI based analyses, voxel level TACs have a comparatively higher degree of noise, which can affect quantification accuracy.

Partial volume effect

As a result of the relatively poor spatial resolution of PET, the measured concentration of radioactivity in a given voxel reflects different tissue fractions as well as contributions from adjacent regions (Figure 8).[217] This is referred to as the partial volume effect (PVE), and leads to inaccuracies in radioactivity concentration estimates in reconstructed images, and, correspondingly, in derived parametric images.[217] Several methods have been proposed to correct for this effect,[218] including MRI driven approaches that rely on segmentation maps (i.e. assigning each voxel a tissue class: grey matter (GM), white matter (WM), CSF. In one such method, proposed by Müller-Gärtner et al.,[219] spill-over between white and grey matter compartments can be estimated and accounted for using tissue segmentation fractions, providing a GM specific correction. Though adjustment for PVE has been proposed to improve quantitative accuracy, methods reliant on anatomical information have been shown to be affected by the quality of the segmentation and image registration steps.[220,221] shown vs proposed.

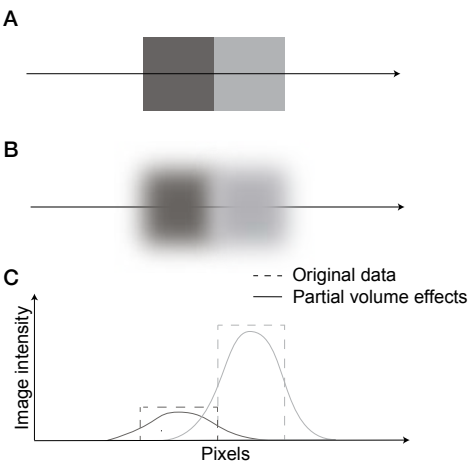

Figure 8. *Schematic representation of the impact of PVE on pixel data. Two adjacent pixels with different radioactivity concentrations (true data; A). Due to PVE, the intensity of the signal in each pixel spills out (B), resulting in a dilution of the signal (C). PVE results in a lower measured image intensity, as well as an overlap in the signal measured from both structures. Adapted from Heurling K, Characterization of [^{18}F]flutemetamol binding properties. Doctoral thesis, Uppsala University, 2015.*

1.5.2 Amyloid imaging

The first study using the carbon-11 ligand Pittsburgh Compound-B ([^{11}C]PIB), a thioflavin-T derivative specific for Aβ, showed increased retention in cortical areas in AD dementia patients, as compared to controls,[222] a finding that has since been reproduced in numerous studies.[223] The widespread success of [^{11}C]PIB and the limitations of carbon-11 prompted the development and commercialisation of fluorine-18 labelled compounds for wide availability.[224-227] As for [^{11}C]PIB, these tracers have as their substrate the tertiary β-pleated sheet conformation of fibrillar amyloid.[228] Studies using [^{11}C]PIB and these longer-lived compounds have shown that approximately 30% of cognitively unimpaired (CU) elderly[225,229-233] and 60% of MCI[229,234-237] patients show amyloid positivity. These findings match autopsy studies showing comparable percentages meeting neuropathological criteria for AD.[139,236,238-240] Among patients diagnosed as AD dementia, roughly 10% are amyloid negative using PET;[225,229,230,235,241] given the high correspondence between PET and neuropathological assessments,[242] these cases are largely assumed to represent clinical misdiagnosis.[231,243]

Importantly, amyloid PET positivity in CU and MCI subjects is interpreted to represent AD in its preclinical and prodromal phases, respectively, and is associated with an increased likelihood of abnormal neurodegenerative biomarkers and cognitive decline.[244] Emergence of significant Aβ pathology (i.e. amyloid positivity) has been suggested to occur for many in their mid-50s;[245] Aβ deposition is then thought to increase in a slow and continuous fashion, with sigmoidal kinetics over time. Specifically, using [^{11}C]PIB, it has been shown to take 12 years to progress from mean SUVR levels seen in amyloid negative CU older adults to the threshold for positivity, and a further 19 years to reach SUVR values seen in AD dementia patients.[246] In studies that have looked at the rate of change in amyloid PET as a function of uptake at baseline,[246-248] after an initial accumulation phase, a peak is reached, followed by a decline to an accumulation rate of nearly zero, implying a plateau in amyloid load.[247] Though a fairly substantial window of opportunity for secondary prevention studies was established based on these studies,[247] the consistent failure of clinical trials employing anti-amyloid compounds[249] suggests that by the time brain amyloid deposition has reached a plateau, amyloid may be less relevant as a target, with the disease course instead driven by downstream processes.[249]

Among the above-mentioned fluorine-18 amyloid tracers, three have been approved by both the European Medicines Agency (EMA) and the US Food and Drug Administration (FDA), including [^{18}F]AV-45 ([^{18}F]florbetapir; Amyvid),[226] [^{18}F]-BAY94-9172 ([^{18}F]florbetaben; Neuraceq)[250] and [^{18}F]3′-F-PIB ([^{18}F] flutemetamol; Vizamyl),[227] (Figure 9) in order to estimate Aβ neuritic plaque burden in cognitively impaired patients who are being investigated for AD and related causes of cognitive decline. Currently, these tracers are validated for binary

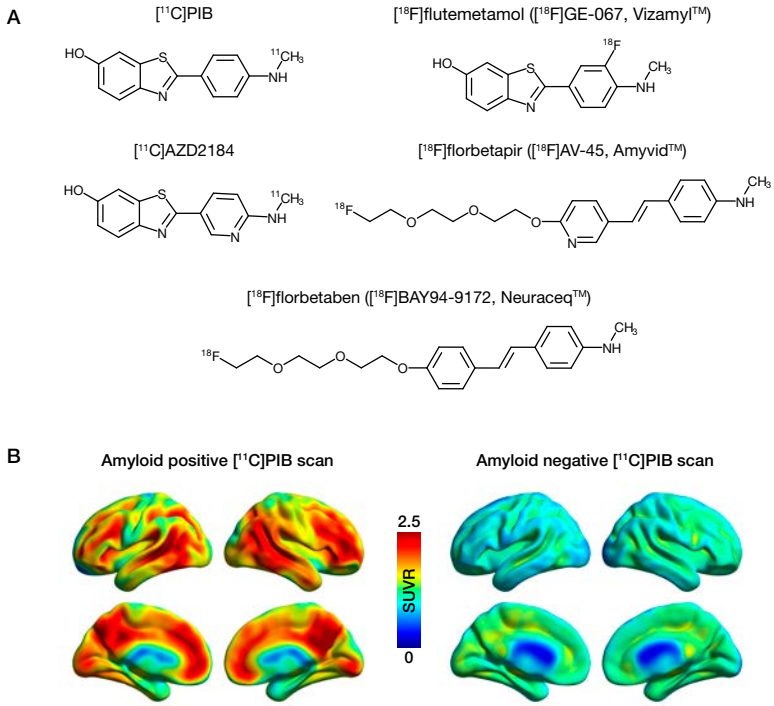

Figure 9. *Chemical structure of [^{11}C]PIB and related fluorine-18 commercial amyloid PET ligands (A). Representative [^{11}C]PIB SUVR cortical projection images (B) in an amyloid positive patient with AD dementia (left) and in a cognitively unimpaired amyloid negative older control (right).*

visual reads only, whereby images are rated as positive (abnormal) or negative (normal).[251,252] Clinical studies using these compounds, while few in number, suggest that amyloid imaging can increase diagnostic confidence and alter patient management.[253-255] Large-scale multicentric US (Imaging Dementia – Evidence for Amyloid Scanning; IDEAS) and European studies (Amyloid imaging to prevent Alzheimer's disease; AMYPAD) are also underway, aiming to examine the clinical utility of amyloid PET, including its cost-effectiveness.[256]

1.5.2.1 Appropriate use criteria for amyloid imaging

In connection with the availability of fluorine-18 amyloid tracers, appropriate use criteria (AUC) were published by an Amyloid Imaging Taskforce (AIT) assembled by the Nuclear Medicine and Molecular Imaging and the Alzheimer's Association.[257,258] Broadly, amyloid imaging was defined as appropriate in patients with objective cognitive impairment of unclear aetiology (though with AD as a potential diagnosis) and when findings are expected to result in increased diagnostic certainty and altered patient management. More specifically, in MCI patients for

whom the syndrome is persistent and of unclear aetiology; in patients fulfilling core clinical criteria for AD dementia but with an atypical or etiologically mixed presentation (i.e. possible AD),[259] and in dementia patients with atypical age of onset (i.e. below age 65). The application of these criteria is to be performed by a dementia expert, defined as a physician with training and board-certification in psychiatry, neurology, or geriatric medicine with ≥ 25% of patient contact being with adults suffering from cognitive impairment or dementia.[258] Similar consensus based practice guidelines have been proposed by the Specialized Task force on Amyloid imaging in Canada (STAC)[260] and the Society of Nuclear Medicine and Molecular Imaging (SNMMI)/ European Association of Nuclear Medicine (EANM).[261]

1.5.3 Tau imaging

The latest addition to the armamentarium of tools available for the study of neurodegenerative disorders, tau imaging has largely emerged from international efforts aiming to replicate the success of amyloid PET.[262] As a molecular target, tau is challenging:[262] located intracellularly, it can assume six different isoforms; these can combine in various ways, and are further subject to post-translational modifications,[263] leading to heterogeneity among ultrastructural conformations (Table 2).[264] Further, though Aβ and tau deposits are known to co-localize, the concentrations of tau are far lower than those for Aβ.[265,266] Despite these challenges, remarkable progress has been made in the development of tau-selective ligands (Figures 10 and 11), with first-generation tracers (namely, [^{18}F]AV1451, [^{18}F]THK5317, [^{18}F]THK5315, and [^{11}C]PBB3) widely used in research studies[267-271] and second-generation tracers (such as, [^{18}F]MK-6240, [^{18}F]RO6958948), [^{18}F]PI2620, and under development.[272-276]

Table 2. Varied tauopathies and their tau isoform characteristics.

Type	Pathology	Isoform	Light microscope	Electron microscope
I	Alzheimer's disease	3R and 4R	NFTs	PHFs and SFs
	Down's syndrome	3R and 4R	NFTs	PHFs and SFs
II	Corticobasal degeneration	4R	Astrocytic plaques	SFs and TFs
	Progressive supranuclear palsy	4R	Globose tangles; tufted astrocytes	SFs and TFs
III	Pick's disease	3R	Pick's bodies	RCFs and TFs
IV	Myotonic dystrophy	Short 3R	NFTs	–

3R, Three repeat tau; 4R, Four repeat tau; NFTs, Neurofibrillary tangles; –, Not available; PHF, Paired helical filament; RCF, Random coil filament; SF, Straight filament; TF, Twisted filament. Adapted from Villemagne VL, Fodero-Tavoletti MT, Masters CL, Rowe CC. Tau imaging: early progress and future directions. Lancet Neurol. 2015;14(1):114-124

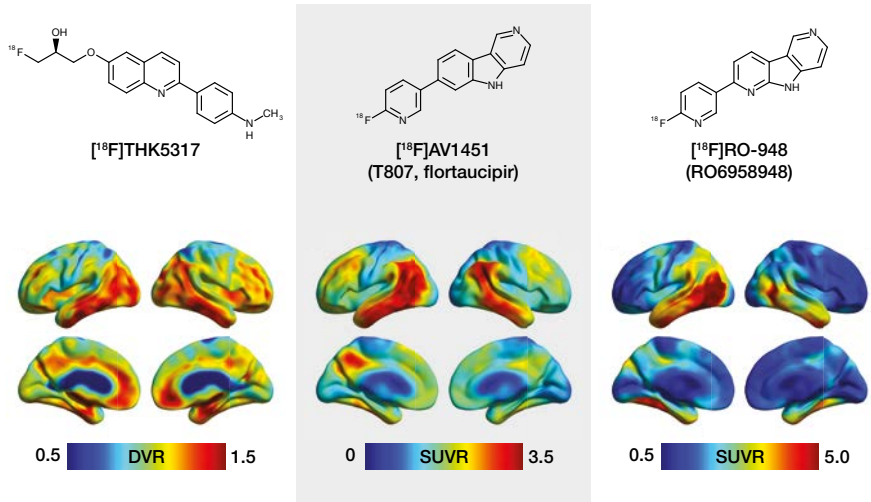

Figure 10. *Chemical structures and representative uptake images in amyloid positive AD patients using selected first- and second-generation tau PET tracers. For the creation of parametric images for all tracers, areas of the cerebellar cortex were used as reference. The [^{18}F]AV1451 image is courtesy of the Alzheimer's Disease Neuroimaging Initiative (ADNI); the [^{18}F]RO-948 image is courtesy of Professor Oskar Hansson and the Swedish Biomarkers for Identifying Neurodegernative Disorders Early and Reliably (BioFINDER) 2 study. Though direct comparison is complicated by between-patient differences, one can observe the preferential binding of the first- and second-generation tracers in AD relevant areas of the temporal lobes, and the broader dynamic range seen with [^{18}F]RO-948. DVR, distribution volume ratio; SUVR, standardised uptake value ratio.*

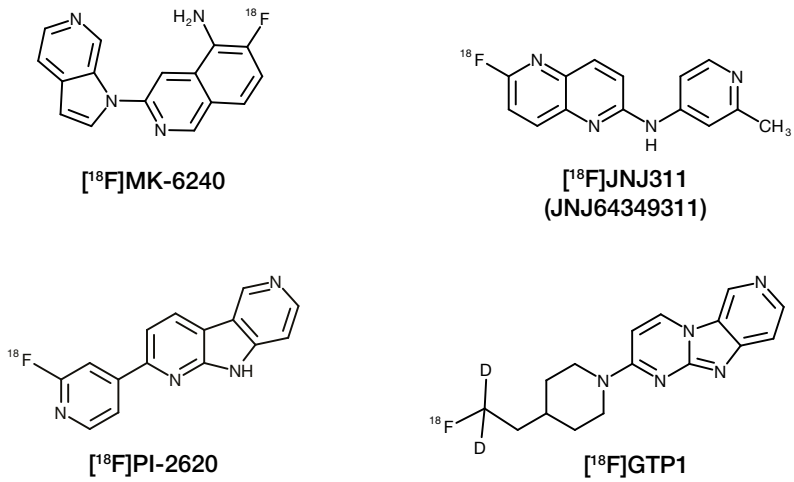

Figure 11. *Chemical structures of selected second-generation tau PET tracers*

In vitro studies using first-generation tracers showed high binding affinity to and specificity for tau aggregates, with high overlap between observed binding patterns and tau-immunohistochemistry (e.g. AT8, PHF-1) in AD brain tissue.[267,268,270,271,277,278] Further, early *in vivo* studies showed tracer retention to be elevated in patients with AD, as compared to CU elderly individuals.[268,270,279-281] Findings in MCI have varied between restricted elevations in medial temporal cortices to neocortical binding at a level comparable to AD, likely reflecting between study differences in the proportion of amyloid positive subjects.[81,82,280,281] Several studies have also shown a close correspondence between the pattern of ligand uptake and the known distribution of tau pathology based on post-mortem studies.[63,238] Combined with cross-sectional findings showing tau PET to associate with measures of neurodegeneration (hypometabolism; cortical atrophy)[271,282,283] and cognition,[80,284,285] this suggests that tau imaging may be useful in predicting the evolution of AD and/or as a marker of disease stage.[276,286] Longitudinal findings, however, suggest the lack of a linear association between tau pathology and 2-deoxy-2-[^{18}F]fluoro-D-glucose ([^{18}F]FDG) PET.[287] Although the number of publications using second-generation tau tracers are to date few and in limited samples,[288-290] available findings are consistent with those using first-generation ligands.

Though the majority of studies with tau imaging have focused on AD, those in non-AD tauopathies, such as corticobasal syndrome (CBS) and PSP have shown patterns of tracer retention that accord with the expected spatial distribution of tau based on neuropathology studies.[268,291-294] *In vivo* studies in PSP have generally shown distinct pattern of tracer uptake in subcortical brain regions and the cerebellar dentate nuclei.[295-298] Comparison of *ante-* and *post-mortem* findings in PSP, however, has shown that in some patients, there tracer binding was absent in structures showing signal *in vivo*,[299,300] possibly reflecting a low binding affinity of [^{18}F]AV1451 for 4R tau.[276] Further, comparative studies between tau ligands suggest that they differ in their sensitivity and specificity toward AD-type PHF tau, highlighting both the complexity of tau pathology and the potential need for multiple tracers to properly characterize primary tauopathies.[301,302] A further limitation of tau imaging is the observation of off-target binding to multiple targets, including monoamine oxidase A (MAO-A) and B (MAO-B)[303-306] this phenomenon, however, appears so far reduced or absent in second-generation tracers.[273,274]

1.5.4 Cerebral glucose metabolism

The primary substrate for energy production in the brain, glucose metabolism has been closely tied to neuronal (synaptic) and, more recently, astrocytic, activity.[307-310] Consumption of glucose in the brain can be measured using [^{18}F]FDG, a fluorine-18 labelled glucose analogue.[311,312] Following transport into the brain by the same carrier that transports glucose across the BBB,[313] [^{18}F]FDG is phosphorylated by hexokinase,

yielding [^{18}F]FDG-6-phosphate. Lacking a hydroxyl group, however, this labelled product cannot proceed further along the glycolytic pathway,[312] becoming trapped in the cerebral tissue, at least over the time course of a typical PET study.

A considerable body of work using [^{18}F]FDG PET has identified a characteristic pattern of metabolic changes in clinically established AD (Figure 12).[314-317] This ensemble includes the posterior cingulate/precuneus, the inferior parietal lobe, as well as the posterolateral and medial temporal lobe. Decline in the uptake of [^{18}F]FDG within these regions has been shown to associate with clinical progression across the continuum of AD,[318-322] including the emergence of MCI among elderly subjects,[323,324] and to correlate with the neuropathologic diagnosis of AD at autopsy.[325,326] Further, distinct spatial patterns of hypometabolism have been associated with atypical focal cortical presentations of AD,[203,327,328] and have been of value in the differentiation of AD from other dementia disorders, including frontotemporal dementia (FTD) and dementia with Lewy bodies (DLB).[329]

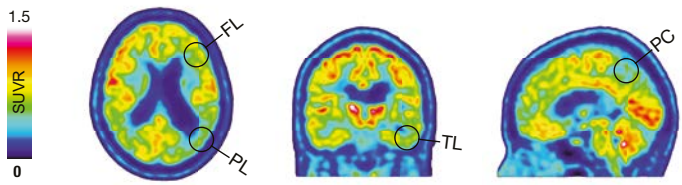

Figure 12. *[^{18}F]FDG PET scan in a patient with AD dementia; circles indicate areas typically showing hypometabolism in AD, including the temporal (TL) and parietal (PL) lobes, as well as the precuneus (PC). Involvement of the frontal lobe (FL) can be seen later on the disease course, while metabolism within the occipital lobe is typically preserved.*

1.5.5 Cerebral blood flow

Though classically measured using PET with oxygen-15 labelled water ([O^{15}]H_2O),[330-332] cerebral blood flow (CBF) can also be estimated through the application of reduced configuration models to dynamic PET data.[204] Replacing arterial plasma with a reference tissue as the source of the input function, such models provide perfusion information in the form of the parameter R_1 (Figure 13), [206,333,334] shown to be highly correlated with regional CBF, as measured by [O^{15}]H_2O.[335] A related measure, perfusion SUVR (p-SUVR), defined as the calculation of SUVR over the initial minutes post tracer injection, has also been used as a proxy of CBF (Figure 13).[336] In contrast to R_1, however, this parameter does not require kinetic modelling due the assumption that the initial portion of tracer uptake reflects K_1,[337] with p-SUVR thus reflecting CBF.

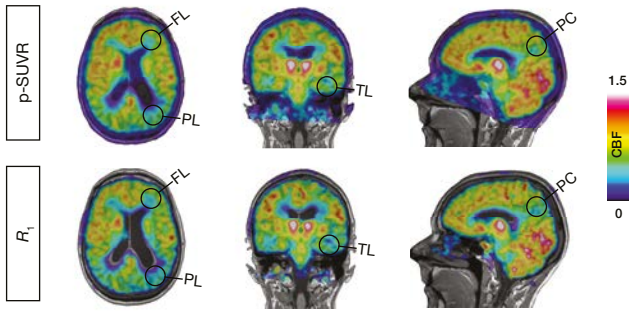

Figure 13. *[^{18}F]THK5317 perfusion (p-SUVR and R_1) images in a patient with AD dementia. Decrements in cerebral blood flow can be seen in temporoparietal (TL, temporal lobe; PL, parietal lobe) and frontal (FL) areas, as well as in the posterior cingulate (PC), a spatial topography similar to that seen with [^{18}F]FDG PET.*

1.5.5.1 Coupling between cerebral blood flow and glucose metabolism

Blood flow and glucose consumption in the brain have been shown to be closely linked under physiological conditions[338] and in those with AD and related neurodegenerative disorders.[317,339] As a result of this linkage, studies have explored the use of regional CBF estimates derived from dynamic amyloid PET studies as proxies for [^{18}F]FDG metabolic imaging.[336,340-343] Additional studies have used the dopamine transporter tracer [^{11}C]PE2I,[344] and the tau tracers [^{18}F]AV1451[345] and [^{18}F]THK5317.[340,346] Overall, these studies have shown that regional perfusion estimates correlate strongly with [^{18}F]FDG and may prove of value in the context of differential diagnosis between dementia disorders. Some findings suggest, however, that conditions may exist under which the parallelism between these parameters may become decreased.[346-349]

1.6 STRUCTURAL BRAIN IMAGING

Information pertaining to the structural (i.e. anatomical) integrity of the brain can be obtained using computed tomography (CT) and MRI. CT is a computerized x-ray based imaging technique whereby a narrow beam of x-rays is rotated around the head, generating tomographic images.[350] These can then be digitally concatenated, yielding a three-dimensional image of the brain.[350] MRI, by contrast, involves the use of a strong magnetic field and electromagnetic (radio) waves in order to manipulate hydrogen nuclei (protons) within the body; this results in the patient or subject being scanned emitting a signal, which can be received and reconstructed into an image.[351] Given that proton content varies across tissue types, combinations (sequences) of radio wave pulses and gradations in the external magnetic field of the scanner can be used to modulate the signal from a given tissue class.[351] In

the context of brain imaging, for example, the relative signal from GM, WM and CSF can be adjusted, according to what one wishes to examine (e.g. morphology, vascular changes, cerebrovascular disease).

In AD, CT and MRI studies have shown that atrophy typically begins in the entorhinal cortex, followed closely by the hippocampus, amygdala, and parahippocampus.[352-356] Volumetric loss then spreads to involve lateral aspects of the temporal lobe, followed by neocortical association areas.[357-359] This pattern of atrophy progression has been shown to closely follow the known spatial distribution of neurodegenerative changes in AD from autopsy studies,[63,360,361] and to correlate strongly with cognitive decline;[362] as such, atrophy is considered a good marker of disease progression.[363] In clinical practice, visual rating of medial temporal lobe atrophy is commonly performed in specialist memory centres as this measure carries good positive predictive value for AD, both in terms of differentiation from normal aging[364-366] and identifying MCI subjects at risk for progression to dementia.[367,368] Visual assessment of additional brain areas can further be of help when attempting to discriminate AD from other dementia disorders,[369,370] and in the recognition of atypical forms of AD where wide variation in medial temporal atrophy exists.[371,372]

In the context of memory clinics, detection of atrophy (medial temporal, global cortical) and WM changes has been shown to be comparable using visual rating of images on a newer CT scanner and a 1.5T MRI.[373] Though CT carries several advantages over MRI,[374] including increased availability, more rapid data acquisition, lower cost, and the ability to image patients with MR-incompatible ferromagnetic objects such as pacemakers, MRI is better able to detect cerebrovascular lesions when compared with most currently used CT scanners,[375] has higher resolution, and lacks ionizing radiation.[376] The utility of MRI, moreover, is broader; in addition to a growing interest in the automation of pattern classification,[377] additional measures of cerebral perfusion,[378] integrity of WM fibre pathways,[379] brain activation (both at rest and in response to tasks),[380] and perturbations in brain biochemistry[381] are a major focus within the field, given the belief that they might be more sensitive than anatomic measures to early disease-related changes.[382] These measures, however, lack validation and as yet are not established for use in clinical practice.

1.7 CEREBROSPINAL FLUID BIOMARKERS

CSF fills the ventricles and surrounds the brain and the spinal cord. Its functions include cushioning the brain against trauma, removal of metabolic by-products generated by the activity of neurons and glial cells, and the circulation of biologically active substances within the brain.[383] Production of CSF is accomplished largely by the choroid plexus, a specialized organ within the lateral, third and fourth ventricles, with the remainder (~10-20%) arising from bulk flow of interstitial fluid along perivascular spaces and axonal tracts.[384] In adults, the intracranial volume of CSF has been estimated at roughly 155 mL; CSF turn-over is high (~0.4 mL/min),

with an average of 650 mL produced daily.[385-387] Due its direct contact with the central nervous system, CSF is considered an ideal source of information for the detection and measurement of biochemical abnormalities within the brain parenchyma,[388] and can be sampled via lumbar puncture (LP), a safe and well-tolerated procedure.[389-392] Analytes of interest in CSF can then be quantified using a range of techniques, including enzyme linked immunosorbent assays (ELISAs), electrochemiluminescence, and mass spectrometry (MS).

1.7.1 Assays

1.7.1.1 Immunoassays

A powerful method for the detection and quantification of selected molecules in complex solutions and tissue preparations, the ELISA was first developed in the early 1970s[393,394] due advances in the production of antigen-specific monoclonal antibodies[395] and methods to achieve their chemical linkage to biological enzymes able to emit a measurable signal.[396-398] Although a number of ELISA variants exist, all are characterized by the same basic elements: an antigen, one or several antibodies specific to that antigen, and a system to quantify the amount of antigen present.

Given the low abundance of most CSF based proteins,[399,400] the capture or sandwich ELISA is widely used due its high sensitivity and specificity (Figure 14). First, a capture antibody, highly specific for the antigen, is attached to a solid phase (e.g., detection plate surface, membranes and beads). The antigen (sample or calibrator) is then added, followed by detection antibody, bound, directly or indirectly, to a reporter system (e.g. signal-generating enzyme or fluorophore). For detection, the appropriate substrate is added, with the observed signal (colorimetric or fluorometric) proportional to the amount of antigen in the sample. Simultaneous quantification of multiple analytes (multiplexing) can also be performed using the xMAP Luminex[401] and Meso Scale Discovery (MSD) platforms;[402] these rely on bead-based technology (capture antibodies coupled to dyed beads or microspheres with varied emission spectra) and an electrochemiluminescent label conjugated to the detection antibody, respectively.

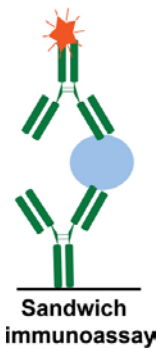

Figure 14. *A schematic diagram illustrating a sandwich ELISA. Using sandwich assays, the analyte of interest (blue sphere) is measured using two antibodies: a capture antibody (bottom) and a detection antibody (top), coupled to a reporter system (star symbol; e.g. horse radish peroxidase). Following addition of a substrate (e.g. p-Nitrophenyl-phosphate), a signal (colorimetric or fluorometric) is emitted in proportion to the amount of target antigen in the sample. Adapted with permission from Landegren U, Al-Amin RA, Bjorkesten J. A myopic perspective on the future of protein diagnostics. N Biotechnol. 2018; 45:14-18. Copyright Elsevier, 2018.*

In contrast to traditional analogue ELISA systems, in which the intensity of the detection signal increases as a function of analyte concentration, digital ELISA allows for the measurement of individual molecules.[403-405] This technique has recently been extended to a bead-based approach that uses an arrangement of femtoliter-sized reaction chambers termed single-molecule arrays (Simoa).[406] Using this ultrasensitive method, single molecule immunocomplexes can be detected, with sample and reagent volumes, cost, and analysis times below those for conventional immunoassays.[407]

1.7.1.2 Mass spectrometry based quantification

MS is an antibody-independent analytical technique used to determine the molecular composition of a compound.[408] The first step in a mass spectrometric analysis is the transformation of the sample into an ionized gas; these ions are then accelerated through the use of electric and/or magnetic fields, and, following fragmentation, are separated according to their mass-to-charge (m/z) ratio. Detected in proportion to their abundance, a mass spectrum (relative ion abundance against m/z; ordinate and abscissa, respectively) is thus produced. MS can also be performed in parallel (MS/MS), allowing for analysis of an analyte and its fragments.

Within clinical laboratory medicine, reference measurement procedures (RMPs) and certified reference materials (CRMs) are considered the gold standards for CSF measurements.[409-413] Defined as a method producing metrologically traceable results that can be linked to an established higher-order standard (i.e. the International System of Units) through a chain of unbroken comparisons, an RMP can be used to assign or verify the concentration of a CRM (with a known concentration in SI units) for the analyte of interest, which can subsequently be distributed for assay calibration. Establishment of a CRM can be achieved using an MS based RMP known as selected reaction monitoring (SRM) (Figure 15).[414] In this approach, solid phase extraction (SPE) and liquid chromatography (LC) are included prior to the MS step in order to concentrate and extract, respectively, the desired analyte.[415] MS/MS is then used to increase selectivity, with quantification of the endogenous analyte possible through comparison of its signal to that of a stable isotopically labelled internal standard.[414,416]

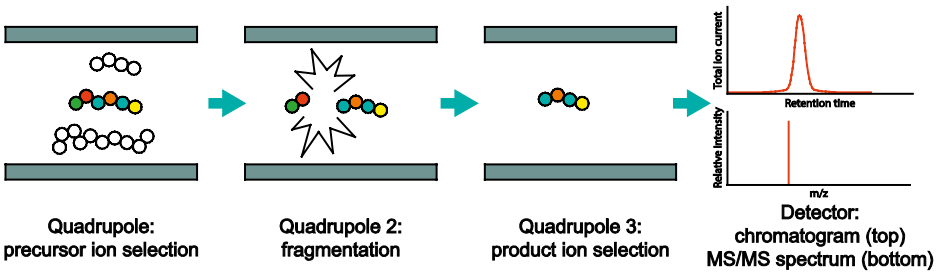

Figure 15. *Selected reaction monitoring (SRM) mode on a triple quadrupole mass spectrometer. SRM is a targeted mass spectrometry based analysis involving the use of a triple quadrupole mass spectrometer comprising three consecutive quadrupole mass analysers. The first quadrupole is set to transmit a precursor ion based on its mass-to-charge (m/z) ratio. In the second quadrupole, which is filled with an inert gas such as argon or nitrogen, collision induced dissociation is then used to fragment this ion as it collides with the gas molecules. The third quadrupole is set to transmit one or more specific product ions generated in the second quadrupole to the detector. SRM greatly increases selectivity compared to single ion monitoring, since interfering ions with identical m/z co-isolated in the first quadrupole will most likely not give rise to product ions with identical m/z to that of the analyte of interest. Adapted from Pannee J, Mass spectrometric quantification of amyloid-beta in cerebrospinal fluid and plasma. Doctoral thesis, University of Gothenburg, 2015.*

1.7.2 Standardisation efforts

Though commercial assays for AD biomarkers ($A\beta_{1\text{-}42}$, p-tau_{181p}, and t-tau) show similar diagnostic accuracy in the separation of AD patients from those with related neurodegenerative diseases or controls,[286,401] reported analyte concentrations have been shown to vary significantly.[417] This is thought to reflect the sensitivity of these assays to pre-analytical (e.g. sample handling and storage),[418-422] analytical (e.g. between/within differences in laboratory procedures),[423,424] and assay-related (e.g. manufacturing based variations in the analytical kit components) factors.[418,424] As a result of differences in absolute concentrations, different cut-offs have been used between centres, complicating clinical practice and comparability in single and multicentre studies.[425] International efforts to standardise CSF procedures are currently ongoing, however,[426] including a QC program monitoring within and between laboratory measurement variability.[417,427,428] In a step towards the implementation of universal cut-off levels, SRM MS-based RMPs have been published for $A\beta_{1\text{-}42}$;[429] these methods will be used to establish CRMs that can then be used for assay calibration by manufacturers.[409,426]

1.7.3 Amyloid-β pathology

The precursor to Aβ, the APP is a transmembrane protein comprising a large extracellular N-terminal region and a lesser intracellular tail.[430] Two pathways exist for the degradation of APP: in the nonamyloidogenic pathway (so-called due it precluding the generation of Aβ), APP is cleaved within the Aβ domain by the protease α-secretase, resulting in the production of an 83-amino acid C-terminal fragment (C83) and a soluble APP (α-sAPP) fragment. C83 is subsequently cleaved by γ-secretase, yielding a truncated peptide ($A\beta_{17-32}$, or p3). This fragment, however, has been found in senile plaques[431] and may possess neurotoxic properties,[432] suggesting that the pathway moniker may be somewhat of a misnomer. In the amyloidogenic pathway, APP is by contrast cleaved by β-secretase, producing a large N-terminal fragment (β-sAPP) and an intracellular 83-amino acid C-terminal fragment (C99); in a second step, C99 is cleaved by γ-secretase, releasing Aβ peptides. Among these, $A\beta_{1-40}$ has been shown to be the most predominant variant, followed by $A\beta_{1-38}$ and $A\beta_{1-42}$.[433]

Initial studies examining CSF Aβ did not differentiate between isoforms (i.e. total Aβ). Though some studies found a slight decrease in this measure in AD,[434-436] large overlap was observed in comparison to controls, with other studies finding no change.[437-439] Following the discovery of multiple C-terminal forms of Aβ, and the observation that the 42-amino acid isoform was highly aggregation prone[440] and predominant in diffuse and senile plaques,[441,442] ELISAs specific to $A\beta_{1-42}$ were developed.[438,443] Using this method, a marked reduction in $A\beta_{1-42}$ was found in AD dementia patients[438,444] with levels shown to correlate inversely with cortical plaque load in AD brain tissue in both post-mortem[445,446] and biopsy studies.[447] Reduced $A\beta_{1-42}$ has been hypothesized to reflect the preferential deposition of $A\beta_{1-42}$ in plaques, resulting in a reduction in the amount available for passage into the CSF.[438,448,449] Reduced CSF $A\beta_{1-42}$ has also been observed in disorders without plaques, however, including amyotrophic lateral sclerosis[450] and CJD,[451] suggesting the involvement of additional mechanisms.

The high abundance of $A\beta_{1-40}$ in CSF,[452] combined with its lower potential for aggregation,[453] suggests that its levels can theoretically provide a better index of amyloidogenic APP processing, in comparison to $A\beta_{1-38}$ or $A\beta_{1-42}$. Moreover, the use of $A\beta_{1-40}$ in ratio with $A\beta_{1-42}$ ($A\beta_{1-42}$/ $A\beta_{1-40}$) has been proposed as a method to adjust for interindividual differences in Aβ production levels.[433,454] Indeed, some studies have shown improved discrimination between AD and non-AD disorders using this measure,[454-456] as well as improved power to predict AD in subjects with MCI.[457]

1.7.4 Tau pathology

The identification of Aβ as the main component in plaques,[458,459] and the subsequent cloning of *APP*,[129] occurred nearly in parallel to the discovery that tangles

were composed of abnormally hyperphosphorylated tau.[77] Though multiple phosphorylation sites exist on the tau protein,[460] the most commonly used assays for phosphorylated tau (p-tau) use antibodies targeting phosphorylation at threonine 181 (p-tau$_{181}$) or 231 (p-tau$_{231}$).[461,462] Studies using these measures have consistently shown an increase in p-tau in AD;[463] these subtypes of p-tau have further been shown to strongly correlate and exhibit similar diagnostic performance.[464] In addition to p-tau, levels of total tau (t-tau), determined using monoclonal antibodies able to detect all tau isoforms, independent of their phosphorylation state,[465] have also been shown to be markedly increased in AD.[466-468] Elevations in both measures have been shown to correlate with more rapid progression from MCI to AD, the rate of hippocampal atrophy,[469] and faster cognitive decline in AD.[470-473]

Though positive correlations have been reported between CSF tau (p-tau, t-tau) and neocortical tangle burden at autopsy,[445,447,474-477] associations for p-tau appear to be specific to threonine 231;[474,475] p-tau$_{231}$ may, further, have greater sensitivity for NFTs as it been shown to detect tau pathology in layer II of the entorhinal cortex, an area considered to be the earliest site affected by tangles in AD.[478] Current thinking, however, suggests that p-tau may best reflect the phosphorylation state of tau in the brain, which, in turn, is related to the development of tangle pathology, as opposed to the burden of tangles per se.[424] While the level of t-tau may partially reflect the release of tau from degenerating neurons affected by tangle pathology, its marked elevation in acute disorders such as stroke and brain trauma[479-481] and conditions characterized by rapid neurodegeneration (e.g. CJD)[482] suggests that it primarily reflects the intensity of neuronal injury and degeneration.[424] Indeed, CSF t-tau is considered as such a marker in the recently proposed AD biomarker classification scheme (see "A/T/N", section 1.11).[483,484]

1.7.5 Neurodegeneration

A key feature of AD pathophysiology, the degeneration and loss of synapses has been shown to more strongly correlate with cognitive deficits in AD than either Aβ plaque or tangle load.[87,485] The hypothesis that synaptic markers might thus show a strong association to cognition in AD led to the identification of several synaptic proteins in CSF, including neurogranin.[91,486] A postsynaptic dendritic protein highly expressed by excitatory neurons in the cortex and hippocampus,[487,488] neurogranin has been shown to play a key role in synaptic plasticity and induction of long-term potentiation.[489,490] High CSF levels have been observed in AD[491-494] and have further been shown to correlate with both the rate of hippocampal atrophy and extent of metabolic reduction on [^{18}F]FDG PET.[495] Moreover, high CSF neurogranin seems to be specific to AD, as this finding was absent among patients with a range of other neurodegenerative disorders.[496] A further measure, neurofilament light (NFL), a marker of large-caliber axonal degeneration, has also been shown to be increased in MCI and AD, and to associate with structural brain changes and cognitive decline.[497]

1.8 RELATIONSHIP BETWEEN PET AND CSF BIOMARKERS

Following the first study showing an inverse association between global cortical retention of [^{11}C]PIB and CSF $A\beta_{1-42}$[498] have numerous publications since confirmed this finding.[234,499-504] Across these studies, approximately 90% of subjects showed concordance between amyloid biomarkers (i.e. both abnormal or normal), with discordant cases divided nearly equally between isolated low CSF $A\beta_{1-42}$ and isolated PET positivity.[505] Investigation of discordant cases has shown biomarker disagreement to vary by disease stage, with isolated CSF $A\beta_{1-42}$ positivity highest in CU elderly, intermediate in MCI and lowest in AD dementia.[244] Further, CSF $A\beta_{1-42}$ was found to more strongly relate to carriage of the apolipoprotein E (*APOE*) ε4 allele, with amyloid PET, by contrast, showing the strongest relationship to CSF tau (p-tau181p and t-tau) levels and cognitive decline. This was interpreted as indicating that CSF $A\beta_{1-42}$ may be more sensitive to early Aβ pathology, with amyloid PET, by contrast, more sensitive to disease progression.[244] Though it has been proposed that fibrillar Aβ may be detectable prior to declines in CSF $A\beta_{1-42}$,[501] isolated amyloid PET positivity may in fact better relate to the use of cut-offs for $A\beta_{1-42}$ that are in fact too low and to false negative results tied to high Aβ production levels.

For tau imaging, a modest positive correlation has been reported between [^{18}F]AV1451 uptake in CU older adults, patients with AD and non-AD neurodegenerative disorders, including PSP and FTD, and CSF tau ($p\text{-}tau_{181p}$ and t-tau).[506-509] Though agreement between biomarkers was generally greater in AD dementia, in comparison to preclinical and prodromal stages, overall concordance rates reached 70%.[508] In a related study examining the diagnostic performance of these markers,[510] CSF tau and [^{18}F]AV1451 uptake exhibited comparable performance in prodromal AD; [^{18}F]AV1451, however, showed superior performance in the dementia stage of AD. These findings, combined with studies showing early plateauing of CSF tau[511-513] and increases in tau PET signal in AD,[285,506,507] suggest that CSF tau may behave as disease state markers, reflecting the intensity of the AD process, with tau imaging, by contrast, best described as a stage marker, reflecting disease progression.[286,514] In the one study that has to date examined tau biomarkers in non-AD subjects, [^{18}F]AV1451 and CSF tau showed similar performance in differentiating non-AD from Aβ-positive AD patients, suggesting that these measures are largely reflective of AD-type PHF tau.[509] In light of recent findings showing that a range of tau fragments exist in CSF, with these characterized by differing kinetics,[515,516] and a stronger relationship between such fragments and tau imaging (e.g. theronine 205 an 207, as compared to 181, with [^{18}F]GTP1 PET)),[517] novel measures may be required in order to achieve optimal concordance with tau imaging. Previous studies addressing the relationship between CSF tau and cross-sectional [^{18}F]FDG PET in AD have shown inconsistent results for both $p\text{-}tau_{181p}$ and t-tau.[518-522]

1.9 RECOMMENDATIONS FOR THE DIAGNOSTIC USE OF CSF AD BIOMARKERS

Recently, international multidisciplinary based recommendations were proposed for the clinical implementation of CSF AD biomarkers ($A\beta_{1-42}$, p-tau_{181p} and t-tau) in the diagnostic evaluation of patients with MCI and dementia.[523,524] According to their interpretation scheme, positive $A\beta_{1-42}$ and tau markers indicate that MCI is likely due to AD. This pattern in dementia patients increases the probability that AD is the underlying cause; as such, AChEIs or memantine (an NMDA glutamate receptor antagonist) and nonpharmacological treatments should be offered. Abnormal $A\beta_{1-42}$ and normal tau should be followed by examining CSF cell count/albumin and cut-offs, sample reanalysis and/or inclusion of other imaging biomarkers. In cases with normal $A\beta_{1-42}$ / abnormal tau, non-AD neurodegenerative disorders should be considered and additional biomarkers, such as $A\beta_{1-40}$ or imaging based measures, added. In patients with normal CSF biomarkers, other medical conditions such as depression should be considered.

Given the high variability commonly seen with CSF biomarker measurements (up to 10%), fairly broad gray (border) zones exist,[525] complicating binary classification; in such cases, sample reanalysis is recommended. Importantly, however, both sets of recommendations emphasized that the current evidence base surrounding the choice of AD biomarkers (CSF or imaging) was conflictual or insufficient, highlighting the need for further studies. Strong support for the use of CSF in conjunction with clinical measures was only reported for the prediction of functional/cognitive decline in MCI, and to rule out AD as the underlying aetiology in patients with mild dementia. Novel fully automated instruments, showing high precision and low variability across lots and laboratories, have however been developed;[526] their use, alongside standardisation efforts, including those addressing preanalytical sample handling procedures, should result in the wider use of $A\beta_{1-42}$ CSF measurements in routine clinical practice; similar progress for CSF tau will be made in the near future. This, combined with the growing use of fluorine-18 amyloid PET (and likely, soon, tau) ligands will generate the data required to refine current recommendations.

1.10 DIAGNOSTIC ASSESSMENT OF COGNITIVE IMPAIRMENT

An important tool in directing the use of evidence-based practice in the diagnosis and management of dementia disorders, clinical practice guidelines have been advanced by guideline development groups, including the European Federation of Neurological Sciences.[527] Intended to optimize patient care, these recommendations are developed by a multidisciplinary panel of experts and are guided by a systematic evidence review.[528]

In Sweden, national guidelines have been developed addressing the clinical handling of patients presenting to health care professionals due to cognitive impairment.[529] According to these, a detailed history of the presenting complaints is taken from the patient and their spouse or close family member; in addition, brief cognitive tests are administered (e.g. the Mini-Mental State Examination (MMSE),[530] and Clock-Drawing Test,[531] assessing global cognition and visuospatial/executive function, respectively). Physical, neurological, and psychiatric examinations are also performed, in addition to blood work, functional assessment (the patient's ability to perform activities of daily living),[532] and structural brain imaging with either CT or MRI. In the event of uncertainty following this first-level assessment, or if the patient is below age 65, a referral for a more expanded work-up is undertaken; this may include detailed testing by a neuropsychologist and/or speech pathologist, CSF sampling, and PET based investigations (glucose metabolism and/or amyloid).

1.11 REVISED RESEARCH DIAGNOSTIC CRITERIA FOR AD

Though widely used in clinical research and therapeutic trials, the original NINCDS-ADRDA criteria have recently been revised in order to incorporate advances made along clinical, biological, and conceptual lines. These revisions, initiated by an International Working Group (IWG-1 and 2)[41-43,533] and the National Institute on Aging and the Alzheimer's Association (NIA-AA),[44,46,259,534] include the recognition of nonamnestic presentations of AD,[535-537] and the incorporation of biomarkers of the underlying disease process; a distinction between clinical expressions of AD pathophysiology was also drawn, with the resulting recognition of preclinical (accrual of AD pathology in the absence of symptoms) and symptomatic pre-dementia (prodromal AD or MCI due to AD) states.

Despite their similarities, these criteria differ somewhat in their overall approach and terminology, as well as in their application of cognitive and biological markers.[538,539] The IWG-1 criteria, for instance, require impairment in episodic memory and at least one biomarker supportive of AD (e.g. temporo-parietal hypometabolism on [^{18}F]FDG PET, CSF showing decreased $A\beta_{1-42}$ and elevated tau, or a positive amyloid PET scan) for a diagnosis of prodromal AD;[42] in contrast, cognitive impairment can be in any cognitive domain in the IWG-2 criteria, supported by either CSF (decreased $A\beta_{1-42}$ and increased tau) or amyloid PET.[43] According to the NIA-AA criteria for MCI due to AD,[44] cognitive impairment need not be memory based, with biomarker abnormalities required for amyloid (decreased CSF $A\beta_{1-42}$ or positive amyloid PET) or neuronal injury (medial temporal atrophy on MRI, increased CSF tau, or [^{18}F]FDG hypometabolism), with the number of abnormal biomarkers (both, one, none) translating into an estimate of the likelihood that the observed MCI syndrome is due to AD.

In a recent multicentre study in patients with MCI, the IWG-1, IWG-2, and NIA-AA criteria were compared with respect to the proportion of subjects fulfilling criteria for prodromal AD/MCI due to AD and the rate of conversion to AD-type dementia.[539] Though performing similarly in a broad sense, findings showed that the proportion of MCI classified as prodromal AD was greater using IWG-1 criteria, while IWG-2 and NIA-AA criteria showed somewhat better performance at predicting progression to AD dementia. Despite comparable accuracy in predicting cognitive decline, this study indicates that one set of criteria may be favoured over another depending on the setting and availability of biomarkers:[539,540] in clinical trials, for instance, where a high rate of conversion is needed, IWG-2 prodromal AD or those fulfilling the NIA-AA high AD likelihood criteria would be best (i.e. any MCI, assuming availability of biomarkers for amyloid and neuronal injury). If only neuronal injury biomarkers are available, the IWG-1 criteria should, by contrast, be considered due its higher specificity tied to the requirement of an amnestic MCI phenotype. In clinical settings, where a more refined prognosis is required, the NIA-AA criteria, with its broad definition of MCI, may provide the most accurate prognosis.

Based on the scientific advances made since the 2011 NIA-AA diagnostic criteria for AD,[44,46,259,534] a biomarker focused research framework was recently proposed to unify and update initial recommendations.[483] This framework incorporates the so-called "A/T/N" system,[484] in which biomarkers can be grouped into those for amyloid-β (A; elevated amyloid PET or low CSF $A\beta_{1-42}$ or $A\beta_{1-42}$/ $A\beta_{1-40}$), abnormal tau (T; elevated tau PET or CSF phosphorylated tau (p-tau)), and neurodegeneration (N; hypometabolism on [^{18}F]FDG PET, atrophy on MRI, or elevated CSF total tau (t-tau)). In defining a given individual's biomarker (A/T/N) profile, either CSF or imaging biomarkers can be used alone or in combination (e.g. CSF $A\beta_{1-42}$ and P-tau for A and T, respectively, and MRI as N). According to this framework, AD is no longer regarded as three clinically distinct entities (preclinical, MCI, AD) but rather as a continuum, with whether or not an individual is in this continuum defined using biomarkers (e.g. AD, A+/T+/N- or A+/T+/N+) (Figure 16). These biomarker profiles can be combined with two different cognitive staging schemes; the first involves traditional syndromic labels and is applicable to all biomarker profiles (i.e. AD and non-AD), while the second six-stage numeric scheme applies only to those in the AD continuum.

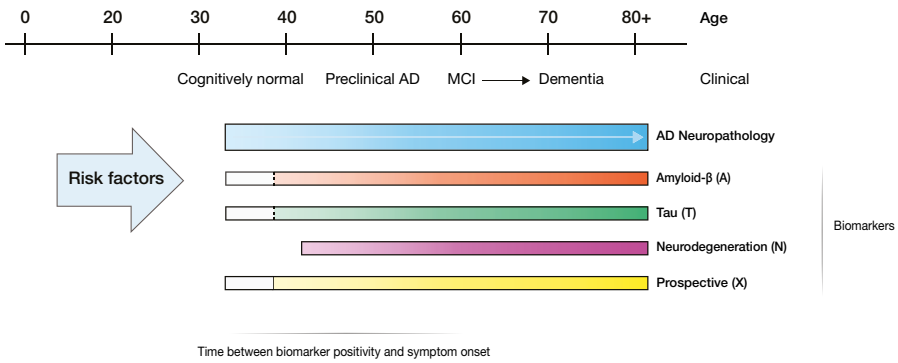

Figure 16. *Hypothetical time course of Alzheimer's disease. AD neuropathological changes are thought to precede symptom onset by some 20-30 years; this process can be detected with current recognized biomarkers. Importantly, the relationship between a given individual's cognitive status and biomarker profile is thought to be influenced by risk factors, including genetic risk alleles, cognitive reserve (the brain's ability to compensate for pathology), and comorbid brain pathologies. The grey zones on the left-ward end of the bars for amyloid and tau are in acknowledgement of the fact that it has yet to be definitively established whether amyloid precedes tau pathology, with medial temporal tau potentially preceding amyloid. The prospective (X) bar is in recognition of the fact with we will likely learn a great deal from new and upcoming biomarkers for targets such as α-synuclein, TDP-43, and the synaptic vesicle protein 2A. Colour scales indicate theoretical changes over time. Adapted with permission from Silverberg N, Elliott C, Ryan L, Masliah E, Hodes R. NIA commentary on the NIA-AA Research Framework: Towards a biological definition of Alzheimer's disease. Alzheimers Dement. 2018;14(4):576-578. Copyright Elsevier, 2018.*

1.12 TIME COURSE OF ALZHEIMER'S DISEASE

On the basis of cross-sectional autopsy and biomarker data, a hypothetical ordering of changes in AD biomarkers and clinical disease phases was proposed in 2010 by Jack and colleagues.[541] In this model, Aβ dyshomeostasis is considered a triggering event, upstream to hyperphosphorylation of tau, neurodegeneration and cognitive impairment. As such, Aβ biomarkers (CSF $A\beta_{1-42}$ and amyloid PET) were considered to become abnormal first, followed by neurodegenerative biomarkers (CSF tau, [^{18}F]FDG PET, and structural MRI). The model incorporated biomarker abnormalities in CU individuals, with cognitive decline (i.e. the onset and progression of symptoms) closely tied to the extent and rate of change in neurodegenerative biomarkers.[362,542,543] Importantly, biomarker trajectories were viewed as following a non-linear temporal course, likely sigmoidal in shape.[544,545]

Widely accepted by the research community, a revised version of the model was proposed in 2013,[546] incorporating slight changes in the ordering and shape of biomarker trajectories, as well as the concept of low and high risk for cognitive impairment due to AD pathophysiology (due genetic profile, cognitive reserve, lifestyle factors and comorbid brain pathologies). This model also acknowledged findings suggesting that in many individuals, a subcortical tauopathy may be the earliest pathophysiological process in AD; Aβ pathology is thought to then emerge later and independently, yet to synergistically accelerate this pre-existing tauopathy, leading to the neocortical spread of tangle pathology.[139,547]

A number of additional models have also been described; similar to the model originally proposed by Jack et al., these too incorporated AD biomarkers on the ordinate and clinical stages on the abscissa.[548-551] Of these, two have incorporated neuroinflammation (astrocytosis and/or microglial activation),[548,550] as well as oligomeric forms of Aβ and disruptions in cholinergic neurotransmission.[548] More recently, curves relating CSF tau to tau PET imaging were derived from subjects with autosomal dominant AD, with changes in the former preceding changes in the latter,[551] similar to the ordering proposed for Aβ biomarkers.[552,553]

2 AIMS

The overarching aim of this thesis was to gain new insight into how different PET and CSF based functional and molecular measures interrelate in AD, and to examine their potential utility from a clinical standpoint. Study specific aims were as follows:

In **paper I,** to compare concordance between [^{11}C]PIB PET and CSF $A\beta_{1\text{-}42}$ in a multicentric cohort, using historical and centrally reanalysed CSF measures; $A\beta_{1\text{-}42}$/ $A\beta_{1\text{-}40}$ was also included to examine its effect on agreement levels with [^{11}C]PIB PET.

In **paper II**, to examine the impact of amyloid imaging with [^{18}F]flutemetamol PET on diagnostic decision making and treatment management in tertiary memory clinic patients with an unclear diagnosis.

In **paper III**, to investigate the association between [^{18}F]THK5317 retention and CSF tau, using assays for both classical and novel fragments, in a cohort of patients with AD (prodromal and dementia).

In **paper IV**, to explore the potential use of [^{18}F]THK5317 perfusion parameters (p-SUVR and R_1) as proxies for metabolic imaging with [^{18}F]FDG PET in patients in the prodromal and dementia stages of AD.

In **paper V**, to determine the reproducibility of [^{18}F]THK5317 perfusion parameters as well as their longitudinal relationship to [^{18}F]FDG and tau pathology in patients from study IV who underwent follow-up investigations.

3 PARTICIPANTS AND METHODS

3.1 PARTICIPANTS

3.1.1 Paper I

The study cohort comprised 243 subjects (230 patients and 13 CU older controls) from seven European memory clinics belonging to BIOMARKAPD (Biomarkers for Alzheimer's and Parkinson's Disease),[554] a research program aiming to optimize and standardise the collection, analysis and interpretation of biomarkers in AD and PD.[524] All had [^{11}C]PIB PET and historical CSF $A\beta_{1\text{-}42}$ data available, as well as aliquots of CSF available for reanalysis. Patients had been referred on the basis of cognitive complaints and assessed clinically according to standard local routines. All diagnoses (AD, n=122; MCI, n=81; FTD, n=20; vascular dementia (VaD), n=7) were made according to standard criteria,[30,45,555,556] using a consensus-based multidisciplinary approach, including neurologists, clinical neuropsychologists, specialist nurses, psychiatrists, and speech-language therapists.[557] CU controls were recruited from among relatives and patient caregivers. Inclusion criteria were: the absence cognitive complaints, independence in activities of daily living, and normal neurological and psychiatric examinations.

3.1.2 Paper II

207 patients were included from the Clinic for Cognitive Disorders, Theme Aging, Karolinska University Hospital, Stockholm, Sweden. Referral sources included primary care physicians as well as other hospital clinics. Following diagnostic workup, including medical and neurological examination, clinical rating batteries for depression and neuropsychiatric symptoms, neuropsychological assessment, structural imaging, and, in a subset, CSF analyses ($A\beta_{1\text{-}42}$, p-tau_{181p}, t-tau; n=152), and [^{18}F]FDG PET (n=76), the clinical picture remained unclear. Diagnoses were made prior to and following [^{18}F]flutemetamol PET, according to standard diagnostic criteria,[3,18,30,45,555,556,558] and followed a multidisciplinary consensus based approach.

3.1.3 Papers III-IV

Twenty patients were recruited from the Clinic for Cognitive Disorders, Theme Aging, Karolinska University Hospital, Stockholm, Sweden. All had completed a comprehensive battery of investigations, including a detailed history taking, physical examination, routine blood work, cognitive and neuropsychological testing, CSF sampling, and structural imaging. Patients diagnosed as prodromal AD

(n = 11) and AD dementia (n = 9) fulfilled classical criteria for MCI and probable AD, respectively, and, in addition, showed *in vivo* evidence of Aβ pathology (abnormal [^{11}C]PIB).

The number of patients per study varied, however. Fourteen patients, evenly divided between prodromal and dementia groups, were included in study III, including ten (6 prodromal, 4 dementia) with follow-up data; in this study, the limiting factor was the availability of CSF for reanalysis. Study III also included nine CU individuals (THK-controls: five young, four elderly: 20-30 and 58-71 years old, respectively), recruited through Clinical Trial Consultants AB (Uppsala University Hospital, Uppsala, Sweden) or from patients' relatives as part of an earlier study;[280] all were free from medication and non-smokers, completed extensive clinical evaluations, and were included in the absence of known neurological/ psychiatric disorders, head injury, or cognitive complaints. A further 15 individuals were included from the Sahlgrenska University Hospital as CSF negative controls; these were patients with minor cognitive complaints, where basic (cell count, albumin ratio, IgG index) and core ($A\beta_{1-42}/A\beta_{1-40}$, p-tau$_{181p}$, and t-tau) CSF biomarkers fell within normal ranges. In contrast to study IV (n=20), study V included only 16 patients (10 prodromal, six dementia) due this being the number for which longitudinal [^{18}F]FDG and [^{18}F]THK5317 had been performed. One patient with CBS, recruited as part of the initial study describing our findings with [^{18}F]THK5317,[280] was also included in the test-retest component of study V.

3.2 COMPLIANCE WITH ETHICAL AND REGULATORY STANDARDS

Prior to participation in the above described studies, all participants and their caregivers provided written informed consent prior. These were performed in accordance with the Declaration of Helsinki and subsequent revisions. All studies were approved by the Regional Ethical Review Board in Stockholm, Sweden, and the Radiation Safety committees at the Karolinska University Hospital, Stockholm, Sweden and the Uppsala University Hospital, Uppsala, Sweden. Ethical approval had been obtained from local ethics committees in the case of study I. The CSF samples from CSF-controls included in study III were de-identified left-over aliquots from clinical routine analyses, following a procedure approved by the Ethics Committee at University of Gothenburg (EPN 140811).

3.3 IMAGING DATA ACQUISITION AND PROCESSING

3.3.1 Paper I

In this study, [^{11}C]PIB PET data was pooled from seven European research centres, where scanning platforms and protocols differed: 0-60 min (Coimbra and Lisbon, Portugal; Karolinska, Sweden, using Philips PET/CT Gemini GXL and Siemens EXACT HR + scanners, respectively); 40-60 min (Ulm, Germany; Siemens Biograph mCT Flow); 40-70 min (Copenhagen, Denmark; GE PET/CT Lightspeed, Siemens Biograph PET/CT, Siemens PET/MRI, and Siemens ECAT HRRT); 50-70 min (Barcelona, Spain; Siemens EXACT HR +); and 60-90 min (Turku, Finland; GE Advance PET scanner).

Dynamic [^{11}C]PIB studies were first corrected for subject motion using a rigid realignment procedure between frames (VOIager, version 4.0.7, GE Healthcare Ltd., Uppsala, Sweden).[559] Summation images (40-60, 40-70, 50-70, and 60-90 min) were then created in VOIager, and images spatially normalised to a population based [^{11}C]PIB template,[560] using the Normalise function in Statistical Parametric Mapping, version 8 (SPM8). Partial volume correction was not performed due to the inclusion of visual ratings previously performed on non-partial volume corrected summation images and between centre differences in scanner resolution.

3.3.2 Paper II

PET investigations were performed at the department of Medical Radiation Physics and Nuclear Medicine Imaging, Karolinska University Hospital, Stockholm, Sweden, using a Siemens/CTI Biograph mCT PET/CT. For [^{18}F]flutemetamol, the acquisition protocol consisted of a 20 min scan (list-mode), 90 min post injection of 185 MBq. Static 15-min [^{18}F]FDG studies were performed 30-min after an intravenous bolus injection of 3 MBq/kg. All appropriate corrections, including time-of-flight (TOF), were applied, with a low dose CT scan used for attenuation correction. Reconstruction was done with ordered subset expectation maximisation (OSEM; 5 iterations, 21 subsets, 2.0 mm Gaussian filter), yielding an effective resolution of 3 mm. Structural T1-weighted MRI was performed at various radiology departments in Stockholm and neighbouring counties, using different platforms and protocols.

Dynamic late-phase (90-110 min) [^{18}F]flutemetamol data was processed using a fully automated software under commercial development (Hermes Medical Solutions, Stockholm).[561] A PET driven approach, images were first realigned, summed over the 90-110 min interval, and spatially normalised into Montreal Neurology Institute (MNI)-152 stereotaxic space. Similar to study I, partial volume correction was not performed due the inclusion of visual ratings performed on uncorrected summation images.

3.3.3 Papers III-IV

Patients in studies III-V underwent amyloid ([^{11}C]PIB), tau ([^{18}F]THK5317), and metabolic ([^{18}F]FDG) PET imaging within a short time period (median (days), inter-quartile range (IQR): [^{11}C]PIB to [^{18}F]THK5317: 0 [0, 7]; [^{18}F]FDG to [^{18}F]THK5317: 58 [40, 80]); 16 patients (10 prodromal AD and six AD dementia), underwent follow-up [^{18}F]THK5317 and [^{18}F]FDG PET investigations after a median period of 17 months IQR: 15, 18] (studies III-IV). Dynamic (0-60 min) [^{18}F]THK5317 and [^{11}C]PIB scans were acquired on an Siemens/CTI ECAT EXACT HR+ scanner (n=16) or a GE Discovery ST PET/CT scanner (n=4) at the Uppsala PET Centre. Static (30-45 min) [^{18}F]FDG PET studies were performed on a Siemens Biograph mCT PET/CT scanner at the department of Medical Radiation Physics and Nuclear Medicine Imaging, Karolinska University Hospital, Stockholm, Sweden. Test-retest [^{18}F]THK5317 data was collected in a subset of five patients (four prodromal AD, one CBS), within 22 days [IQR: 13, 27].

Structural (T1-weighted) MR scans were available for all subjects (10 performed same day as [^{18}F]THK5317, eight before, two after), and were used for anatomical co-registration and ROI definition; the median interval between MRI and [^{18}F] THK5317 PET was 32 days [IQR: 0, 509]. MR scans were performed on three different platforms, at three different sites: Karolinska University Hospital, Stockholm (Siemens Magneton Symphony 1.5T, n=9); Uppsala PET Centre (Siemens Magneton Trio 3T, n=8); and Aleris Röntgen Sabbatsberg, Stockholm (Philips Diamond Select Achieva 1.5T, n=3). For controls, structural MRI data was also collected (eight at Uppsala PET Centre, one with an earlier acquisition at Aleris Röntgen Sabbatsberg,) in addition to [^{18}F]THK5317 PET (ECAT EXACT HR+, n=6; GE Discovery ST PET/CT, n=3); elderly controls also performed [^{11}C] PIB PET studies to rule out Aβ pathology.

Individual dynamic ([^{18}F]THK5317 and [^{11}C]PIB) and static ([^{18}F]FDG) PET scans were co-registered to their respective T1-MR images using PMOD (v.3.5; PMOD Technologies Ltd., Zurich, Switzerland). Structural images were segmented into tissue classes (GM, WM and CSF) using SPM8, with the inverse transformation matrix used to spatially warp a probabilistic atlas[214] from into native T1 image space. GM masks generated during the segmentation step were then applied to the atlas subject-wise, yielding individual GM VOIs.

In study III, [^{18}F]THK5317 data was first partial volume corrected in PMOD, using the Müller-Gärtner method.[219] Here, the focus on how CSF biomarkers related to [^{18}F]TH5317 DVR within regions of interest motivated the application of a correction method (Müller-Gärtner),[219] given the known effects of partial volume, particularly in medial temporal regions.[280] In studies IV and V, where [^{18}F]TH5317 was also used, correction for partial volume effects was not applied due the focus on perfusion information and, in the case of study V, the fact that the Müller-Gärtner correction induces spatial distortions when applied at the voxel level.[563,564]

3.4 PET QUANTIFICATION

3.4.1 Paper I

Spatially normalised [^{11}C]PIB summation images were multiplied by a set of anatomically defined GM VOIs, previously derived from the multiplication of a standard digital atlas[216] with an averaged eroded gray matter mask.[560] SUVR images were then created over the various time windows, using the cerebellar cortex as reference tissue, and resulting parametric maps sampled to obtain VOI uptake values. In order to obtain a global measure of Aβ burden, a composite neocortical [^{11}C]PIB value was calculated as the voxel-weighted average SUVR across frontal, parietal, temporal, occipital, and cingulate cortices. An abnormal [^{11}C]PIB scan was then defined as a composite SUVR above 1.41 (upper 95% confidence limit in CU age-matched controls).[560]

Due to the variability in scanning windows between centres and the known impact of this on SUVR,[212] composite neocortical SUVR values were standardised to a 100-point scale using a linear scaling procedure.[565] The units of this scale are termed "Centiloids", with 0 representing the average [^{11}C]PIB uptake in Aβ negative subjects and 100, the average in mild-to-moderate AD when scanned 50- to 70-min. As per the outlined process, we first validated our pipeline using a publically available data set ([^{11}C]PIB and matching T1 MR images from 34 Aβ-negative young controls and 45 Aβ-positive AD patients) (Figure 17). Then, using average SUVR values from a subset of this data set with imaging up to 90-min, specific parameters for the provided conversion equations were estimated, and composite neocortical [^{11}C]PIB values for all subjects, as well as the cut-off of 1.41, were converted to Centiloid values (Figure 17).

3.4.2 Paper II

[^{18}F]Flutemetamol SUVR was calculated using an isocortical composite region, comprising brain areas known to typically display a high burden of Aβ, including the frontal, lateral temporal, cingulate, and parietal cortices. The pons was used as the reference region.

3.4.3 Paper III

Reference Logan DVR and SUVR were calculated voxel-wise using partial volume corrected [^{18}F]THK5317 (30-60 min, cerebellar cortex) and [^{18}F]FDG (30-45 min, pons) scans, respectively. In addition to the GM VOIs used in studies IV and V, two composite regions based on Braak stages for tau pathology were included:[63] limbic (stage III/IV), comprising the hippocampus, amygdala, parahippocampus and fusiform gyri, anterior and middle/inferior temporal cortex, orbital and straight gyri, cuneus and temporo-parietal carrefour; and isocortical (stages V/VI), comprising all cortical regions save the pre- and postcentral gyri.[280]

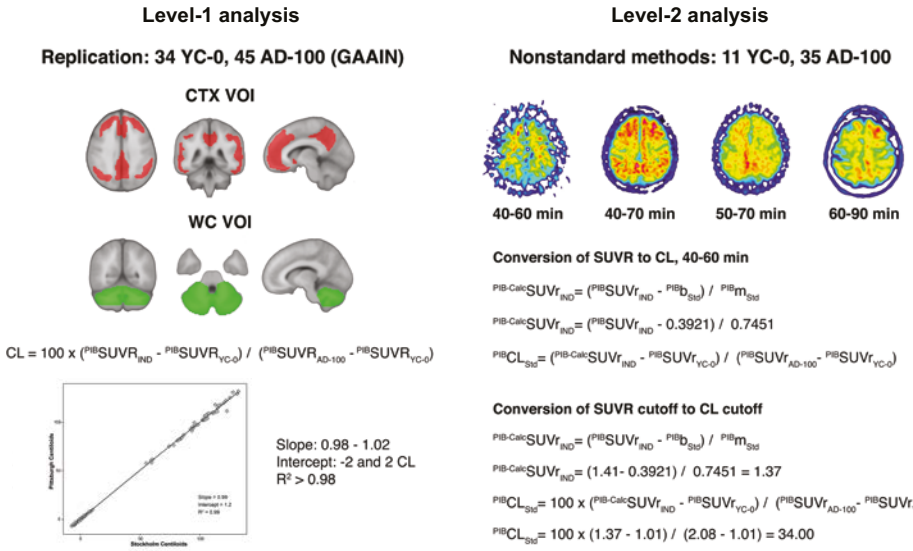

Figure 17. *Overview of the conversion of [^{11}C]PIB data to the Centiloid scale. Conversion of [^{11}C]PIB SUVR findings to Centiloid (CL) units was carried out in a two-step process. First, a level-1 analysis was performed in order to set the "typical" 0- and 100-anchor points for all future scaling operations. These correspond to average uptake levels in relatively young amyloid negative subjects (YC-0) and typical AD patients (AD-100), respectively. To do this, [^{11}C]PIB data was downloaded from the Global Alzheimer's Association Information Network (GAAIN) website and processed (SUVR) using a cortical composite (CTX) meta-region and the whole cerebellum (WC) as reference region. After validation of our pipeline via comparison of calculated (CL equation) and reference CL values (linear regression; scatterplot), the level-2 analysis (required when an approach other than 50- to 70-min SUVR using CTX and WC VOIs is used) was performed owing to varied scanning windows across centres. Conversion of SUVR data (example shown for 40-60 min) and our cut-off was then performed using provided equations. Klunk WE, Koeppe RA, Price JC, et al. The Centiloid Project: standardizing quantitative amyloid plaque estimation by PET. Alzheimers Dement. 2015;11(1):1-15 e11-14.*

3.4.4 Papers IV-V

Parametric p-SUVR and SRTM R_1 ([^{18}F]THK5317 and [^{11}C]PIB), reference Logan DVR ([^{18}F]THK5317, 30-60 min) and SUVR ([^{18}F]FDG, 30-45 min) maps were created in PMOD, using the cerebellar cortex as reference region. In contrast to study III, where the pons was used as reference region for [^{18}F]FDG SUVR, the cerebellum was chosen in studies IV and V in order to ensure a common reference region across parameters. Selection of time intervals for p-SUVR were based on correlation analyses with R_1 and [^{18}F]FDG SUVR.[566] In order to obtain VOI based values, parametric images were sampled using individual GM atlases; in study V, however, R_1 values were obtained via kinetic modelling (SRTM) of regional time-

activity curves. Examined VOIs were largely identical to those used in study IV: frontal, parietal, temporal (medial and lateral), occipital, and posterior cingulate cortices, with a neocortical meta-VOI encompassing all regions save the medial temporal lobe.

3.5 CSF SAMPLING AND ANALYSES

CSF analyses were included in studies I, II, and III. CSF had been collected via LP (~ 10 mL) and stored in polypropylene tubes. After discarding the first 0.5 mL, samples were centrifuged and stored at -80 °C in 1mL aliquots. All CSF samples were analysed at the Clinical Neurochemistry Laboratory at the Sahlgrenska University Hospital, Mölndal, Sweden; historical values from study I were determined locally.

3.5.1 Enzyme linked immunosorbent assays

In studies I, II, and III, commercial INNOTEST ELISAs from Fujirebio (Ghent, Belgium) were used for $A\beta_{1\text{-}42}$,[419] p-tau_{181p}[462] and t-tau,[465] using the following monoclonal capture/detection antibodies: 21F12/3D6, HT7/AT270, AT120/HT7 and BT2, respectively.[567] All analyses were performed according to kit inserts. In study III, two additional in-house ELISAs (University of Gothenburg) were used: 1) for neurogranin, using NG22 (mouse monoclonal in-house antibody) and biotinylated NG2 (mouse monoclonal in-house antibody) as coating and primary antibodies, respectively, with enhanced streptavidin-HRP complex (Kem En Tech #4740N) for detection and recombinant neurogranin full-length protein-GST as calibrator; 2) for tau N-Mid, using Tau12 (Nordic Biosite, binding region aa9-18) and a combination of biotinylated HT7 (Thermo Scientific, aa159-163) and BT2 (Thermo Scientific, aa194-198) as coating and primary antibodies, respectively, with an enhanced streptavidin-HRP complex for detection and full-length recombinant Tau 441 2N4R (rPeptide) as calibrator.

3.5.2 Electrochemiluminescence assay

The MSD (Gaithersburg, Maryland, USA) triplex assay was used in studies I and III, providing levels of $A\beta_{1\text{-}42}$, $A\beta_{1\text{-}40}$, and $A\beta_{1\text{-}38}$ (V-PLEX, Aβ Peptide Panel 1 (6E10) Kit).[568] This assay uses capture antibodies specific to each Aβ peptide, with the n-terminal, anti-Aβ (1-16) antibody (6E10 clone) as the detection antibody.

3.5.3 Mass spectrometry assay

LC-MS/MS was used in study I ($A\beta_{1\text{-}42}$, $A\beta_{1\text{-}40}$, and $A\beta_{1\text{-}38}$). For calibration and sample preparation, native (unlabelled) and ^{15}N uniformly labelled $A\beta_{1\text{-}40}$ and $A\beta_{1\text{-}42}$ and ^{13}C uniformly labelled $A\beta_{1\text{-}42}$ (rPeptide) were prepared as described elsewhere, aliquoted, and stored at -80 °C. Preparation of artificial CSF and calibration samples

for $A\beta_{1-42}$ were prepared according to previously established methods.[429,569] For $A\beta_{1-40}$, artificial CSF was spiked to a final concentration of 1.5, 5, 10, 20, 30 and 40 ng/mL native $A\beta_{1-40,}$ with a constant concentration of ^{15}N-$A\beta_{1-40}$ at 1600 pg/ml used as internal standard. Unknown samples (180 µL) were spiked with 20 µL internal standard to a final concentration of 1600 pg/mL, ^{13}C-$A\beta_{1-42}$ and ^{15}N-$A\beta_{1-40}$. SPE and LC, as well as the processing and analysis of MS data, were performed as described elsewhere.[429]

3.5.4 Single molecule array assay

Tau-368 was measured through a Simoa HD-1 analyzer (Simoa, Quanterix, Lexington, MA, USA) using magnetic beads conjugated with capture antibody anti-Tau368,[570] using the conjugation protocol provided by the manufacturer. As detection antibody, biotin-labeled KJ9A (Sigma) was used, with series diluted tau 1-368 recombinant protein[570] used as calibrator.

3.6 DETERMINATION OF BIOMARKER CUT-OFFS

In the present thesis, cut-offs were used in studies I, II, and III. In study I, the cut-off for [^{11}C]PIB Centiloids (34) was based on the upper 95% confidence interval of a group of CU elderly controls (global SUVR > 1.41).[560] For historical CSF $A\beta_{1-42}$ derived from the INNOTEST assay , a pre-existing cut-point was selected based on the Youden index (sum of sensitivity and specificity – 1)[571] that best predicted amyloid PET positivity.[503] Mixture modelling, whereby an expectation maximization algorithm is used to cluster individuals according to their probability of belonging to a given group (here, normal and abnormal CSF $A\beta_{1-42}$ or $A\beta_{1-42}$/$A\beta_{1-40}$),[572] was used to generate cutpoints for the additional MSD and MS-RMP measurements (Figure 18). In study III, cut-offs for regional [^{18}F]THK5317 were determined using the mean plus two standard deviations of the DVR values among controls; in study II, the cut-off for isocortical composite [^{18}F]flutemetamol SUVR had been previously established in a subset of subjects from a phase II study[573] using the value that provided the best discrimination between AD and controls. Similar approaches were used for CSF INNOTEST measures ($A\beta_{1-42}$, p-tau_{181p} and t-tau) in studies II and III, and for tau N-Mid and tau-368/t-tau in study III.

3.7 STATISTICAL ANALYSES

Between group comparisons were performed using Kruskal-Wallis ANOVA for continuous variables; Mann Whitney U-tests were performed *post-hoc* where appropriate. Chi-square or Fisher's exact test were used for categorical variables. Analysis of imaging data was performed at both the ROI and voxel-based level, as discussed below. Significance for group level comparisons was generally set as

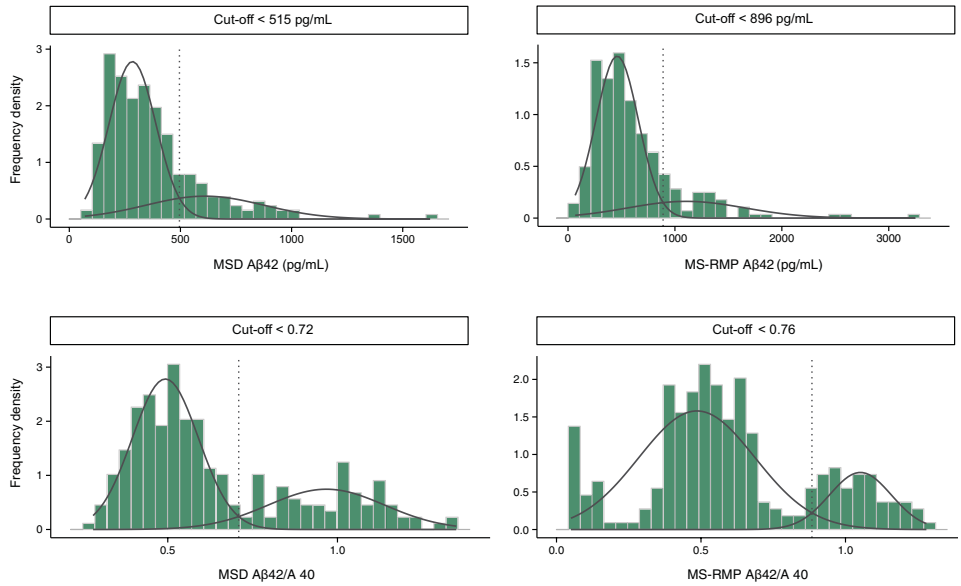

Figure 18. *Mixture modelling derived frequency density plots of MSD and MS-RMP based CSF Aβ42 and Aβ42/Aβ40 measurements from BIOMARKAPD. The dashed lines represent the cut-offs for CSF Aβ positivity.*

$p < 0.05$ (two-sided, uncorrected); in studies I and IV, however, false discovery rate (FDR) and Bonferroni corrected (correlations) p-values were reported, respectively. Statistical analyses were performed using different versions of the software R (R Foundation for Statistical Computing, Vienna Austria, http://www.R-project.org/).

3.7.1 Region of interest-based analyses

To investigate the relationship between PET and CSF based measures, linear and nonparametric rank-based estimation multilinear regression models were used; in the latter models, 2-way interactions were assessed using simple slopes analyses. Longitudinal change in PET, as well as longitudinal associations between pairs of regional PET measures, were assessed using linear mixed models. Associations between PET measures were also investigated using bivariate and partial Pearson correlation analyses. Differences between bivariate correlations using Williams' modification of Hotelling's t-test. The ability of different PET measures to discriminate between patient groups was assessed using receiver operating characteristic (ROC) analyses. Agreement between visual assessment as well as between visual read and semi-quantitative values was achieved using percentage agreement and Fleiss' kappa, with diagnostic and treatment change assessed using 1-sample proportions test.

3.7.2 Voxel-based analyses

Correlation analyses between PET measures were performed using Biological Parametric Mapping (v. 3.3), an SPM based toolbox. Annual percentage change images were created subject-wise as follows: [(Follow-up - Baseline)/ Baseline]/ Time interval between scans (years) x 100%; after averaging individual images, binarisation (masking) was performed using the isocortical composite repeatability (test-retest) of [^{18}F]THK5317 perfusion parameters. All voxel-based analyses were performed in MATLAB 2015a (The MathWorks, Inc., Natick, Massachusetts, USA).

4 RESULTS AND REFLECTIONS

4.1 MAIN FINDINGS

4.1.1 Paper I – PET and CSF based amyloid biomarkers

4.1.1.1 Concordance between [^{11}C]PIB and CSF $A\beta_{1-42}$

Using the combined sample, agreement between dichotomized [^{11}C]PIB (Centiloid) and CSF $A\beta_{1-42}$ was 73% (INNOTEST), 77% (MSD) and 76% (MS-RMP) (Figure 19). These figures were lower than reported concordance rates, which averaged 88% [505] across 10 studies;[234,499-502,518,574-577] this was likely due to differences in study design and sample composition. In contrast to these studies, which were either single centre[234,499,500,574,575,577] or based on data from highly selected convenience samples,[501,502,518,576,578] ours was a multicentre study drawn from several tertiary memory clinics showing variable concordance figures (range, 55% to 97%). The centres with the lowest concordance (i.e. 55% and 67%) were those which had most of the non-AD patients, the group showing the most disagreement between amyloid biomarkers. When excluding these centres, overall concordance was 87%. The low concordance we observed within this group in comparison to the high agreement reported in one of these studies[577] can likely be traced to differences in the non-AD subtypes included and the finding that CSF $A\beta_{1-42}$ levels can vary markedly in these disorders.[580]

One of the aims of this study was to see whether concordance would be improved by reanalysing CSF batch-wise in one laboratory; this was based on findings showing that ELISA derived CSF $A\beta_{1-42}$ measurements are sensitive to a number of factors, including how the samples are handled and stored, choice of calibrator peptide, and kit lot.[417] Though the overall concordance rates using reanalysed data were not substantially higher than that achieved using historical $A\beta_{1-42}$ (Figure 20), this was again driven by continued low-concordance in the non-AD group, and, to some degree, by an increase in discordance among CU subjects. Only in the AD group was concordance consistently higher using reanalysed data. Though the shift, among AD and a subset of CU cases, from largely borderline positive findings to clearly lowered values may reflect, for example, the removal of variability tied to differing kit lots, the use of different assays complicates direct comparison.[418] All groups, however, showed improved concordance when using $A\beta_{1-42}/A\beta_{1-40}$ (Figure 20); this effect was greatest among FTD and VaD patients. This result suggested that, in addition to adjusting for interindividual differences in Aβ production, $A\beta_{1-42}$ in ratio with $A\beta_{1-40}$ might also help differentiate true amyloid positive case (an isolated drop in $A\beta_{1-42}$, specific to AD) from conditions characterized by a general decrease in Aβ isoforms.[581,582]

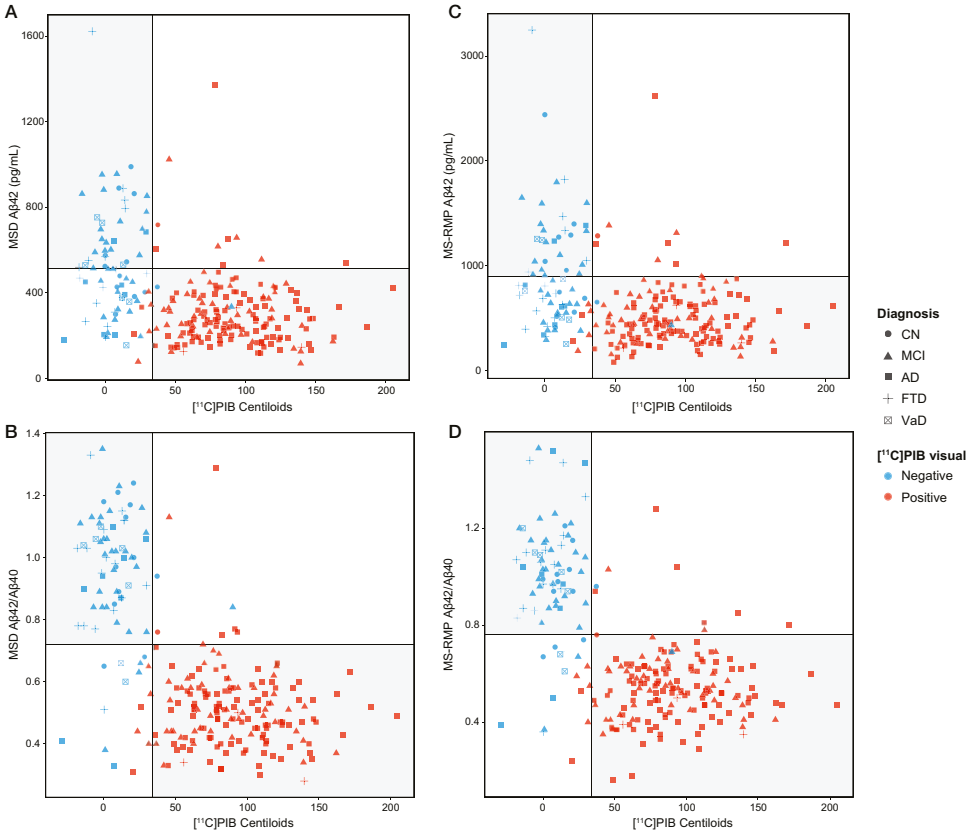

Figure 19. *Scatterplots reflecting concordance between [^{11}C]PIB Centiloids and CSF Aβ. (A) MSD Aβ42 (cut-off < 515 pg/mL). (B) MSD Aβ42/40 (cut-off < 0.72); (C) MS-RMP Aβ42 (cut-off < 896 pg/mL), and (D) MS-RMP Aβ42/40 (cut-off < 0.76). Grey circles indicate cognitively normal healthy control (CN) subjects, triangles indicate mild cognitive impairment (MCI), squares Alzheimer's disease (AD), crosses frontotemporal dementia (FTD), and crossed squares vascular dementia (VaD) patients. The vertical lines reflect the Centiloid cut-off of 34; the horizontal lines the cut-offs of 515 pg/mL, 0.72, 896 pg/mL, and 0.76 for MSD (Aβ42, Aβ42/40) and MS-RMP (Aβ42, Aβ42/40), respectively. Blue indicates [^{11}C]PIB scans visually rated as negative, red as positive. The grey quadrants indicate concordance between amyloid biomarkers (top left, concordant negative: [^{11}C] PIB-/ CSF Aβ-; bottom right, concordant positive: [^{11}C]PIB+/ CSF Aβ+). The white quadrants indicate discordance between amyloid biomarkers (bottom left, discordant with isolated CSF positivity: [^{11}C]PIB-/ CSF Aβ+; top right, discordant with isolated [^{11}C]PIB positivity: [^{11}C]PIB+/ CSF Aβ-). Adapted from Leuzy A, Chiotis K, Hasselbalch SG, et al. Pittsburgh compound B imaging and cerebrospinal fluid amyloid-beta in a multicentre European memory clinic study. Brain. 2016;139(Pt 9):2540-2553.*

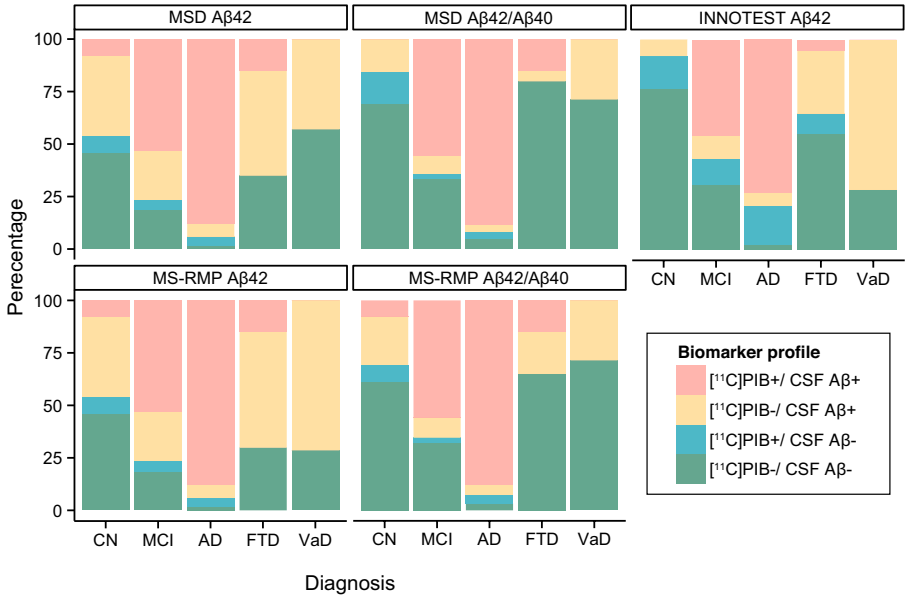

Figure 20. *Frequency plots showing different agreement profiles between [^{11}C]PIB PET and CSF Aβ. Cut-offs of < 557 pg/mL (INNOTEST Aβ42), < 515 pg/mL (MSD Aβ42), < 0.72 (MSD Aβ42/40), < 896 pg/mL (MS-RMP Aβ42), < 0.76 (MS-RMP Aβ42/40), and global ([^{11}C]PIB Centiloid value > 34 were used to classify subjects as concordant positive ([^{11}C]PIB+ /CSF Aβ+), concordant negative ([^{11}C]PIB-/CSF Aβ-), discordant with CSF positivity ([^{11}C]PIB-/CSF Aβ+), and discordant with [^{11}C]PIB positivity ([^{11}C] PIB+/CSF Aβ-). Adapted from Leuzy A, Chiotis K, Hasselbalch SG, et al. Pittsburgh compound B imaging and cerebrospinal fluid amyloid-beta in a multicentre European memory clinic study. Brain. 2016;139(Pt 9):2540-2553.*

4.1.1.2 Agreement between visual and Centiloid-based [^{11}C]PIB classification

Overall, agreement between visual assessment and Centiloid based classification was seen in 235 of 243 [^{11}C]PIB scans (97%) (Figure 19). Among the eight instances of disagreement, two were classified as visually negative/Centiloid positive (one CU and one MCI), and six as visually positive/Centiloid negative (four MCI, two AD). Interpretation of the visually negative/Centiloid positive cases was complicated by poor image quality and high spill over from WM; all classified as visually positive/Centiloid negative showed borderline Centiloid values. Taking visual ratings as the standard of truth, however, these findings showed that the Centiloid method could be successfully implemented in precisely the type of context it was developed for.[565]

4.1.1.3 Cut-off selection for Centiloid and CSF based classification

As described in section 3.7, the Centiloid cut-point (34) used was based on a global SUVR of 1.41, previously established in CU individuals using our image processing pipeline;[560] by comparison, other available cut-offs for Centiloid (27.48 and 19) were derived from SUVR values of 1.40 and 1.42, respectively, generated using post-mortem data (27.48) and a method whereby the selected threshold was based on that which reliably predicted an increased rate of change in [^{11}C]PIB SUVR (19).[583] Back calculation of these CL cut-offs to SUVR using our processing pipeline gave values of 1.38 (27.48) and 1.21 (19), illustrating the impact differing methods can have on SUVR estimation, and the attendant importance of standardisation in settings involving the use of varied acquisition and processing protocols.

The use of different cut-offs also raises an important point pertaining to the selection of appropriate thresholds for the detection of biologically meaningful signal using amyloid PET.[584-586] Though measurements of between 1.40 and 1.50 SUVR are routinely used to define amyloid status, these thresholds may be too high, misclassifying subjects with substantial plaque pathology as amyloid negative.[584] In our material, isolated abnormal CSF $A\beta_{1\text{-}42}$ was the more common discordance profile; while low $A\beta_{1\text{-}42}$ can be seen in the absence of amyloid plaques,[450] amyloid can also be seen as a co-pathology in non-AD disorders.[587] This raises the possibility that the applied cut-off for [^{11}C]PIB was too conservative, which may have resulted in the misclassification of at least a subset of these discordant cases. Lastly, our use of Gaussian mixture modelling to establish cut-points for CSF measures assumed that $A\beta_{1\text{-}42}$ and $A\beta_{1\text{-}42/}$ $A\beta_{1\text{-}40}$ data were composed of two different normal distributions.[502,572] Although this assumption was valid in our cohort, these cut-points may not generalize to population-based samples, where unimodal frequency distributions have been reported for amyloid biomarkers.[583]

4.1.2 Paper II – Clinical impact of [^{18}F]flutemetamol PET in a memory clinic setting

4.1.2.1 Structural imaging, [^{18}F]FDG and CSF based investigations

Most of the patients were relatively young (mean age < 65 years), with the majority showing a diagnosis of MCI (n=131, 63%), followed by AD (n=41, 20%), dementia not otherwise specified (dementia NOS) (n=20, 10%), non-AD (n=10, 5%) and SCD (n=5, 2%). With respect to rating of the temporal lobe, no atrophy or only minimal widening of the choroid fissure was predominant across MCI, AD, dementia NOS and SCD; mild atrophy, however, was noted in nearly half of those in the non-AD group. In terms of global atrophy and WM changes, most patients showed scores consistent with mild changes. Of the 76 patients who underwent [^{18}F]FDG PET, patterns suggestive of, but not typical for, AD were the most common finding

in MCI and AD (39% and 56% respectively), with findings in dementia NOS nearly evenly divided between atypical for AD and non-AD. In the non-AD group, half of patients showed a metabolic pattern suggestive of a non-AD disorder; the other half, along with SCD patients, showed only nonspecific changes.

CSF sampling was not performed in a little over a quarter of patients (n=55, 27%) due to use of anticoagulants (n=18, 33%), spinal stenosis or related problems (n=6, 10%), LP refusal (n=12, 22%), and technical problems (n=19, 35%). Of the 154 subjects from whom CSF was successfully sampled, 24% showed only abnormal CSF $A\beta_{1\text{-}42}$, 23% only abnormal tau (p-tau_{181p} or t-tau), 21% abnormal $A\beta_{1\text{-}42}$ in combination with abnormal tau, and 32% showed a negative CSF profile ($A\beta_{1\text{-}42}$ and tau above and below cut-offs, respectively). Overall agreement between CSF biomarkers and [^{18}F]flutemetamol PET was 66% for $A\beta_{1\text{-}42}$, 66%, 76% for p-tau_{181p}, 76% and 77% for t-tau; across all three measures, isolated PET positivity was the more the more common discordance profile. Preanalytical (e.g. specimen shipment/storage) and assay related factors may have impacted CSF findings, and, consequently, concordance with [^{18}F]flutemetamol. Additional possibilities include the young age of our cohort (average age 64 years, with 58% fulfilling criteria for an early onset dementia disorder, i.e. onset < 65 years), which may have been associated with not yet fully distinguished biomarker profiles,[580] and heterogeneity in the underlying neuropathology and associated differences in amyloid metabolism and neurodegenerative mechanisms.[588] Though disagreement between Aβ biomarkers may relate to the cut-point used for CSF, application of a more lenient value (647 pg/mL) derived using the same INNOTEST assay provided the same overall level of concordance.

4.1.2.2 Referral for [^{18}F]flutemetamol PET

As noted above, 55 patients were referred for [^{18}F]flutemetamol PET as CSF biomarker data was not available. Among those with CSF findings available, the main reason for [^{18}F]flutemetamol PET in our cohort was a negative or unclear (isolated $A\beta_{1\text{-}42}$ or tau) CSF profile in the context of suspected AD based on clinical, neuropsychological and imaging (CT/MRI, [^{18}F]FDG PET) findings (117 of 152 patients with CSF; 77%). A clinically unclear picture in combination with suspected AD and a supportive CSF profile (low $A\beta_{1\text{-}42}$ and one or both tau markers positive), was the second most common reason (35 of 152 patients, 23%).

4.1.2.3 Change in diagnosis and patient management following [^{18}F]flutemetamol PET

Following visual evaluation of [^{18}F]flutemetamol scans, amyloid positivity was found in 69/131 (53%) of patients with MCI as their initial diagnosis, 28/41 AD (68%), 2/10 non-AD (20%), 4/20 dementia NOS (20%) and 3/5 SCD (60%). Representative [^{18}F]flutemetamol summation images are shown in Figure 21.

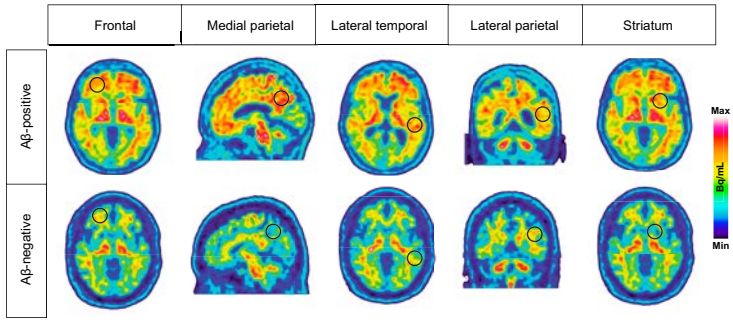

Figure 21. *Representative [^{18}F]flutemetamol PET summation images in two patients initially diagnosed as MCI. The first patient (top row) had a positive scan, the second patient (bottom row), a negative scan. Both showed inconclusive CSF, MRI and [^{18}F] FDG biomarker findings; the first patient received a post-[^{18}F]flutemetamol diagnosis of prodromal AD; the second patient, FTD. Scan classification is based on the identification of high cortical uptake in several brain regions (black circles), as outlined in the electronic training programme designed by the manufacturer of [^{18}F]flutemetamol, GE Healthcare, Buckley CJ, Sherwin PF, Smith AP, Wolber J, Weick SM, Brooks DJ. Validation of an electronic image reader training programme for interpretation of [^{18}F] flutemetamol beta-amyloid PET brain images. Nucl Med Commun. 2017;38(3):234-241.*

Amyloid status in the diagnostic groups before and after [^{18}F]flutemetamol investigations, as well as changes in diagnosis, are summarised in Figure 22. As shown in this figure, a majority of patients with a final diagnosis of MCI after [^{18}F]flutemetamol PET were amyloid negative. The vast majority of patients in the pre-[^{18}F] flutemetamol PET MCI group who were amyloid positive received a diagnosis of prodromal AD or AD (54 of 60, 90 %). In the pre-[^{18}F]flutemetamol PET AD group, the diagnosis of AD was dismissed in 5 amyloid negative cases. Finally, all patients in the pre-[^{18}F]flutemetamol dementia NOS group, and almost all in patients in the non-AD group, were amyloid negative. Overall, [^{18}F]flutemetamol PET led to a significant change in diagnosis (n=92, 44%; $p < 0.05$). Among MCI, dementia NOS, AD, and non-AD, the highest percentage change in diagnosis was observed in the MCI group (n=67, 5 %), as well as in dementia NOS (n=12 %), while a smaller percent change was seen in non-AD and AD patients (n=3, 30% and n=8, 20%, respectively). In the SCD group, which only consisted of five patients (3 amyloid positive and 2 negative), initial diagnoses were changed in three patients (MCI, prodromal AD, and AD).

The outcome of [^{18}F]flutemetamol PET resulted not only in changes to initial diagnoses but also in an increase in the use of AChEIs ($p < 0.001$). Among patients with a pre-[^{18}F]flutemetamol diagnosis of MCI, AChEI use increased from nine to 62 patients, and in AD, from 22 to 38. Among dementia NOS, non-AD and SCD patients, AChEIs were initiated in only a handful of patients who had a positive

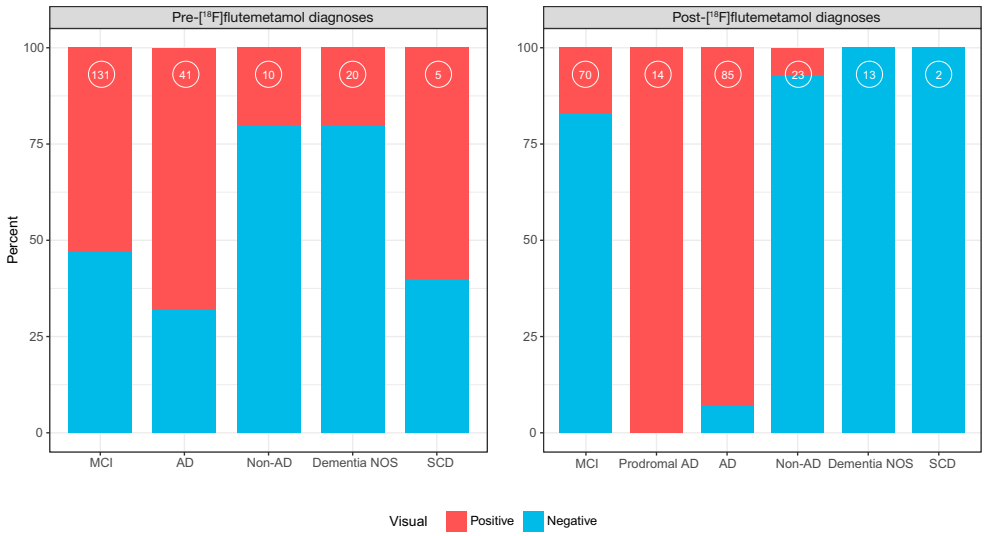

Figure 22. *Diagnostic groups along with visual ratings for [^{18}F]flutemetamol scans before and after [^{18}F]flutemetamol PET. Stacked bar charts showing diagnoses before (A) and after (B) [^{18}F]flutemetamol investigations; the number of patients per group are indicated at the top of each bar. Red and blue indicate visual ratings of positive and negative, respectively.*

[^{18}F]flutemetamol scan. Among those in whom treatment was initiated following [^{18}F]flutemetamol (n=75), most had a positive scan (n=69) and a final diagnosis of AD (n=67; additional diagnoses included three MCI and one DLB; the six [^{18}F] flutemetamol negative cases included two patients with a post-scan diagnosis of AD, two of MCI, one FTD and one DLB). Among the 34 on AChEIs prior to [^{18}F]flutemetamol, most were [^{18}F]flutemetamol positive (n=24) and had a final diagnosis of AD; ten, however, were [^{18}F]flutemetamol negative and did not have AD as a final diagnosis. In one case, an amyloid negative MCI, treatment was discontinued following [^{18}F]flutemetamol due to cholinergic side effects.

4.1.3 Paper III – CSF tau in relation to [^{18}F]THK5317 and [^{18}F]FDG

4.1.3.1 Relationship between baseline PET measures and CSF tau

Associations between CSF tau and baseline PET measures ([^{18}F]THK5317 and [^{18}F]FDG) are summarized in Figure 23. P-tau$_{181p}$ related to baseline [^{18}F]THK5317 uptake within lateral temporal and parietal cortices, as well within isocortical composite and Braak V/VI ROIs. By contrast, t-tau related only to isocortical composite [^{18}F]THK5317 DVR. Tau-368 related to [^{18}F]THK5317 uptake within

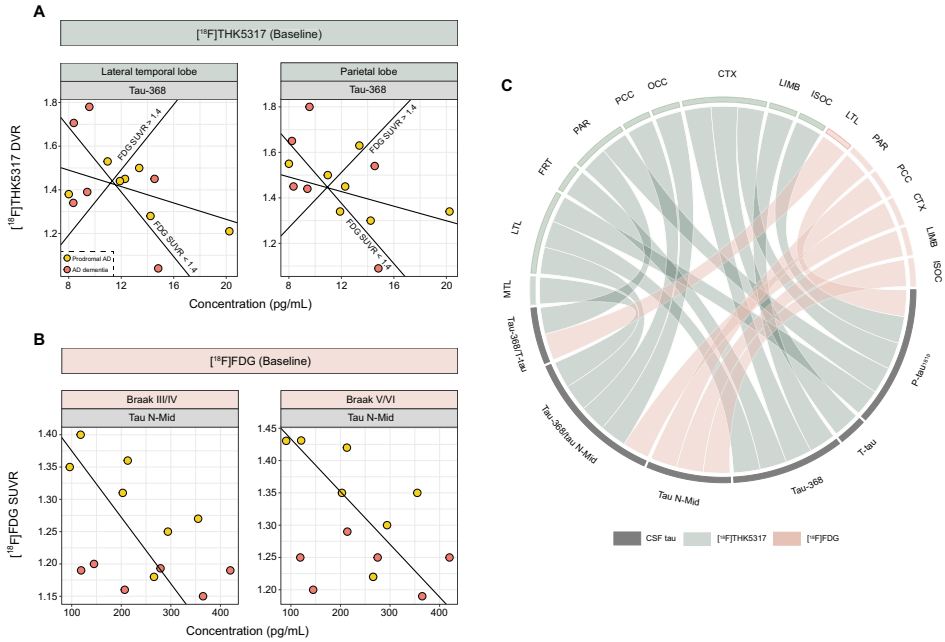

Figure 23. *Scatter plots showing the relationship between baseline [18F]THK5317 DVR and CSF tau-368 (A) and between baseline [18F]FDG SUVR and tau N-Mid (B). For [18F]THK5317, though overall fits were negative, an interaction between effect was seen whereby positive slopes were observed in those with an isocortical [18F]FDG SUVR > 1.4, with negative slopes seen in those with [18F]FDG SUVR < 1.4. Findings from multilinear regression analyses are summarized in the chord diagram (C), with each band indicating a significant relationship. MTL, medial temporal; LTL, lateral temporal; FRT, frontal; PAR, parietal; PCC, posterior cingulate; OCC, occipital; CTX, isocortical composite; LIMB, Braak III/IV; ISOC, Braak V/VI.*

lateral temporal, frontal, isocortical and Braak III/IV ROIs; Tau-368 in ratio to t-tau associated significantly to parietal [^{18}F]THK5317 uptake, with tau-368/tau N-Mid relating to temporal, posterior cingulate, and occipital [^{18}F]THK5317 DVR. Since p-tau$_{181p}$ and tau-368 are thought to reflect, respectively, a pathologic state associated with the development of tangle pathology,[483] with tau-368 reflecting an expansion in the pool of C-terminal fragments that make up PHF tau.[570] It would thus be expected that these two measures would parallel one another, and perhaps show regional overlap with tau-368 ratios, measures thought to provide an estimate of tangle pathology. Though regional overlap between these measures was limited to the lateral temporal and parietal cortices, as well as more broadly, across all cortical regions combined, the associations that emerged as significant at baseline involved areas affected in later Braak stages,[63,124] in support of this idea. Further, recent findings suggest that the development of tangle pathology may not adhere precisely to the Braak staging scheme.[84,589]

Group level (all subjects combined) regression fits between baseline [^{18}F]THK5317 and CSF tau were negative; though this finding conflicted with previous studies, which showed positive associations between CSF and PET,[506,507,509,510,514,590] an interaction effect was found whereby [^{18}F]THK5317 and CSF tau were positively associated in subjects with more preserved isocortical glucose metabolism ([^{18}F]FDG SUVR > 1.4); those with more impaired glucose metabolism ([^{18}F]FDG SUVR < 1.4) showed a negative association, similar to the observed group level fit. With respect to the inverse association seen in those with more impaired metabolism, several studies suggest that following initial increases, p-tau$_{181p}$ and t-tau may decrease in AD with symptomatic progression,[591-594] possibly reflecting a deceleration in neurodegeneration and/or a reduction in the number of viable neurons releasing tau and the sequestration of p-tau in NFTs. Though certain studies have shown little to no change in CSF tau longitudinally,[595-599 511-513,595-598,600-608] others have shown decreases in tau in those with high baseline concentrations[591,593,594,596,607] as well as initial increases followed by decreases through the MCI and dementia phases, respectively.[592,594,609] Longitudinal stability in CSF tau has also been interpreted as a slowing in the rate of increase due this deceleration in neuronal loss.[594] Though a decrease in CSF tau could be due to a dilution effect,[599] our application of a ventricular volume correction would argue against this.

Though methodological differences, including study duration and patient selection, complicate comparisons, the above described data, in the aggregate, support the idea that negative trajectories for CSF tau may be biologically driven. Further support for this idea comes from a recent study that used a stable isotope labelling kinetics (SILK) method (involving the marking and quantification of cells marked with a stable isotopically labelled tracer, $^{13}C_6$-leucine)[610] to monitor the half-life and turnover rate and of tau in the human CNS.[516] Applied to CU and AD subjects, this study suggested that while an equilibrium exists between brain soluble tau and CSF tau under physiological conditions (stage A, normal), triggering events, including, potentially, Aβ aggregation, result in the increased production or extracellular release of tau (stage B, asymptomatic). Elevated soluble tau then results in the seeding and spread (via mono- and trans-synaptic connections) of misfolded (insoluble) tau. This process is detectable using tau PET imaging, and results in a decrease in CSF tau (stage C, very mild AD; Braak stage I/II).[611] The accumulation and further spread of tau aggregates (stage D, mild AD; Braak III/IV) would be characterized by further decreases in CSF tau.

Using baseline [^{18}F]FDG, p-tau$_{181p}$ was inversely related to parietal SUVR; significant negative associations were also found between tau N-Mid and [^{18}F]FDG SUVR within the posterior cingulate and Braak composite regions. Tau ratios positively related to metabolism within lateral temporal (tau-368/T-tau) and isocortical composite (tau-368/tau N-Mid) regions. By comparison, overall findings for [^{18}F]FDG, in terms of the number of significant regression models, were less than half those for [^{18}F]THK5317. Though considered interchangeable as biomarkers of

neurodegeneration,[483,484] no significant associations were found between t-tau and [^{18}F]FDG; previous studies addressing the relationship between t-tau and imaging biomarkers of neurodegeneration have shown inconsistent results in MCI and AD, with positive associations only mild in strength.[509,514,518,520-522,612,613] Associations with tau N-Mid, however, were specific to [^{18}F]FDG. These differences between [^{18}F]THK5317 and [^{18}F]FDG suggest a temporal delay between tau pathology and hypometabolism,[280,287] possibly due endogenous neuroprotective mechanisms,[614-616] and that tau N-Mid, in contrast to the other measures of soluble tau here investigated, may capture tau related synaptic dysfunction.

4.1.3.2 Relationship between rate of change in PET measures and CSF tau

Considering the smaller number of subjects who underwent follow-up [^{18}F]THK5317 studies, the interaction term with [^{18}F]FDG SUVR was not included, with regional [^{18}F]THK5317 values instead regressed onto CSF tau measures. Based on these models (Figure 24), a positive association was found between p-tau$_{181p}$ and the rate of change in [^{18}F]THK5317 DVR in the parietal cortex. As described above, p-tau$_{181p}$ was also related to parietal metabolism at baseline. This pattern of CSF relating to baseline [^{18}F]FDG SUVR and to the rate of change in [^{18}F]THK5317 DVR within the same ROI was also seen for tau-368/t-tau (lateral temporal), tau-368/tau N-Mid (isocortical composite), and tau N-Mid (posterior cingulate and Braak regions). These findings, combined with previous observations, provide further support for the idea of a nonlinear association between tau pathology and neurodegeneration,[287,614-616] with closer correspondence during the dementia phase of AD.[617-620] Furthermore, in light of cross-sectional associations, longitudinal findings associations with tau N-Mid suggest this measure may prove sensitive to both tangle pathology and synaptic impairment.

4.1.3.3 Concordance between tau biomarkers

Cut-offs for [^{18}F]THK5317 across ROIs were set using the mean DVR plus two standard deviations of controls (young and elderly combined). This yielded the following regional values: 1.11 (medial temporal lobe), 1.28 (lateral temporal lobe), 1.29 (posterior cingulate), 1.38 (parietal lobe), 1.44 (frontal lobe), 1.34 (isocortical composite), 1.22 (Braak III/IV), and 1.33 (Braak V/VI). Concordance findings with CSF measures are summarized in Figure 25. Across prodromal AD and AD dementia patients combined, agreement between [^{18}F]THK5317 and INNOTEST tau measures (p-tau$_{181p}$, t-tau) was approximately 50%. Overall concordance was similar when using N-Mid tau (53%), and improved when using tau-368 in ratio to t-tau (71%). Isolated [^{18}F]THK5317 positivity was the predominant form of discordance when using INNOTEST measures and tau N-Mid. Using tau-368/t-tau, only isolated CSF positivity was found. These findings held when prodromal AD and AD dementia patients were analysed separately; concordance, however, was overall higher among AD dementia subjects.

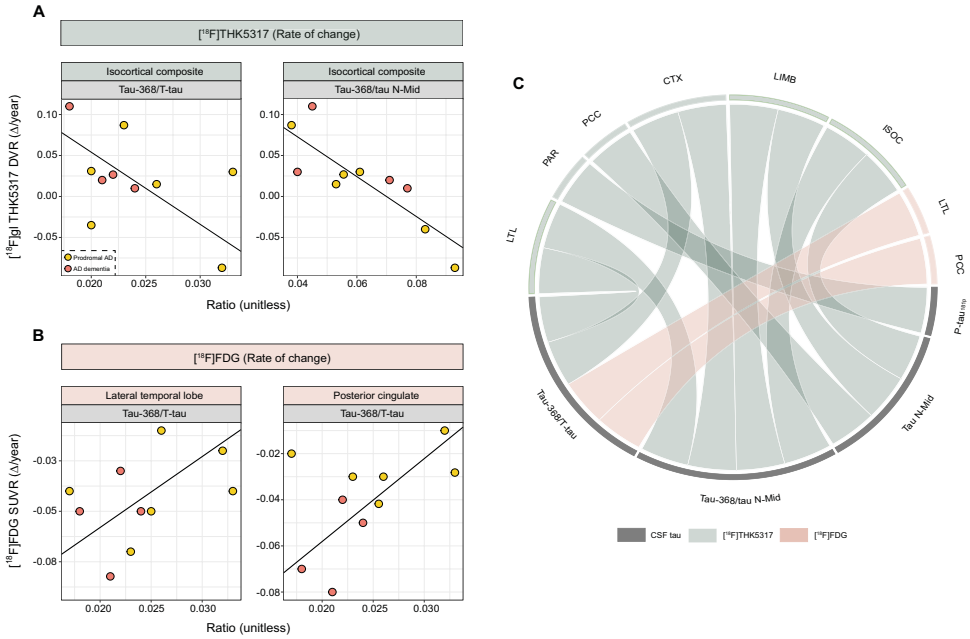

Figure 24. *Scatter plots showing the relationship between the annual rate of change in [^{18}F]THK5317 DVR and tau-368 in ratio with T-tau and tau N-Mid (A) and between the annual rate of change in [^{18}F]FDG SUVR and tau-368/T-tau (B). Multilinear regression model findings are summarized in the chord diagram (C), with each band indicating a significant finding. MTL, medial temporal; LTL, lateral temporal; FRT, frontal; PAR, parietal; PCC, posterior cingulate; OCC, occipital; CTX, isocortical composite; LIMB, Braak III/IV; ISOC, Braak V/VI.*

Concordance figures between dichotomized CSF tau and [^{18}F]THK5317 were somewhat lower than those reported in the only other study to so far examine agreement between tau biomarkers ([^{18}F]AV1451; p-tau$_{181p}$ and t-tau).[514] This discrepancy may relate to differences between cohorts, including age and CSF tau levels, the interval between CSF and tau PET, ROI selection, use of a different tau tracer, and the control subjects used to define regional tau PET cut points. Similar to the study by Mattsson et al.,[514] however, we also found that the degree of concordance was higher overall among AD dementia subjects in comparison to the prodromal AD group. This observation possibly aligns with the explanation that while tau biomarkers may disagree, they will prove concordant over time given the chronic nature of AD.[483] This reflects the fact that while CSF reflects production/clearance rates at a given time point, tau PET captures the cumulative burden of accumulated pathology. With respect to the idea of a decrease in CSF tau during the dementia phase of AD, higher concordance compared to prodromal AD might be accounted for by high baseline levels, variability across subjects, and increases in tau PET signal.

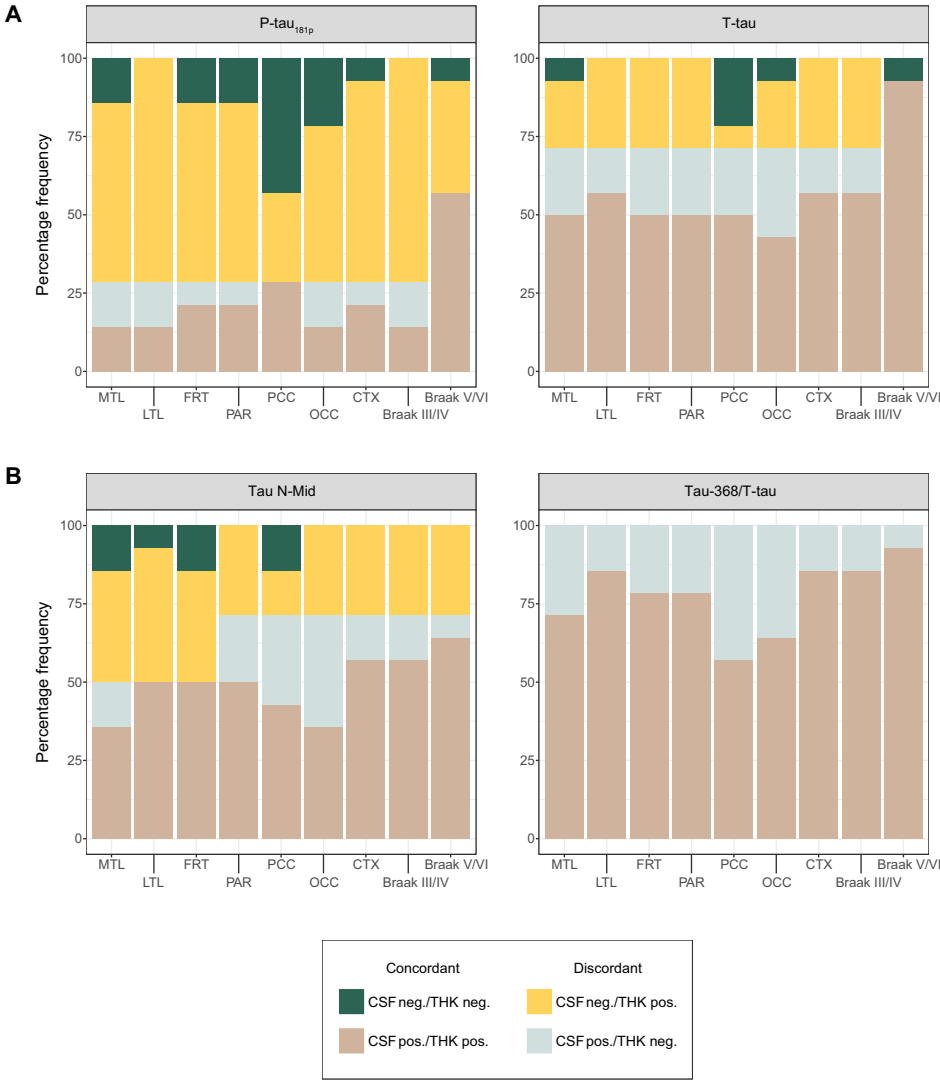

Figure 25. *Concordance figures showing agreement between binarised regional [^{18}F] THK5317 DVR and CSF tau: INNOTEST tau (A), tau N-Mid and tau-368/T-tau (B). MTL, medial temporal; LTL, lateral temporal; FRT, frontal; PAR, parietal; PCC, posterior cingulate; OCC, occipital; CTX, isocortical composite; LIMB, Braak III/IV; ISOC, Braak V/VI.*

4.1.3.4 Illustrative biomarker profiles in selected AD patients

Prodromal AD

Two prodromal AD cases showing differing tau biomarker profiles are shown in Figure 26A and C. High cortical [^{18}F]THK5317 uptake (surpassing cut-offs in all (case 1) and eight of nine (case 2) ROIs, respectively) and temporoparietal hypometabolism was noted in both individuals at baseline. Using P-tau$_{181p}$ and T-tau, case 1 was concordant positive with [^{18}F]THK5317, while CSF levels were below cut-offs in case 2. Longitudinally, case 1 showed increased [^{18}F]THK5317 retention, mainly in temporal and parietal regions, with decreased metabolism in the lateral temporal, posterior cingulate, and parietal cortex; case 2 also exhibited increased [^{18}F]THK5317 DVR in posterior regions, though with more widespread changes in metabolism. CSF levels of N-Mid tau in case 1 were nearly double those of case 2; this difference also held for tau ratios. Tau-368 levels, however, were similar. At clinical follow-up, case 1 showed cognitive decline and received a diagnosis of AD dementia; by contrast, case 2 showed relative cognitive stability and retained the diagnosis of prodromal AD.

AD dementia

Two cases of AD dementia showing concordant and discordant tau biomarker profiles are shown in Figure 26B and C. Using P-tau$_{181p}$ and T-tau, the first patient (case 3) showed a concordant positive profile, while the second (case 4) showed only [^{18}F]THK5317 positivity. At baseline, both showed high [^{18}F]THK5317 DVR values in cortical regions (above cut-offs in all regions, save for a borderline value in the posterior cingulate of case 4) and low [^{18}F]FDG SUVR in temporal, parietal, and frontal regions. Increased retention of [^{18}F]THK5317 was noted in frontal and parietal regions longitudinally for both cases, with case 3 showing additional involvement of temporal areas. Both patients showed metabolic decline, predominantly in temporal areas. Large differences were seen in N-Mid tau-368 and tau-368/tau N-Mid; both patients showed similar values, however, for tau-368/T-tau. Cognitively (MMSE), no decline was seen in case 3 at follow-up, while a decline of 2 points was seen in case 4.

4.1.3.5 Interchangeability of tau biomarkers

These cases illustrate how despite the same baseline diagnosis and a similar imaging profile, widely differing CSF tau profiles can be observed. Further, they highlight how CSF tau profiles can vary in the context of low Aβ_{1-42}, in contrast to the CSF signature of high tau and low Aβ_{1-42} expected in AD.[621] In combination with concordance findings to date,[514] these results underline the importance of recent recommendations for the interpretation of ambiguous CSF results in the work up of patients presenting with cognitive impairment,[523,524] and suggest that CSF and tau PET biomarkers may not be invariably interchangeable.

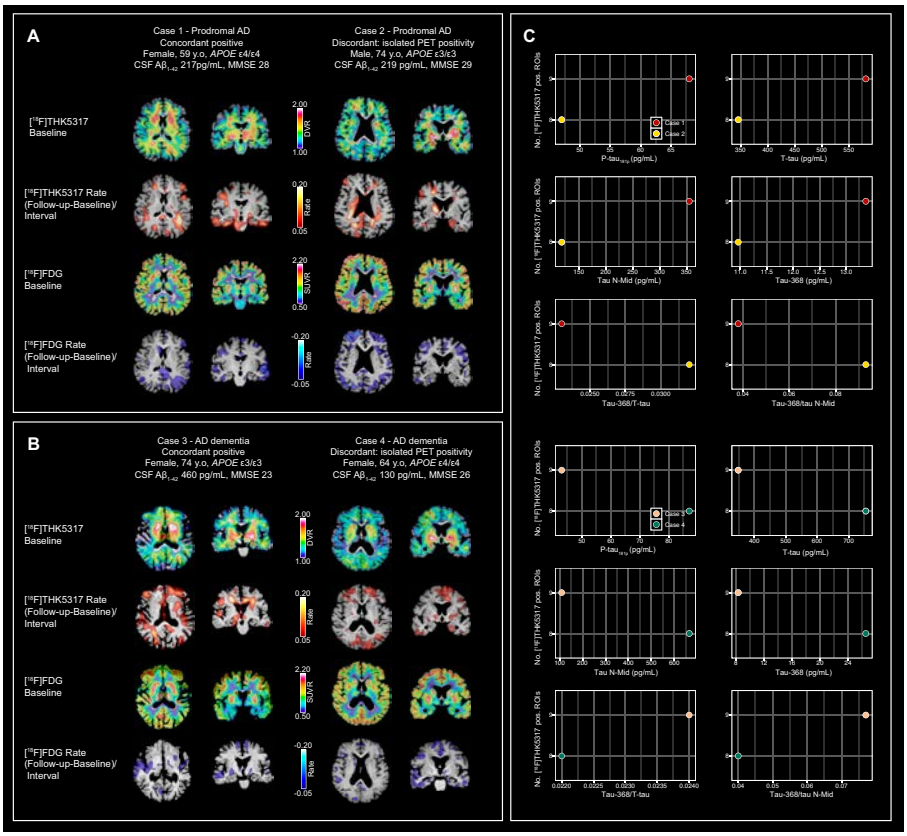

Figure 26. *Imaging and CSF profiles for patients with baseline diagnoses of prodromal AD (A, C), and AD dementia (B, C). As P-tau$_{181p}$ and T-tau are established measures in the clinical work-up of dementia disorder patients, these were selected to define concordance (A,B). [^{18}F]THK5317 positivity was ascribed owing to the high percentage of ROIs showing DVR values above THK-control defined cut-offs.*

4.1.4 Papers IV and V – [^{18}F]THK5317 perfusion parameters in relation to [^{18}F]FDG PET

4.1.4.1 Selection of [^{18}F]THK5317 perfusion SUVR interval

In order to determine the time interval for [^{18}F]THK5317 p-SUVR, several initial starting points (0, 1, and 2 min) and frame durations (1 to 10 min) were used. Using a subset of nine patients (four prodromal AD, five AD dementia), the optimal interval for p-SUVR was then determined as that providing the highest correlation between p-SUVR and both [^{18}F]FDG and R_1 across ROIs (0-3 min). For [^{11}C]PIB, a time window of 1–8 min was used based on previous findings showing that this interval provided the highest correlation between p-SUVR and both [^{18}F]FDG and K_1.[336] In other studies using p-SUVR from [^{11}C]PIB and [^{18}F]AV45, similar time

intervals have been reported (0-6;[343] 1-4[566]; 1-6[622]; 1.33-8 min[342]; and 1-6 min,[623,624] respectively). In the only other study to thus far derive p-SUVR from a tau tracer ([^{18}F]AV1451), the interval 1-6 min was selected as optimal.[345] Variability in the p-SUVR time window largely reflects methodological differences across studies; though the impact of small shifts around upper and lower boundaries are unlikely to exert much of an effect on correlation strengths, the risk of signal contamination from specific binding should be kept in mind.

4.1.4.2 Reproducibility of [^{18}F]THK5317 perfusion parameters

In study V, the reproducibility (test-retest variability: [(Retest – Test)/ Test]) of [^{18}F]THK5317 perfusion parameters was investigated in a subset of five patients (four prodromal AD, one CBS) who underwent two [^{18}F]THK5317 scans within an interval of 37 days. Using an isocortical meta-ROI, the average absolute difference between scans across subjects was 2.43% for p-SUVR, and 3.13% for R_1. Test-retest variability in individual ROIs was also low. For example, in the parietal and posterior cingulate cortices, regions of high interest in AD, reproducibility estimates were 4.18% and 3.10%, respectively, for p-SUVR, and 3.11% and 3.78%, respectively, for R_1. By comparison, an average isocortical composite test-retest of approximately 4.5% has been reported for fluorine-18 labelled amyloid ligands,[625] with reports of between ~1.5% ([^{18}F]AV1451)[626] and 1.8% ([^{18}F]THK5317)[280] for tau imaging. In addition to the evaluation of tracers' utility in studies involving repeated measurements (such as those measuring treatment effects), test-retest studies can also provide useful information for selection of optimal quantification methods and more broadly, for understanding measurement variability across regions of the brain.[627]

4.1.4.3 [^{18}F]THK5317 perfusion parameters in comparison to [^{18}F]FDG

In study IV, both [^{18}F]THK5317 p-SUVR and R_1 were found to positively correlate with [^{18}F]FDG, with the highest coefficients observed in the lateral temporal, parietal and occipital cortices. [^{18}F]THK5317 p-SUVR and R_1 were found to strongly correlate positively, as did perfusion parameters from [^{18}F]THK5317 and [^{11}C]PIB. Representative images of these measures are shown in Figure 27. Voxel-wise analyses revealed a similar pattern (Figure 28), with widespread positive correlation between [^{18}F]THK5317 perfusion parameters and [^{18}F]FDG; Reperformance of these cross-sectional analyses in study V using a subset of subjects from study IV yielded similar results, using both baseline and follow-up data. Overall, cross-sectional findings from these two studies matched well with the literature showing that p-SUVR and R_1 from amyloid ligands ([^{11}C]PIB and [^{18}F]AV-45)[336,342,343,566,622-624] and [^{18}F]AV1451 tau imaging[345] strongly relate to [^{18}F]FDG metabolic imaging PET, using both ROI and voxel-based analyses, as well as visual comparison of images. Regional variability in correlational strength and percentage of shared variance, however, suggest that though grossly similar, CBF and metabolism may not relate in a one-to-one fashion throughout the brain.

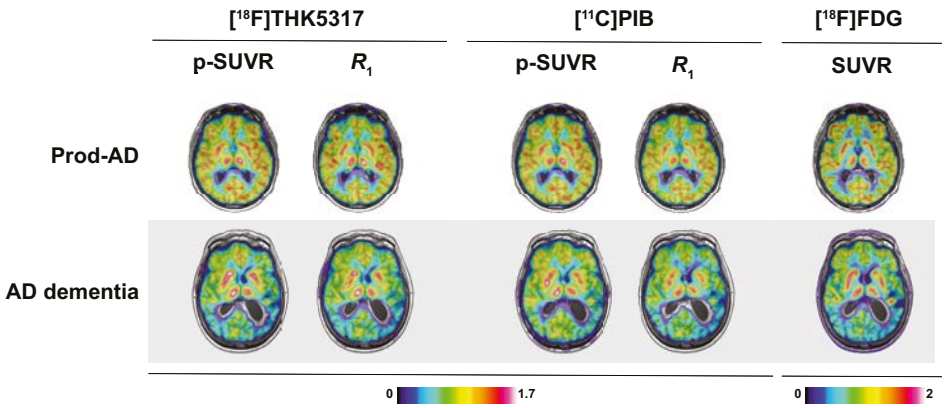

Figure 27. *Comparison of perfusion images (p-SUVR and R_1) from [^{18}F]THK5317 and [^{11}C]PIB with [^{18}F]FDG in a patient with prodromal AD (top row) and AD dementia (bottom row). Adapted from Rodriguez-Vieitez E, Leuzy A, Chiotis K, Saint-Aubert L, Wall A, Nordberg A. Comparability of [^{18}F]THK5317 and [^{11}C]PIB blood flow proxy images with [^{18}F]FDG positron emission tomography in Alzheimer's disease. J Cereb Blood Flow Metab. 2016.*

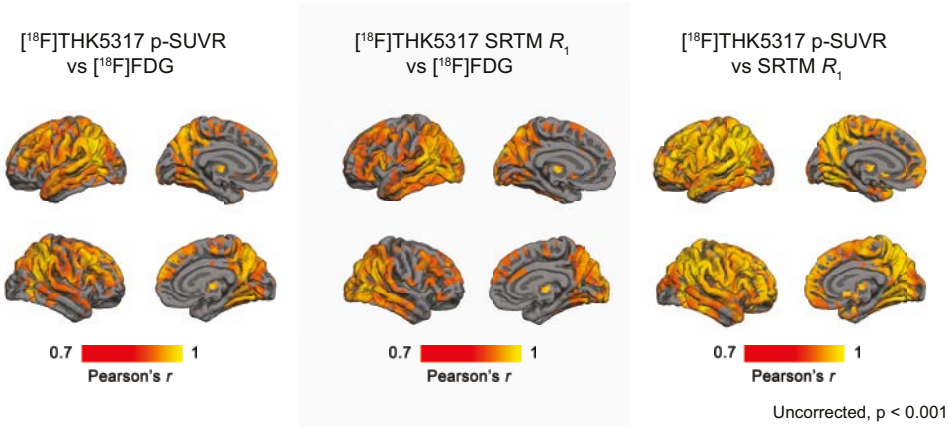

Figure 28. *Biological Parametric Mapping derived voxel-wise Pearson's correlation maps in 20 patients with AD (p<0.001, uncorrected; cluster extent > 20 voxels): [^{18}F]THK5317 p-SUVR vs [^{18}F]FDG (left), [^{18}F]THK5317 R_1 vs [^{18}F]FDG (middle) and [^{18}F]THK5317 p-SUVR vs R_1 (right). Adapted from Rodriguez-Vieitez E, Leuzy A, Chiotis K, Saint-Aubert L, Wall A, Nordberg A. Comparability of [^{18}F]THK5317 and [^{11}C]PIB blood flow proxy images with [^{18}F]FDG positron emission tomography in Alzheimer's disease. J Cereb Blood Flow Metab. 2017; 37(2):740-749.*

In study V, voxel-wise annual percentage change for [^{18}F]THK5317 perfusion measures and [^{18}F]FDG was investigated (Figure 29). Though p-SUVR and R_1 both showed similar changes in lateral temporal and parietal areas, greater change was seen for p-SUVR in cingulate, prefrontal, and orbitofrontal cortices, as well as in the precuneus and occipital cortex. Changes in [^{18}F]FDG were predominant in temporal, medial parietal, and prefrontal regions, and showed greater overlap with declines in p-SUVR, relative to R_1. Further, comparison of binarised percentage change maps for each measure showed that the overlap between metabolism and R_1 was greatest in temporoparietal areas, with a more frontal predominant pattern for p-SUVR. These observations strengthened the notion of disruptions to neurovascular coupling in AD, and underscored the question of interchangeability between perfusion measures. Further, the limited overlap (medial temporal) observed between p-SUVR and areas showing increased [^{18}F]THK5317 DVR (frontal, temporal and occipital) highlighted the concept of a spatiotemporal offset between pathophysiological processes in AD.

Hypothesizing that the relationship between PET measures might vary as a function of disease stage, correlation analyses were repeated by sub-group (prodromal AD, AD dementia) (Figure 30). These showed that while the overlap between [^{18}F]THK5317 perfusion parameters and [^{18}F]FDG maps was greater in AD dementia; spatial correspondence between p-SUVR and R_1, however, was seemingly greater in prodromal AD. Linear mixed modelling, including the interaction term time point (baseline, follow-up) x sub-group, showed that the decline in metabolism was comparatively greater in AD dementia. Focal increases in [^{18}F]THK5317 DVR were seen in both groups; overlap with p-SUVR, however, was largely restricted to a small basal temporal cluster, in AD dementia. Taken together, these findings were interpreted as suggesting that the effects of amyloid and tau on synaptic integrity and cerebral vasculature differ by disease stage, with the closer alignment of CBF and metabolism in AD dementia possibly reflecting the loss of a glial phenotype that has been shown to exert a protective effect on metabolism.[116,628] While the overall inconsistencies observed between p-SUVR and R_1 may relate to how these parameters are estimated,[335,345] their greater spatial divergence in AD dementia may be due to contamination of the p-SUVR signal by very early binding to tau aggregates,[345] an effect an effect that may have been masked by the threshold used to binarise the rate of change images.

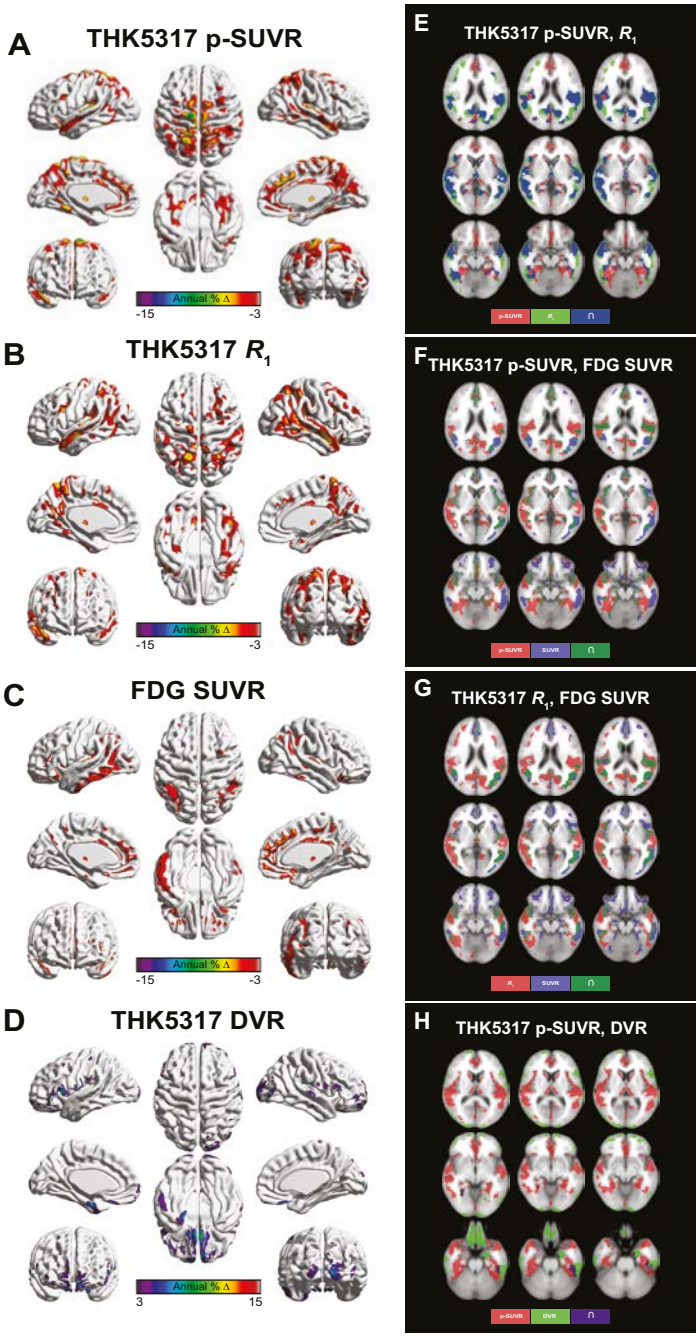

Figure 29. *Group-level annual percentage change maps for perfusion (A, B), metabolism (C), and tau (D). Spatial overlap between images binarised using the average test-retest repeatability of [^{18}F] THK5317 perfusion measures is shown for [^{18}F]THK5317 perfusion measures (E), [^{18}F]THK5317 p-SUVR and [^{18}F]FDG SUVR (F), and [^{18}F]THK5317 R_1 and [^{18}F] FDG SUVR (G). For the overlap between perfusion and [^{18}F] THK5317 DVR (H), [^{18}F]THK5317 p-SUVR was chosen because of the potentially greater clinical applicability of this measure due the fact that it does not require dynamic imaging and the fact that identical overlap was obtained when using [^{18}F]THK5317 R_1. Adapted from Leuzy A, Rodriguez-Vieitez E, Saint-Aubert L, et al. Longitudinal uncoupling of cerebral perfusion, glucose metabolism, and tau deposition in Alzheimer's disease. Alzheimers Dement. 2018;14(5):652-663.*

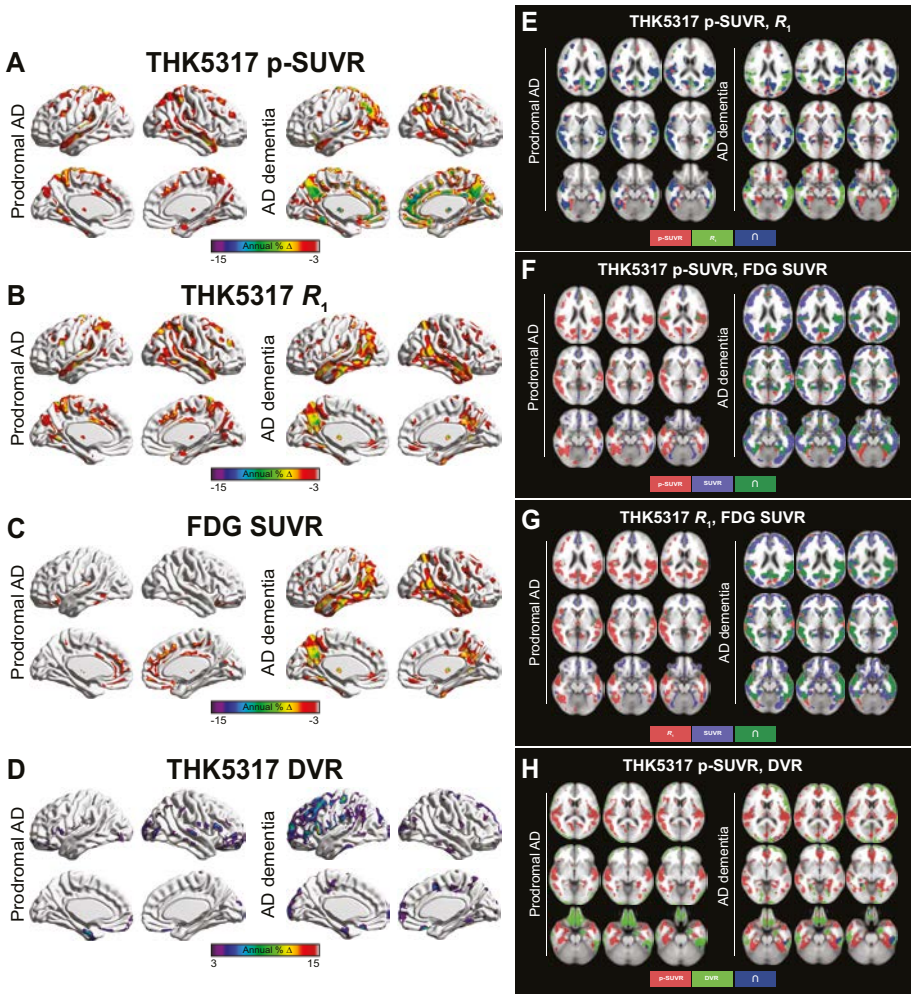

Figure 30. *Subgroup-level (prodromal AD, AD dementia) annual percentage change maps for perfusion (A, B), metabolism (C), and tau (D). Spatial overlap between images binarised using the average test-retest repeatability of [^{18}F]THK5317 perfusion measures is shown for [^{18}F]THK5317 perfusion measures (E), [^{18}F]THK5317 p-SUVR and [^{18}F]FDG SUVR (F), and [^{18}F]THK5317 R_1 and [^{18}F]FDG SUVR (G). For the overlap between perfusion and [^{18}F]THK5317 DVR (H), [^{18}F]THK5317 p-SUVR was chosen because of the potentially greater clinical applicability of p-SUVR due the fact that it does not require dynamic imaging and the fact that identical overlap was obtained when using [^{18}F]THK5317 R_1. Adapted from Leuzy A, Rodriguez-Vieitez E, Saint-Aubert L, et al. Longitudinal uncoupling of cerebral perfusion, glucose metabolism, and tau deposition in Alzheimer's disease. Alzheimers Dement. 2018;14(5):652-663.*

4.1.4.4 Discriminative ability of [^{18}F]THK5317 perfusion parameters

In study IV, the accuracy of [^{18}F]THK5317 perfusion parameters with respect to the discrimination of prodromal AD *vs* AD dementia patients was investigated using AUC area under the curve values derived from ROC analyses. These were compared to those for [^{11}C]PIB perfusion parameters and [^{18}F]FDG SUVR. No significant differences were found between values, however, indicating that these measures performed equally well in separating these two groups. These findings accord with previous studies that compared the diagnostic accuracy of [^{11}C]PIB p-SUVR[566] and [^{123}I]IMP-SPECT[339] with [^{18}F]FDG, though other studies showed slightly superior performance for [^{11}C]PIB p-SUVR[336] and [^{18}F]FDG.[342] Of interest, however, was the observation that perfusion to metabolism ratios,[623] using both [^{18}F]THK5317 and [^{11}C]PIB differed slightly by brain region, aligning with previous findings showing relative hyper- and hypoperfusion, compared to glucose metabolism, of limbic and cortical regions, respectively.[629] Future studies will be required to clarify the potential impact of this, particularly with respect to the separation of AD from disorders that are affected by mainly subcortical pathology.

4.2 METHODOLOGICAL CONSIDERATIONS

4.2.1 PET based measures

PET based measures used in the present thesis included SUVR (studies I-V), p-SUVR and SRTM R_1 (studies IV-V), and reference Logan DVR (studies III and V). As these measures were all derived from reference tissue methods, common to them are a number of assumptions for reference tissues, including the suitability of a 1-TC model to describe ligand kinetics, negligible blood volume contribution, a lack of specific/displaceable binding, and the same non-displaceable volume of distribution as target regions.[630] Although important, violations to these assumptions and the related impact of this were not directly addressed in this thesis. Though recent evidence suggests off-target binding of [^{18}F]THK5351 to MAO-B,[304,631,632] it remains unclear how well this extrapolates to findings with [^{18}F]THK5317,[306,633] particularly given the very low levels of MAO-B across the neocortex and cerebellar GM.[634]

4.2.1.1 Partial volume correction

In the present thesis, [^{18}F]THK5317 PET data was pre-processed using PMOD. Using this software, two approaches exist for partial volume correction: the Müller-Gärtner (MG) method[219] and the geometric transfer matrix (GTM) method.[635] Though both rely on anatomical information from structural imaging and provide correction for both spill-in and spill-out,[563] the former provides a GM specific correction at the voxel level, while the latter provides a regional correction after having segmented the brain into distinct ROIs. Due to the combination of the GTM not taking into account signal variability within regions (i.e. activity within each

region is assumed to be homogeneous) and the focality of findings with tau PET, the MG method was selected over the GTM for study III. Accordingly, dynamic [^{18}F]THK5317 studies were first corrected voxel-wise; kinetic modelling was then performed on the PVE-corrected images, with ROI DVR values extracted via application of the Hammers atlas to parametric images.

4.2.2 CSF measurements

In study I, historical INNOTEST A$\beta_{1\text{-}42}$ values were included from several centres belonging to the BIOMARKAPD project. These values had been determined locally as part of routine clinical practice, with CSF samples thus analysed sample by sample, as opposed to batch-wise. Though board-certified laboratory technicians performed all analyses according to kit-inserts, using procedures accredited by national certification and inspection bodies, participation in the Alzheimer's Association QC program varied.[417,427,428] As such, the longitudinal stability of measurements may have differed somewhat across the included laboratories; this, in turn, could have impacted the cross-sectional measurements included. While unlikely to have exerted a large effect on our findings, this variable participation, combined with the use of two different commercial assays, was suboptimal from a methodological standpoint given the aim to directly compare concordance rates using local and central results.[579]

4.2.3 Biomarker cut-offs

Continuous biomarker measures are often dichotomized as positive or negative in order, for instance, to facilitate clinical decision making or to simplify statistical analyses in a research framework. A number of statistical approaches exist for cut-point selection, ranging from setting sensitivity and specificity *apriori* to accuracy maximization.[636] Broadly speaking, cut-point selection involves the determination of an acceptable balance between the risk of falsely classifying a non-diseased individual as diseased (false positive) and vice versa (false negative), with this trade-off dependent on the context in which the measure is to be applied.[636] The approaches used in this thesis relied mainly on normal reference limits; a possible limitation of this is the inadvertent inclusion of subjects who, while being negative for amyloid or tau at the time-point of inclusion, may show increases longitudinally. Similarly, while mixture modelling assumes that the overall sample in fact consists of two distinct subpopulations (one with AD pathology, the other without), subjects instead likely lie on a continuum of AD pathology, complicating interpretation of the identified mixture components.[637] Ultimately, only an extended follow-up period (i.e. to post-mortem) would allow for an accurate assessment of how well these dichotomized biomarkers perform with respect to AD pathology.

5 CONCLUDING REMARKS

- Visual based assessment of [^{11}C]PIB scans was comparable across centres, with standardisation of SUVR data feasible using the Centiloid method. Centralized batch-wise re-analysis of CSF for $A\beta_{1-42}$ did not invariably improve agreement with [^{11}C]PIB imaging. This suggests a biological component to discordance, as opposed to this phenomenon merely reflecting methodological aspects of PET or CSF processing. Findings using $A\beta_{1-42}/A\beta_{1-40}$ support its use instead of $A\beta_{1-42}$ alone.
- Amyloid imaging with [^{18}F]flutemetamol PET exerted a meaningful impact in terms of diagnostic change and altered drug treatment among diagnostically uncertain tertiary memory clinic patients. These findings, paired with the current literature on this topic and the extensive biomarker investigations performed in the majority of patients prior to [^{18}F]flutemetamol, support the utility of amyloid imaging in clinical practice.
- CSF tau may show both positive and negative correlations with tau PET, possibly as a function of neurodegeneration. In contrast to established CSF tau measures (i.e. p-tau$_{181p}$, t-tau), novel fragments (i.e. tau N-Mid and tau-368, alone, or incorporated into ratios, (tau-368/tau N-Mid, tau-368/T-tau) may better capture both cross-sectional and longitudinal findings with tau and [^{18}F]FDG PET.
- Cross sectional findings support the use of tau PET derived perfusion measures (p-SUVR and R_1) as alternatives for metabolic imaging with [^{18}F]FDG PET. Longitudinal observations, however, suggest that the coupling between CBF and metabolism, as well as the interchangeability of perfusion metrics, may vary across both the course of AD and brain regions.

6 FUTURE OUTLOOK

The increasing use of CSF measures and PET in clinical settings (amyloid and [^{18}F] FDG, with tau PET imaging likely soon to follow), and the current view of AD as a biological construct – definable using biomarkers for its core neuropathological features – highlights the relevance of understanding how they interrelate. However, fairly large scale longitudinal studies incorporating serial CSF and imaging in individuals across the AD continuum, and in related disorders, will be required to properly address this question. Further studies comparing CSF and PET biomarkers with those based in blood are also of importance given the advantages carried by plasma measures.[638] Though further studies addressing the cost-effectiveness of amyloid PET are required, accrued evidence thus far indicates that it carries clinical utility based on its impact on changes in diagnosis, diagnostic confidence, number of ancillary investigations, and patient treatment. Finally, given the flexibility of the recently proposed A/T/N classification scheme for biomarkers used in AD and research on brain aging, additional studies are warranted addressing the use of perfusion imaging as a substitute for neurodegeneration, via comparison to [^{18}F]FDG and related markers of neurodegeneration, including CSF t-tau, neurogranin, and NFL.

6.1 PET AND CSF BIOMARKERS FOR AMYLOID, TAU, AND NEURODEGENERATION

Studies addressing concordance between amyloid biomarkers show a level of agreement that is high, but imperfect; studies for tau biomarkers, though few in number, show lower rates of agreement lower than those for amyloid. Explanations for disagreement include variability in Aβ production levels, isolated low CSF $A\beta_{1\text{-}42}$ in non-AD disorders, and, for tau, possibly, that CSF levels vary over the disease course. Cut-offs used to define abnormality in CSF are also relevant; due the lack of common calibrators, a multitude of values are currently used for defining abnormal measurements. Standardisation efforts have so far come the furthest for $A\beta_{1\text{-}42}$, with the publication of two MS-based RMPs, now certified by the Joint Committee for Traceability in Laboratory Medicine,[429,639] and a CSF-based reference material currently under evaluation.[640] These developments, combined with fully automated assays carrying low coefficients of variation,[526] should move the field closer to the introduction of universal cut-offs for defining abnormal $A\beta_{1\text{-}42}$ values. Similar advances will hopefully soon follow for tau, with one candidate RMP for t-tau recently reported.[641] In the interim, recent work using one such automated assay has shown 90% concordance between CSF (tau/$A\beta_{1\text{-}42}$ ratios) and amyloid PET;[642] the fact that this resulted from tau in ratio with $A\beta_{1\text{-}42}$ also highlights comparative studies between these measures and $A\beta_{1\text{-}42}$ in ratio with shorter Aβ peptides as an important line of research. Lastly, further exploration of novel tau fragments that better track the development of neurofibrillary pathology

will likely be required to achieve optimum concordance with tau PET imaging, as are studies addressing the proposed reclassification of t-tau as a marker of neurodegeneration.[483]

While visual reads remain the standard for amyloid PET in clinical practice, with this approach likely to also be used with tau imaging should it become approved for clinical use, quantitative approaches carry advantages, including reduced inter-reader variability, and higher sensitivity.[643-645] Using the Centiloid method, amyloid PET findings can be brought into the same range of values, potentially facilitating large scale comparative studies with CSF. Recent findings, however, suggest that this approach does not entirely eliminate differences between analytical approaches, resulting in, for instance, different sensitivity to changes in amyloid burden and varied amyloid positivity thresholds.*[646]* Incorporation of neuropathology findings may help solve these issues.[584,647] Similar approaches to standardise quantitative tau imaging measures will be required; this may prove more challenging, however, given the different spatiotemporal pattern of progression tau is thought to follow.

The above described approaches should, ultimately, facilitate large scale studies examining how PET and CSF measures relate over time, including concordance rates using dichotomised measures; this is critical if these biomarkers are to be treated as interchangeable. The current literature suggests discordance between amyloid biomarkers is more often in the form of isolated low CSF $A\beta_{1-42}$,[505] with this type of discordance preferentially found in early disease stages (i.e. CU individuals and early MCI) and seldom in AD dementia.[244] This may not hold true in atypical populations, however (e.g. tertiary memory clinic populations). It is important to stress, however, that these methods do not measure exactly the same thing; from a longitudinal perspective, CSF and PET biomarkers have different trajectories: whereas CSF $A\beta_{1-42}$ and tau plateau (or possibly decrease, in the case of tau), early on, PET based measures remain dynamic into the later stages of the disease.[141,514,553,648] Discordance between CSF and PET amyloid biomarkers in preclinical AD, for instance, may lend itself to the design of prevention trials;[649] those with isolated low $A\beta_{1-42}$, for instance, may prove suitable for long-term studies targeting Aβ production, but not for short term trials examining the effects on an intervention on cognition, tau levels, or brain atrophy.

6.2 CLINICAL VALUE OF AMYLOID IMAGING AND GENERAL APPLICABILITY OF PERFUSION PET

In terms of our findings using [^{18}F]flutemetamol PET, the increases in diagnostic change and in the use of AChEIs, together with previous studies, confirm the clinical value of amyloid PET. Further studies addressing the value of quantitation in amyloid PET, using SUVR and alternative approaches,[561,650] either as an adjunct

to, or substitute for, visual read, are required. The pairing of CBF (early phase SUVR or R_1) and late phase information from amyloid or tau PET imaging carries the advantage of being able to derive both functional and molecular information from a single PET study. From a practical standpoint, however, only p-SUVR would be feasible in clinical settings. Dual-use PET would do away with the need for a separate [^{18}F]FDG PET study, reducing costs, patient discomfort, and radiation exposure. In the event that tau PET gains approval for clinical use, dual-use imaging would circumvent delays between [^{18}F]FDG and tau imaging (similar to those seen for amyloid PET), carrying potential benefits in the form of more rapid diagnosis, improved patient management and decreased ordering of ancillary investigations. Future studies will be required to address this. The possibility of varied parallelism between perfusion and metabolism over the course of AD should also be investigated in longitudinal studies, with these investigations extended to also address the potential of this technique in related non-AD dementia disorders as well as the potential modulatory effects of amyloid and tau pathology, vascular load, and, potentially, neuroinflammation.

7 ACKNOWLEDGMENTS

This dissertation is the culmination of the work of many people. I am especially grateful to:

My supervisor, **Agneta Nordberg**, for teaching me that successful research is not just about having bright ideas; that self-belief, patience, and determination are of equal if not greater importance. Thank you for your guidance, passed on knowledge, and for having played such a central role in my professional and personal development these past years.

To my co-supervisors: **Ove Almkvist**, for being such a class act and for expanding my understanding of cognitive reserve and successful aging; **Elena Rodriguez Vieitez**, for your help and willingness to always lend a hand; for your skillful guidance, particularly early on, and for your admirable dedication to research; and **Kaj Blennow**, for facilitating my discovery of the wonderful world of CSF and its many facets. Your availability, feedback and encouragement have been much appreciated.

To **Konstantinos Chiotis**, for your solidarity on the doctoral front, for introducing me to R based plotting, for your clever and thoughtful perspectives and for fun nights out; **Claudia Cicognola** and **Kina Höglund**, for first highlighting the complexity of tau, and then making it all graspable; you have both been a pleasure to work with; **Laetitia Lemoine,** for your varied and passionate convictions, scientific and otherwise, for broadening my understanding of in vitro techniques, and for your contagious laughter; **Johan Lilja**, for gladly sharing the state-of-the-art in quantification of amyloid PET and for enjoyable collaborations; **Josef Pannee**, for showing me the ins and outs of mass spectrometry and being such a key part of my early thesis work; **Laure Saint Aubert**, for sharing creative solutions to frustrating imaging problems, for your scientific vigour and shared connection to the south-west of France; **Irina Savitcheva**, for your extensive and tireless help in the collection and sifting through of the data for the study on [^{18}F]flutemetamol PET; and **Henrik Zetterberg**, for your enthusiasm, bright ideas and enviable ability to aptly synthesize the latest in the field.

To the bright and talented students and visiting researchers I've had to please of getting to know, learn from, and in many cases, work with: **Morgan Arimbat, Fatima Assenai, Maud Bouwman, Elisa Colato, Fredrik Engman, Jennifer Friman, Lukas Henning, Mona-Lisa Malarte, Mariam Mazrina, Samson Nivins, Rebecca Sjöberg, Unnur Dilja Teitsdottir, Ezije Ukponu,** and **Eduard Vilaplana Martinez.**

All previous and present co-workers at the Division of Translational Alzheimer Neurobiology, now Division of Clinical Geriatrics, especially: **Taher Darreh-Shori** and **Mia Lindskog**, for your sound knowledge and creative approaches to long standing scientific questions; to **Carlos Aguilar, Pavla Cermakova, Soheil Damangir, Farshad-Falahati, Karim Farid, Sara Garcia-Ptacek, Azadeh Karami, Rajnish Kumar, Erica Lana, Maysa Malaskari, Linn Malmsten, Sumonto Mitra, Sathya Mohan, Prashant Murumkar, Ruiqing Ni, Emmy Rannikko, Ipsit Srivastava, Christina Unger, Erika Vazquez-Juarez,** and **Swetha Vijayaraghavan** for helping to create such a scientifically exciting and enjoyable work environment. **Amit Kumar**, for fun times and for keeping my taurine levels high. To **Sara Shams**, thank you for guided tours and chats over lunch; **Göran Hagman**, for shooting the breeze and comic relief.

To my neighbours on the seventh floor; you are a cool and talented bunch: **Olof Lindberg, Alejandra Machado, Gustav Mårtensson, Daniel Ferreira Padilla, Joana Pereira, Konstantinos Poulakis, Emilia Schwertner, Juraj Secnik, Una Smailovic, Olga Voevodskaya**, and **Eric Westman.**

Rita Almeida, for your killer smile, for being so accommodating in the face of my often last minute requests for appointments, and for helping me to better understand statistics.

To varied co-authors: those from BIOMARKAPD, **Steen G. Hasselbalch, Juha O. Rinne,Alexandre de Mendonça, Markus Otto, Alberto Lleó, Miguel Castelo-Branco, Isabel Santana, Jarkko Johansson, Sarah Anderl-Straub, Christine A. F. von Arnim, Ambros Beer, Rafael Blesa, Juan Fortea, and Sanna-Kaisa Herukka** and **Erik Portelius**; from the Uppsala PET Centre, **Gunnar Antoni, Jonas Eriksson, My Jonasson, Mark Lubberink,** and **Anders Wall;** and the Clinic for Cognitive Disorders, Theme Aging, Karolinska University Hospital, **Nenad Bogdanovic, Vesna Jelic,** and **Pia Andersen**. I would also like to warmly thank **Gill Farrar**, GE Healthcare, for her support and interest in our clinical utility study using [^{18}F]flutemetamol PET.

To the computer whizz-kids, **Alfred Nyeko** and **Thomas Westerberg**, for always finding a way around varied IT related problems.

To those who ensure the seamless running of our division at Karolinska Institutet, and who have kindly helped me with the varied and often challenging administrative tasks, both big and small: **Catarina Cleveson, Anette Eidehall, Sofia Fridén, Annette Karlsson, Agneta Lindahl**, and **Maggie Lukasiewicz**. **Selma Wolofsky**, thank you for being so great during my brief stint as a KI web editor.

Alan Evans, Serge Gauthier, and Pedro Rosa-Neto, thank you for your time and valuable guidance over the years. Your continued support and mentorship means a great deal to me.

To **Michael, Nick, Eva, Meera,** and **Johan**, thank you for turning Gothenburg into such a warm and welcoming place. To **Eduardo**, for your support and dependability all these years.

To **Knut, Agneta, Carin, Krister, Ellen,** and **Olle**: You have enriched my life immeasurably and helped make Sweden feel like home. Thank you for everything, especially for taking such excellent care of Ben.

Camilla and **Magnus, Lina** and **Gustav**, **Karin, Eva** and **Stefan**; for being such a pleasure to hang out with and for being good sports about me learning Swedish.

To **Josh**; 15 years of friendship and still going strong, despite the distance. To **Jessie** and **Allan**, for being you. **Linda**, for your shared appreciation of many things I hold dear.

Nina, for being such a great sister; **Robin**, for being a stand-up guy. It's such a pleasure watching **Leo** and **Oliver** grow up.

To my parents, **Vincent** and **Ingrid**; for being there through thick and thin, for your unwavering patience, commitment, support, and love over all these years. This one's for you.

To my darling wife, **Kerstin**; spanning time with you is like a dream. I never knew how bright life could be before I met you.

This thesis was supported by grants from the Axel Linder Foundation, the Dementia Foundation (Demensfonden), the European Research Council, the EU FW7 large-scale integrating project (INMiND), the Gun and Bertil Stohne Foundation, the Hans Osterman's Foundation, the KI Research Foundation, the Knut and Alice Wallenberg Foundation, KTH-SLL, the Old Servants Foundation, the Sigurd and Elsa Goljes Memorial, the Strategic Research Programme in Neuroscience at Karolinska Institutet, the Swedish Alzheimer's Foundation (Alzheimerfonden), the Swedish Brain Foundation (Hjärnfonden), the Swedish Foundation for Strategic Research (SSF), the Swedish Research Council (05817, 02695, 06086), the Regional Agreement on Medical Training and Clinical Research (ALF) for Stockholm County Council, the Torsten Söderberg Foundation, the Wenner-Gren Foundation, and Vinnova.

8 REFERENCES

1. Blazer DG, Yaffe K, Liverman CT, eds. Cognitive Aging: Progress in Understanding and Opportunities for Action.Washington, DC: National Academies Press; 2015. http://www.iom.edu/cognitiveaging. Accessed April 10, 2018.
2. Blazer DG, Yaffe K, Karlawish J. Cognitive aging: a report from the Institute of Medicine. *JAMA*. 2015;313(21):2121-2122.
3. American Psychiatric Association. Diagnostic and Statistical Manual of Mental Disorders. 4th ed. Washington, DC: American Psychiatric Association; 1994.
4. Prince M, Comas-Herrera A, Knapp M, Guerchet M, Karagiannidou M. World Alzheimer Report 2016: Improving healthcare for people with dementia. London, UK: Alzheimer's Disease International; 2016. https://www.alz.co.uk/research/ Accessed May 7, 2018.
5. Winblad B, Amouyel P, Andrieu S, et al. Defeating Alzheimer's disease and other dementias: a priority for European science and society. *Lancet Neurol.* 2016;15(5):455-532.
6. United Nations, Department of Economic and Social Affairs, Population Division. World Population Prospects: The 2017 Revision, Key Findings and Advance Tables. New York, NY: United Nations, Department of Economic and Social Affairs; 2017. https://www.un.org/development/desa/publications. Accessed April 10, 2018.
7. World Health Organization and Alzheimer's Disease International. Dementia: a public health priority. Geneva, Switzerland: World Health Organization; 2012. http://www.who.int/mental_health/publications. Accessed April 10, 2018.
8. World Health Organization. First WHO Ministerial Conference on Global Action Against Dementia. Geneva, Switzerland: World Health Organization; 2015. http:// www.who.int/mental_health/neurology/dementia. Accessed April 10, 2018.
9. James BD, Wilson RS, Boyle PA, Trojanowski JQ, Bennett DA, Schneider JA. TDP-43 stage, mixed pathologies, and clinical Alzheimer's-type dementia. *Brain.* 2016;139(11):2983-2993.
10. Schneider JA, Arvanitakis Z, Bang W, Bennett DA. Mixed brain pathologies account for most dementia cases in community-dwelling older persons. *Neurology.* 2007;69(24):2197-2204.
11. Fleminger S, Oliver DL, Lovestone S, Rabe-Hesketh S, Giora A. Head injury as a risk factor for Alzheimer's disease: the evidence 10 years on; a partial replication. *J Neurol Neurosurg Psychiatry.* 2003;74(7):857-862.
12. Aarsland D, Andersen K, Larsen JP, Lolk A, Nielsen H, Kragh-Sorensen P. Risk of dementia in Parkinson's disease: a community-based, prospective study. *Neurology.* 2001;56(6):730-736.

13. Rabinovici GD, Wang PN, Levin J, et al. First symptom in sporadic Creutzfeldt-Jakob disease. *Neurology.* 2006;66(2):286-287.

14. Holland AJ, Hon J, Huppert FA, Stevens F, Watson P. Population-based study of the prevalence and presentation of dementia in adults with Down's syndrome. *Br J Psychiatry.* 1998;172:493-498.

15. Tripathi M, Vibha D. Reversible dementias. *Indian J Psychiatry.* 2009;51 Suppl 1:S52-55.

16. Abdulrab K, Heun R. Subjective Memory Impairment. A review of its definitions indicates the need for a comprehensive set of standardised and validated criteria. *Eur Psychiatry.* 2008;23(5):321-330.

17. Ossenkoppele R, Jagust WJ. The Complexity of Subjective Cognitive Decline. *JAMA Neurol.* 2017;74(12):1400-1402.

18. Reisberg B, Ferris SH, de Leon MJ, Crook T. The Global Deterioration Scale for assessment of primary degenerative dementia. *Am J Psychiatry.* 1982;139(9):1136-1139.

19. Mitchell AJ, Beaumont H, Ferguson D, Yadegarfar M, Stubbs B. Risk of dementia and mild cognitive impairment in older people with subjective memory complaints: meta-analysis. *Acta Psychiatr Scand.* 2014;130(6):439-451.

20. Rami L, Fortea J, Bosch B, et al. Cerebrospinal fluid biomarkers and memory present distinct associations along the continuum from healthy subjects to AD patients. *J Alzheimers Dis.* 2011;23(2):319-326.

21. Perrotin A, Mormino EC, Madison CM, Hayenga AO, Jagust WJ. Subjective cognition and amyloid deposition imaging: a Pittsburgh Compound B positron emission tomography study in normal elderly individuals. *Arch Neurol.* 2012;69(2):223-229.

22. Visser PJ, Verhey F, Knol DL, et al. Prevalence and prognostic value of CSF markers of Alzheimer's disease pathology in patients with subjective cognitive impairment or mild cognitive impairment in the DESCRIPA study: a prospective cohort study. *Lancet Neurol.* 2009;8(7):619-627.

23. Saykin AJ, Wishart HA, Rabin LA, et al. Older adults with cognitive complaints show brain atrophy similar to that of amnestic MCI. *Neurology.* 2006;67(5):834-842.

24. Scheef L, Spottke A, Daerr M, et al. Glucose metabolism, gray matter structure, and memory decline in subjective memory impairment. *Neurology.* 2012;79(13):1332-1339.

25. Tepest R, Wang L, Csernansky JG, et al. Hippocampal surface analysis in subjective memory impairment, mild cognitive impairment and Alzheimer's dementia. *Dement Geriatr Cogn Disord.* 2008;26(4):323-329.

26. Wang Y, Risacher SL, West JD, et al. Altered default mode network connectivity in older adults with cognitive complaints and amnestic mild cognitive impairment. *J Alzheimers Dis.* 2013;35(4):751-760.

27. Lopez-Sanz D, Bruna R, Garces P, et al. Functional Connectivity Disruption in Subjective Cognitive Decline and Mild Cognitive Impairment: A Common Pattern of Alterations. *Front Aging Neurosci.* 2017;9:109.

28. Jessen F, Amariglio RE, van Boxtel M, et al. A conceptual framework for research on subjective cognitive decline in preclinical Alzheimer's disease. *Alzheimers Dement.* 2014;10(6):844-852.

29. Molinuevo JL, Rabin LA, Amariglio R, et al. Implementation of subjective cognitive decline criteria in research studies. *Alzheimers Dement.* 2017;13(3):296-311.

30. Petersen RC, Smith GE, Waring SC, Ivnik RJ, Tangalos EG, Kokmen E. Mild cognitive impairment: clinical characterization and outcome. *Arch Neurol.* 1999;56(3):303-308.

31. Flicker C, Ferris SH, Reisberg B. Mild cognitive impairment in the elderly: predictors of dementia. *Neurology.* 1991;41(7):1006-1009.

32. Smith GE, Petersen RC, Parisi JE, et al. Definition, course, and outcome of mild cognitive impairment. *Aging, Neuropsychology, and Cognition.* 1996;3(2):141-147.

33. Koepsell TD, Monsell SE. Reversion from mild cognitive impairment to normal or near-normal cognition: risk factors and prognosis. *Neurology.* 2012;79(15):1591-1598.

34. Breitner JC. Mild cognitive impairment and progression to dementia: new findings. *Neurology.* 2014;82(4):e34-35.

35. Winblad B, Palmer K, Kivipelto M, et al. Mild cognitive impairment--beyond controversies, towards a consensus: report of the International Working Group on Mild Cognitive Impairment. *J Intern Med.* 2004;256(3):240-246.

36. Petersen RC. Mild cognitive impairment as a diagnostic entity. *J Intern Med.* 2004;256(3):183-194.

37. Petersen RC, Doody R, Kurz A, et al. Current concepts in mild cognitive impairment. *Arch Neurol.* 2001;58(12):1985-1992.

38. Dubois B. 'Prodromal Alzheimer's disease': a more useful concept than mild cognitive impairment? *Curr Opin Neurol.* 2000;13(4):367-369.

39. Dubois B, Albert ML. Amnestic MCI or prodromal Alzheimer's disease? *Lancet Neurol.* 2004;3(4):246-248.

40. Tounsi H, Deweer B, Ergis AM, et al. Sensitivity to semantic cuing: an index of episodic memory dysfunction in early Alzheimer disease. *Alzheimer Dis Assoc Disord.* 1999;13(1):38-46.

41. Dubois B, Feldman HH, Jacova C, et al. Research criteria for the diagnosis of Alzheimer's disease: revising the NINCDS-ADRDA criteria. *Lancet Neurol.* 2007;6(8):734-746.

42. Dubois B, Feldman HH, Jacova C, et al. Revising the definition of Alzheimer's disease: a new lexicon. *Lancet Neurol.* 2010;9(11):1118-1127.

43. Dubois B, Feldman HH, Jacova C, et al. Advancing research diagnostic criteria for Alzheimer's disease: the IWG-2 criteria. *Lancet Neurol.* 2014;13(6):614-629.

44. Albert MS, DeKosky ST, Dickson D, et al. The diagnosis of mild cognitive impairment due to Alzheimer's disease: recommendations from the National Institute on Aging-Alzheimer's Association workgroups on diagnostic guidelines for Alzheimer's disease. *Alzheimers Dement.* 2011;7(3):270-279.

45. McKhann G, Drachman D, Folstein M, Katzman R, Price D, Stadlan EM. Clinical diagnosis of Alzheimer's disease: report of the NINCDS-ADRDA Work Group under the auspices of Department of Health and Human Services Task Force on Alzheimer's Disease. *Neurology.* 1984;34(7):939-944.

46. Jack CR, Jr., Albert MS, Knopman DS, et al. Introduction to the recommendations from the National Institute on Aging-Alzheimer's Association workgroups on diagnostic guidelines for Alzheimer's disease. *Alzheimers Dement.* 2011;7(3):257-262.

47. Duyckaerts C, Delatour B, Potier MC. Classification and basic pathology of Alzheimer disease. *Acta Neuropathol.* 2009;118(1):5-36.

48. Thal DR, Walter J, Saido TC, Fandrich M. Neuropathology and biochemistry of Abeta and its aggregates in Alzheimer's disease. *Acta Neuropathol.* 2015;129(2):167-182.

49. Labbadia J, Morimoto RI. The biology of proteostasis in aging and disease. *Annu Rev Biochem.* 2015;84:435-464.

50. Nixon RA. The role of autophagy in neurodegenerative disease. *Nat Med.* 2013;19(8):983-997.

51. Zhao Z, Sagare AP, Ma Q, et al. Central role for PICALM in amyloid-beta blood-brain barrier transcytosis and clearance. *Nat Neurosci.* 2015;18(7):978-987.

52. Verghese PB, Castellano JM, Garai K, et al. ApoE influences amyloid-beta (Abeta) clearance despite minimal apoE/Abeta association in physiological conditions. *Proc Natl Acad Sci U S A.* 2013;110(19):E1807-1816.

53. Harper JD, Wong SS, Lieber CM, Lansbury PT. Observation of metastable Abeta amyloid protofibrils by atomic force microscopy. *Chem Biol.* 1997;4(2):119-125.

54. Lambert MP, Barlow AK, Chromy BA, et al. Diffusible, nonfibrillar ligands derived from Abeta1-42 are potent central nervous system neurotoxins. *Proc Natl Acad Sci U S A.* 1998;95(11):6448-6453.

55. Kumar S, Rezaei-Ghaleh N, Terwel D, et al. Extracellular phosphorylation of the amyloid beta-peptide promotes formation of toxic aggregates during the pathogenesis of Alzheimer's disease. *EMBO J.* 2011;30(11):2255-2265.

56. Saido TC, Yamao-Harigaya W, Iwatsubo T, Kawashima S. Amino- and carboxyl-terminal heterogeneity of beta-amyloid peptides deposited in human brain. *Neurosci Lett.* 1996;215(3):173-176.

57. Joachim CL, Morris JH, Selkoe DJ. Clinically diagnosed Alzheimer's disease: autopsy results in 150 cases. *Ann Neurol.* 1988;24(1):50-56.

58. Delaere P, Duyckaerts C, He Y, Piette F, Hauw JJ. Subtypes and differential laminar distributions of beta A4 deposits in Alzheimer's disease: relationship with the intellectual status of 26 cases. *Acta Neuropathol.* 1991;81(3):328-335.

59. Wisniewski HM, Sadowski M, Jakubowska-Sadowska K, Tarnawski M, Wegiel J. Diffuse, lake-like amyloid-beta deposits in the parvopyramidal layer of the presubiculum in Alzheimer disease. *J Neuropathol Exp Neurol.* 1998;57(7):674-683.

60. Thal DR, Sassin I, Schultz C, Haass C, Braak E, Braak H. Fleecy amyloid deposits in the internal layers of the human entorhinal cortex are comprised of N-terminal truncated fragments of Abeta. *J Neuropathol Exp Neurol.* 1999;58(2):210-216.

61. Wisniewski H, Terry R. Reexamination of the pathogenesis of the senile plaques. In: HM Z, ed. *Progress in Neuropathology*. New York: Grune & Straton; 1973:1-15.

62. Ikeda S, Allsop D, Glenner GG. Morphology and distribution of plaque and related deposits in the brains of Alzheimer's disease and control cases. An immunohistochemical study using amyloid beta-protein antibody. *Lab Invest.* 1989;60(1):113-122.

63. Braak H, Braak E. Neuropathological stageing of Alzheimer-related changes. *Acta Neuropathol.* 1991;82(4):239-259.

64. Thal DR, Rub U, Orantes M, Braak H. Phases of A beta-deposition in the human brain and its relevance for the development of AD. *Neurology.* 2002;58(12):1791-1800.

65. Thal DR, Rub U, Schultz C, et al. Sequence of Abeta-protein deposition in the human medial temporal lobe. *J Neuropathol Exp Neurol.* 2000;59(8):733-748.

66. Grothe MJ, Barthel H, Sepulcre J, et al. In vivo staging of regional amyloid deposition. *Neurology.* 2017;89(20):2031-2038.

67. Goedert M, Spillantini MG. A century of Alzheimer's disease. *Science.* 2006;314(5800):777-781.

68. Neve RL, Harris P, Kosik KS, Kurnit DM, Donlon TA. Identification of cDNA clones for the human microtubule-associated protein tau and chromosomal localization of the genes for tau and microtubule-associated protein 2. *Brain Res.* 1986;387(3):271-280.

69. Goedert M, Spillantini MG, Jakes R, Rutherford D, Crowther RA. Multiple isoforms of human microtubule-associated protein tau: sequences and localization in neurofibrillary tangles of Alzheimer's disease. *Neuron.* 1989;3(4):519-526.

70. Andreadis A, Brown WM, Kosik KS. Structure and novel exons of the human tau gene. *Biochemistry.* 1992;31(43):10626-10633.

71. Buee L, Bussiere T, Buee-Scherrer V, Delacourte A, Hof PR. Tau protein isoforms, phosphorylation and role in neurodegenerative disorders. *Brain Res Brain Res Rev.* 2000;33(1):95-130.

72. Murray ME, Kouri N, Lin WL, Jack CR, Jr., Dickson DW, Vemuri P. Clinicopathologic assessment and imaging of tauopathies in neurodegenerative dementias. *Alzheimers Res Ther.* 2014;6(1):1.

73. Gotz J, Probst A, Spillantini MG, et al. Somatodendritic localization and hyperphosphorylation of tau protein in transgenic mice expressing the longest human brain tau isoform. *EMBO J.* 1995;14(7):1304-1313.

74. Delacourte A. Tauopathies: recent insights into old diseases. *Folia Neuropathol.* 2005;43(4):244-257.

75. Sergeant N, Delacourte A, Buee L. Tau protein as a differential biomarker of tauopathies. *Biochim Biophys Acta.* 2005;1739(2-3):179-197.

76. Crowther RA. Straight and paired helical filaments in Alzheimer disease have a common structural unit. *Proc Natl Acad Sci U S A.* 1991;88(6):2288-2292.

77. Grundke-Iqbal I, Iqbal K, Tung YC, Quinlan M, Wisniewski HM, Binder LI. Abnormal phosphorylation of the microtubule-associated protein tau (tau) in Alzheimer cytoskeletal pathology. *Proc Natl Acad Sci U S A.* 1986;83(13):4913-4917.

78. Arriagada PV, Growdon JH, Hedley-Whyte ET, Hyman BT. Neurofibrillary tangles but not senile plaques parallel duration and severity of Alzheimer's disease. *Neurology.* 1992;42(3 Pt 1):631-639.

79. Delacourte A, David JP, Sergeant N, et al. The biochemical pathway of neurofibrillary degeneration in aging and Alzheimer's disease. *Neurology.* 1999;52(6):1158-1165.

80. Scholl M, Lockhart SN, Schonhaut DR, et al. PET Imaging of Tau Deposition in the Aging Human Brain. *Neuron.* 2016;89(5):971-982.

81. Schwarz AJ, Yu P, Miller BB, et al. Regional profiles of the candidate tau PET ligand 18F-AV-1451 recapitulate key features of Braak histopathological stages. *Brain.* 2016;139(Pt 5):1539-1550.

82. Cho H, Choi JY, Hwang MS, et al. In vivo cortical spreading pattern of tau and amyloid in the Alzheimer disease spectrum. *Ann Neurol.* 2016;80(2):247-258.

83. Jones DT, Graff-Radford J, Lowe VJ, et al. Tau, amyloid, and cascading network failure across the Alzheimer's disease spectrum. *Cortex.* 2017;97:143-159.

84. Jack CR, Jr., Wiste HJ, Schwarz CG, et al. Longitudinal tau PET in ageing and Alzheimer's disease. *Brain.* 2018;141(5):1517-1528.

85. Gonatas NK, Anderson W, Evangelista I. The contribution of altered synapses in the senile plaque: an electron microscopic study in Alzheimer's dementia. *J Neuropathol Exp Neurol.* 1967;26(1):25-39.

86. Masliah E, Mallory M, Alford M, et al. Altered expression of synaptic proteins occurs early during progression of Alzheimer's disease. *Neurology.* 2001;56(1):127-129.

87. Terry RD, Masliah E, Salmon DP, et al. Physical basis of cognitive alterations in Alzheimer's disease: synapse loss is the major correlate of cognitive impairment. *Ann Neurol.* 1991;30(4):572-580.

88. Blennow K, Bogdanovic N, Alafuzoff I, Ekman R, Davidsson P. Synaptic pathology in Alzheimer's disease: relation to severity of dementia, but not to senile plaques, neurofibrillary tangles, or the ApoE4 allele. *J Neural Transm (Vienna).* 1996;103(5):603-618.

89. Dickson DW, Crystal HA, Bevona C, Honer W, Vincent I, Davies P. Correlations of synaptic and pathological markers with cognition of the elderly. *Neurobiol Aging.* 1995;16(3):285-298; discussion 298-304.

90. Mukaetova-Ladinska EB, Garcia-Siera F, Hurt J, et al. Staging of cytoskeletal and beta-amyloid changes in human isocortex reveals biphasic synaptic protein response during progression of Alzheimer's disease. *Am J Pathol.* 2000;157(2):623-636.

91. Davidsson P, Blennow K. Neurochemical dissection of synaptic pathology in Alzheimer's disease. *Int Psychogeriatr.* 1998;10(1):11-23.

92. Brinkmalm A, Brinkmalm G, Honer WG, et al. SNAP-25 is a promising novel cerebrospinal fluid biomarker for synapse degeneration in Alzheimer's disease. *Mol Neurodegener.* 2014;9:53.

93. Reddy PH, Mani G, Park BS, et al. Differential loss of synaptic proteins in Alzheimer's disease: implications for synaptic dysfunction. *J Alzheimers Dis.* 2005;7(2):103-117; discussion 173-180.

94. Hubbard BM, Anderson JM. Age-related variations in the neuron content of the cerebral cortex in senile dementia of Alzheimer type. *Neuropathol Appl Neurobiol.* 1985;11(5):369-382.

95. Gomez-Isla T, Price JL, McKeel DW, Jr., Morris JC, Growdon JH, Hyman BT. Profound loss of layer II entorhinal cortex neurons occurs in very mild Alzheimer's disease. *J Neurosci.* 1996;16(14):4491-4500.

96. West MJ, Coleman PD, Flood DG, Troncoso JC. Differences in the pattern of hippocampal neuronal loss in normal ageing and Alzheimer's disease. *Lancet.* 1994;344(8925):769-772.

97. Grignon Y, Duyckaerts C, Bennecib M, Hauw JJ. Cytoarchitectonic alterations in the supramarginal gyrus of late onset Alzheimer's disease. *Acta Neuropathol.* 1998;95(4):395-406.

98. Gomez-Isla T, Hollister R, West H, et al. Neuronal loss correlates with but exceeds neurofibrillary tangles in Alzheimer's disease. *Ann Neurol.* 1997;41(1):17-24.

99. Serrano-Pozo A, Frosch MP, Masliah E, Hyman BT. Neuropathological alterations in Alzheimer disease. *Cold Spring Harb Perspect Med.* 2011;1(1):a006189.

100. Eikelenboom P, Stam FC. Immunoglobulins and complement factors in senile plaques. An immunoperoxidase study. *Acta neuropathologica.* 1982;57(2-3):239-242.

101. Eikelenboom P, Hack CE, Rozemuller JM, Stam FC. Complement activation in amyloid plaques in Alzheimer's dementia. *Virchows Archiv B, Cell pathology including molecular pathology.* 1989;56(4):259-262.

102. Griffin WS, Stanley LC, Ling C, et al. Brain interleukin 1 and S-100 immunoreactivity are elevated in Down syndrome and Alzheimer disease. *Proceedings of the National Academy of Sciences of the United States of America.* 1989;86(19):7611-7615.

103. Eikelenboom P, van Gool WA. Neuroinflammatory perspectives on the two faces of Alzheimer's disease. *J Neural Transm.* 2004;111(3):281-294.

104. Akiyama H, Barger S, Barnum S, et al. Inflammation and Alzheimer's disease. *Neurobiology of aging.* 2000;21(3):383-421.

105. Verkhratsky A, Olabarria M, Noristani HN, Yeh CY, Rodriguez JJ. Astrocytes in Alzheimer's disease. *Neurotherapeutics : the journal of the American Society for Experimental NeuroTherapeutics.* 2010;7(4):399-412.

106. Itagaki S, McGeer PL, Akiyama H, Zhu S, Selkoe D. Relationship of microglia and astrocytes to amyloid deposits of Alzheimer disease. *Journal of neuroimmunology.* 1989;24(3):173-182.

107. Mandrekar S, Jiang Q, Lee CY, Koenigsknecht-Talboo J, Holtzman DM, Landreth GE. Microglia mediate the clearance of soluble Abeta through fluid phase macropinocytosis. *J Neurosci.* 2009;29(13):4252-4262.

108. Akiyama H, Mori H, Saido T, Kondo H, Ikeda K, McGeer PL. Occurrence of the diffuse amyloid beta-protein (Abeta) deposits with numerous Abeta-containing glial cells in the cerebral cortex of patients with Alzheimer's disease. *Glia.* 1999;25(4):324-331.

109. Bamberger ME, Harris ME, McDonald DR, Husemann J, Landreth GE. A cell surface receptor complex for fibrillar beta-amyloid mediates microglial activation. *J Neurosci.* 2003;23(7):2665-2674.

110. Oide T, Kinoshita T, Arima K. Regression stage senile plaques in the natural course of Alzheimer's disease. *Neuropathol Appl Neurobiol.* 2006;32(5):539-556.

111. Cairns NJ, Chadwick A, Luthert PJ, Lantos PL. Astrocytosis, beta A4-protein deposition and paired helical filament formation in Alzheimer's disease. *J Neurol Sci.* 1992;112(1-2):68-75.

112. Wharton SB, O'Callaghan JP, Savva GM, et al. Population variation in glial fibrillary acidic protein levels in brain ageing: relationship to Alzheimer-type pathology and dementia. *Dement Geriatr Cogn Disord.* 2009;27(5):465-473.

113. DiPatre PL, Gelman BB. Microglial cell activation in aging and Alzheimer disease: partial linkage with neurofibrillary tangle burden in the hippocampus. *J Neuropathol Exp Neurol.* 1997;56(2):143-149.

114. Boche D, Nicoll JA. The role of the immune system in clearance of Abeta from the brain. *Brain Pathol.* 2008;18(2):267-278.

115. De Strooper B, Karran E. The Cellular Phase of Alzheimer's Disease. *Cell.* 2016;164(4):603-615.

116. Fan Z, Brooks DJ, Okello A, Edison P. An early and late peak in microglial activation in Alzheimer's disease trajectory. *Brain.* 2017.

117. Fan Z, Okello AA, Brooks DJ, Edison P. Longitudinal influence of microglial activation and amyloid on neuronal function in Alzheimer's disease. *Brain.* 2015;138(Pt 12):3685-3698.

118. Heslegrave A, Heywood W, Paterson R, et al. Increased cerebrospinal fluid soluble TREM2 concentration in Alzheimer's disease. *Mol Neurodegener.* 2016;11:3.

119. Suarez-Calvet M, Kleinberger G, Araque Caballero MA, et al. sTREM2 cerebrospinal fluid levels are a potential biomarker for microglia activity in early-stage

Alzheimer's disease and associate with neuronal injury markers. *EMBO Mol Med.* 2016;8(5):466-476.

120. Ksiezak-Reding H, Tracz E, Yang LS, Dickson DW, Simon M, Wall JS. Ultrastructural instability of paired helical filaments from corticobasal degeneration as examined by scanning transmission electron microscopy. *Am J Pathol.* 1996;149(2):639-651.
121. Mirra SS, Heyman A, McKeel D, et al. The Consortium to Establish a Registry for Alzheimer's Disease (CERAD). Part II. Standardization of the neuropathologic assessment of Alzheimer's disease. *Neurology.* 1991;41(4):479-486.
122. Consensus recommendations for the postmortem diagnosis of Alzheimer's disease. The National Institute on Aging, and Reagan Institute Working Group on Diagnostic Criteria for the Neuropathological Assessment of Alzheimer's Disease. *Neurobiol Aging.* 1997;18(4 Suppl):S1-2.
123. Hyman BT, Phelps CH, Beach TG, et al. National Institute on Aging-Alzheimer's Association guidelines for the neuropathologic assessment of Alzheimer's disease. *Alzheimers Dement.* 2012;8(1):1-13.
124. Braak H, Alafuzoff I, Arzberger T, Kretzschmar H, Del Tredici K. Staging of Alzheimer disease-associated neurofibrillary pathology using paraffin sections and immunocytochemistry. *Acta Neuropathol.* 2006;112(4):389-404.
125. Selkoe DJ. The molecular pathology of Alzheimer's disease. *Neuron*. 1991;6(4):487-498.
126. Beyreuther K, Masters CL. Amyloid precursor protein (APP) and beta A4 amyloid in the etiology of Alzheimer's disease: precursor-product relationships in the derangement of neuronal function. *Brain Pathol.* 1991;1(4):241-251.
127. Hardy J, Allsop D. Amyloid deposition as the central event in the aetiology of Alzheimer's disease. *Trends Pharmacol Sci.* 1991;12(10):383-388.
128. Hardy JA, Higgins GA. Alzheimer's disease: the amyloid cascade hypothesis. *Science.* 1992;256(5054):184-185.
129. Kang J, Lemaire HG, Unterbeck A, et al. The precursor of Alzheimer's disease amyloid A4 protein resembles a cell-surface receptor. *Nature.* 1987;325(6106):733-736.
130. Robakis NK, Ramakrishna N, Wolfe G, Wisniewski HM. Molecular cloning and characterization of a cDNA encoding the cerebrovascular and the neuritic plaque amyloid peptides. *Proc Natl Acad Sci U S A.* 1987;84(12):4190-4194.
131. Goldgaber D, Lerman MI, McBride OW, Saffiotti U, Gajdusek DC. Characterization and chromosomal localization of a cDNA encoding brain amyloid of Alzheimer's disease. *Science.* 1987;235(4791):877-880.
132. Tanzi RE, Gusella JF, Watkins PC, et al. Amyloid beta protein gene: cDNA, mRNA distribution, and genetic linkage near the Alzheimer locus. *Science.* 1987;235(4791):880-884.
133. Olson MI, Shaw CM. Presenile dementia and Alzheimer's disease in mongolism. *Brain.* 1969;92(1):147-156.

134. Goate A, Chartier-Harlin MC, Mullan M, et al. Segregation of a missense mutation in the amyloid precursor protein gene with familial Alzheimer's disease. *Nature.* 1991;349(6311):704-706.

135. Mullan M, Crawford F, Axelman K, et al. A pathogenic mutation for probable Alzheimer's disease in the APP gene at the N-terminus of beta-amyloid. *Nat Genet.* 1992;1(5):345-347.

136. Hardy J, Selkoe DJ. The amyloid hypothesis of Alzheimer's disease: progress and problems on the road to therapeutics. *Science.* 2002;297(5580):353-356.

137. Walsh DM, Klyubin I, Fadeeva JV, et al. Naturally secreted oligomers of amyloid beta protein potently inhibit hippocampal long-term potentiation in vivo. *Nature.* 2002;416(6880):535-539.

138. Hardy J. The amyloid hypothesis for Alzheimer's disease: a critical reappraisal. *J Neurochem.* 2009;110(4):1129-1134.

139. Price JL, Morris JC. Tangles and plaques in nondemented aging and "preclinical" Alzheimer's disease. *Ann Neurol.* 1999;45(3):358-368.

140. Jack CR, Jr., Holtzman DM. Biomarker modeling of Alzheimer's disease. *Neuron.* 2013;80(6):1347-1358.

141. Villemagne VL, Pike KE, Chetelat G, et al. Longitudinal assessment of Abeta and cognition in aging and Alzheimer disease. *Ann Neurol.* 2011;69(1):181-192.

142. Popovitch ER, Wisniewski HM, Barcikowska M, et al. Alzheimer neuropathology in non-Down's syndrome mentally retarded adults. *Acta Neuropathol.* 1990;80(4):362-367.

143. Giannakopoulos P, Herrmann FR, Bussiere T, et al. Tangle and neuron numbers, but not amyloid load, predict cognitive status in Alzheimer's disease. *Neurology.* 2003;60(9):1495-1500.

144. Doody RS, Thomas RG, Farlow M, et al. Phase 3 trials of solanezumab for mild-to-moderate Alzheimer's disease. *N Engl J Med.* 2014;370(4):311-321.

145. Holmes C, Boche D, Wilkinson D, et al. Long-term effects of Abeta42 immunisation in Alzheimer's disease: follow-up of a randomised, placebo-controlled phase I trial. *Lancet.* 2008;372(9634):216-223.

146. Salloway S, Sperling R, Fox NC, et al. Two phase 3 trials of bapineuzumab in mild-to-moderate Alzheimer's disease. *N Engl J Med.* 2014;370(4):322-333.

147. Wiseman FK, Pulford LJ, Barkus C, et al. Trisomy of human chromosome 21 enhances amyloid-beta deposition independently of an extra copy of APP. *Brain.* 2018.

148. Heneka MT, O'Banion MK. Inflammatory processes in Alzheimer's disease. *J Neuroimmunol.* 2007;184(1-2):69-91.

149. Braak H, Del Tredici K. Amyloid-beta may be released from non-junctional varicosities of axons generated from abnormal tau-containing brainstem nuclei in sporadic Alzheimer's disease: a hypothesis. *Acta Neuropathol.* 2013;126(2):303-306.

150. Bartus RT, Dean RL, 3rd, Beer B, Lippa AS. The cholinergic hypothesis of geriatric memory dysfunction. *Science.* 1982;217(4558):408-414.

151. Bowen DM, Smith CB, White P, Davison AN. Neurotransmitter-related enzymes and indices of hypoxia in senile dementia and other abiotrophies. *Brain.* 1976;99(3):459-496.

152. Davies P, Maloney AJ. Selective loss of central cholinergic neurons in Alzheimer's disease. *Lancet.* 1976;2(8000):1403.

153. Mesulam M. A horseradish peroxidase method for the identification of the efferents of acetyl cholinesterase-containing neurons. *J Histochem Cytochem.* 1976;24(12):1281-1285.

154. Whitehouse PJ, Price DL, Clark AW, Coyle JT, DeLong MR. Alzheimer disease: evidence for selective loss of cholinergic neurons in the nucleus basalis. *Ann Neurol.* 1981;10(2):122-126.

155. Drachman DA, Leavitt J. Human memory and the cholinergic system. A relationship to aging? *Arch Neurol.* 1974;30(2):113-121.

156. Summers WK, Majovski LV, Marsh GM, Tachiki K, Kling A. Oral tetrahydroaminoacridine in long-term treatment of senile dementia, Alzheimer type. *N Engl J Med.* 1986;315(20):1241-1245.

157. Lovestone S, Howard R. Alzheimer's disease: a treatment in sight? *J Neurol Neurosurg Psychiatry.* 1995;59(6):566-567.

158. Massoud F, Gauthier S. Update on the pharmacological treatment of Alzheimer's disease. *Curr Neuropharmacol.* 2010;8(1):69-80.

159. Naugle RI, Cullum CM, Bigler ED. Evaluation of intellectual and memory function among dementia patients who were intellectually superior. *The Clinical Neuropsychologist.* 1990;4:355–374.

160. Stern Y. What is cognitive reserve? Theory and research application of the reserve concept. *J Int Neuropsychol Soc.* 2002;8(3):448-460.

161. Stern Y, Alexander GE, Prohovnik I, Mayeux R. Inverse relationship between education and parietotemporal perfusion deficit in Alzheimer's disease. *Ann Neurol.* 1992;32(3):371-375.

162. Stern Y, Alexander GE, Prohovnik I, et al. Relationship between lifetime occupation and parietal flow: implications for a reserve against Alzheimer's disease pathology. *Neurology.* 1995;45(1):55-60.

163. Rentz DM, Huh TJ, Faust RR, et al. Use of IQ-adjusted norms to predict progressive cognitive decline in highly intelligent older individuals. *Neuropsychology.* 2004;18(1):38-49.

164. Rentz DM, Huh TJ, Sardinha LM, et al. Intelligence quotient-adjusted memory impairment is associated with abnormal single photon emission computed tomography perfusion. *J Int Neuropsychol Soc.* 2007;13(5):821-831.

165. Alexander GE, Furey ML, Grady CL, et al. Association of premorbid intellectual function with cerebral metabolism in Alzheimer's disease: implications for the cognitive reserve hypothesis. *Am J Psychiatry.* 1997;154(2):165-172.

166. Schmand B, Geerlings MI, Jonker C, Lindeboom J. Reading ability as an estimator of premorbid intelligence: does it remain stable in emergent dementia? *J Clin Exp Neuropsychol.* 1998;20(1):42-51.

167. Hyman BT, Van Hoesen GW, Kromer LJ, Damasio AR. Perforant pathway changes and the memory impairment of Alzheimer's disease. *Ann Neurol.* 1986;20(4):472-481.

168. Van Hoesen GW. Ventromedial temporal lobe anatomy, with comments on Alzheimer's disease and temporal injury. *J Neuropsychiatry Clin Neurosci.* 1997;9(3):331-341.

169. de Toledo-Morrell L, Goncharova I, Dickerson B, Wilson RS, Bennett DA. From healthy aging to early Alzheimer's disease: in vivo detection of entorhinal cortex atrophy. *Ann N Y Acad Sci.* 2000;911:240-253.

170. Grady CL, Haxby JV, Horwitz B, et al. Longitudinal study of the early neuropsychological and cerebral metabolic changes in dementia of the Alzheimer type. *J Clin Exp Neuropsychol.* 1988;10(5):576-596.

171. Mendez MF, Mendez MA, Martin R, Smyth KA, Whitehouse PJ. Complex visual disturbances in Alzheimer's disease. *Neurology.* 1990;40(3 Pt 1):439-443.

172. Greene JD, Hodges JR, Baddeley AD. Autobiographical memory and executive function in early dementia of Alzheimer type. *Neuropsychologia.* 1995;33(12):1647-1670.

173. Hodges JR, Patterson K. Is semantic memory consistently impaired early in the course of Alzheimer's disease? Neuroanatomical and diagnostic implications. *Neuropsychologia.* 1995;33(4):441-459.

174. Locascio JJ, Growdon JH, Corkin S. Cognitive test performance in detecting, staging, and tracking Alzheimer's disease. *Arch Neurol.* 1995;52(11):1087-1099.

175. Binetti G, Cappa SF, Magni E, Padovani A, Bianchetti A, Trabucchi M. Visual and spatial perception in the early phase of Alzheimer's disease. *Neuropsychology.* 1998;12(1):29-33.

176. Perry RJ, Hodges JR. Attention and executive deficits in Alzheimer's disease. A critical review. *Brain.* 1999;122 (Pt 3):383-404.

177. Galton CJ, Patterson K, Xuereb JH, Hodges JR. Atypical and typical presentations of Alzheimer's disease: a clinical, neuropsychological, neuroimaging and pathological study of 13 cases. *Brain.* 2000;123 Pt 3:484-498.

178. Hansen L, Salmon D, Galasko D, et al. The Lewy body variant of Alzheimer's disease: a clinical and pathologic entity. *Neurology.* 1990;40(1):1-8.

179. Johnson DK, Morris JC, Galvin JE. Verbal and visuospatial deficits in dementia with Lewy bodies. *Neurology.* 2005;65(8):1232-1238.

180. Kraybill ML, Larson EB, Tsuang DW, et al. Cognitive differences in dementia patients with autopsy-verified AD, Lewy body pathology, or both. *Neurology.* 2005;64(12):2069-2073.

181. Ferman TJ, Smith GE, Boeve BF, et al. Neuropsychological differentiation of dementia with Lewy bodies from normal aging and Alzheimer's disease. *Clin Neuropsychol.* 2006;20(4):623-636.

182. Stavitsky K, Brickman AM, Scarmeas N, et al. The progression of cognition, psychiatric symptoms, and functional abilities in dementia with Lewy bodies and Alzheimer disease. *Arch Neurol.* 2006;63(10):1450-1456.

183. Weintraub S, Wicklund AH, Salmon DP. The neuropsychological profile of Alzheimer disease. *Cold Spring Harb Perspect Med.* 2012;2(4):a006171.

184. Weintraub S, Besser L, Dodge HH, et al. Version 3 of the Alzheimer Disease Centers' Neuropsychological Test Battery in the Uniform Data Set (UDS). *Alzheimer Dis Assoc Disord.* 2018;32(1):10-17.

185. Biomarkers Definitions Working G. Biomarkers and surrogate endpoints: preferred definitions and conceptual framework. *Clin Pharmacol Ther.* 2001;69(3):89-95.

186. Hampel H, Frank R, Broich K, et al. Biomarkers for Alzheimer's disease: academic, industry and regulatory perspectives. *Nat Rev Drug Discov.* 2010;9(7):560-574.

187. Mankoff DA. A definition of molecular imaging. *J Nucl Med.* 2007;48(6):18N, 21N.

188. Ossenkoppele R, Prins ND, van Berckel BN. Amyloid imaging in clinical trials. *Alzheimers Res Ther.* 2013;5(4):36.

189. Yaqub M, Tolboom N, Boellaard R, et al. Simplified parametric methods for [11C]PIB studies. *Neuroimage.* 2008;42(1):76-86.

190. van Berckel BN, Ossenkoppele R, Tolboom N, et al. Longitudinal amyloid imaging using 11C-PiB: methodologic considerations. *J Nucl Med.* 2013;54(9):1570-1576.

191. Pike VW. PET radiotracers: crossing the blood-brain barrier and surviving metabolism. *Trends Pharmacol Sci.* 2009;30(8):431-440.

192. Engler H, Damian A, Bentancourt C. PET and the multitracer concept in the study of neurodegenerative diseases. *Dement Neuropsychol.* 2015;9(4):343-349.

193. Green MV, Seidel J, Stein SD, et al. Head movement in normal subjects during simulated PET brain imaging with and without head restraint. *J Nucl Med.* 1994;35(9):1538-1546.

194. Herholz K, Nordberg A, Salmon E, et al. Impairment of neocortical metabolism predicts progression in Alzheimer's disease. *Dement Geriatr Cogn Disord.* 1999;10(6):494-504.

195. Montgomery AJ, Thielemans K, Mehta MA, Turkheimer F, Mustafovic S, Grasby PM. Correction of head movement on PET studies: comparison of methods. *J Nucl Med.* 2006;47(12):1936-1944.

196. Jin X, Mulnix T, Gallezot JD, Carson RE. Evaluation of motion correction methods in human brain PET imaging--a simulation study based on human motion data. *Med Phys.* 2013;40(10):102503.

197. Friston KJ, Ashburner J, Frith CD, Poline JB, Heather JD, Frackowiak RSJ. Spatial registration and normalization of images. *Hum Brain Mapp.* 1995;3:165-189.

198. Mintun MA, Raichle ME, Kilbourn MR, Wooten GF, Welch MJ. A quantitative model for the in vivo assessment of drug binding sites with positron emission tomography. *Ann Neurol.* 1984;15(3):217-227.

199. Minoshima S, Koeppe RA, Frey KA, Kuhl DE. Anatomic standardization: linear scaling and nonlinear warping of functional brain images. *J Nucl Med.* 1994;35(9):1528-1537.

200. Fox PT, Mintun MA, Reiman EM, Raichle ME. Enhanced detection of focal brain responses using intersubject averaging and change-distribution analysis of subtracted PET images. *J Cereb Blood Flow Metab.* 1988;8(5):642-653.

201. Mazziotta J, Toga A, Evans A, et al. A probabilistic atlas and reference system for the human brain: International Consortium for Brain Mapping (ICBM). *Philos Trans R Soc Lond B Biol Sci.* 2001;356(1412):1293-1322.

202. Mazziotta JC, Toga AW, Evans AC, Fox PT, Lancaster JL. Digital brain atlases. *Trends Neurosci.* 1995;18(5):210-211.

203. Madhavan A, Whitwell JL, Weigand SD, et al. FDG PET and MRI in logopenic primary progressive aphasia versus dementia of the Alzheimer's type. *PLoS One.* 2013;8(4):e62471.

204. Gunn RN, Gunn SR, Cunningham VJ. Positron emission tomography compartmental models. *J Cereb Blood Flow Metab.* 2001;21(6):635-652.

205. Innis RB, Cunningham VJ, Delforge J, et al. Consensus nomenclature for in vivo imaging of reversibly binding radioligands. *J Cereb Blood Flow Metab.* 2007;27(9):1533-1539.

206. Lammertsma AA, Hume SP. Simplified reference tissue model for PET receptor studies. *Neuroimage.* 1996;4(3 Pt 1):153-158.

207. Cunningham VJ, Hume SP, Price GR, Ahier RG, Cremer JE, Jones AK. Compartmental analysis of diprenorphine binding to opiate receptors in the rat in vivo and its comparison with equilibrium data in vitro. *J Cereb Blood Flow Metab.* 1991;11(1):1-9.

208. Lammertsma AA, Bench CJ, Hume SP, et al. Comparison of methods for analysis of clinical [11C]raclopride studies. *J Cereb Blood Flow Metab.* 1996;16(1):42-52.

209. Watabe H, Endres CJ, Breier A, Schmall B, Eckelman WC, Carson RE. Measurement of dopamine release with continuous infusion of [11C]raclopride: optimization and signal-to-noise considerations. *J Nucl Med.* 2000;41(3):522-530.

210. Logan J, Fowler JS, Volkow ND, Wang GJ, Ding YS, Alexoff DL. Distribution volume ratios without blood sampling from graphical analysis of PET data. *J Cereb Blood Flow Metab.* 1996;16(5):834-840.

211. Thie JA. Understanding the standardized uptake value, its methods, and implications for usage. *J Nucl Med.* 2004;45(9):1431-1434.

212. Lopresti BJ, Klunk WE, Mathis CA, et al. Simplified quantification of Pittsburgh Compound B amyloid imaging PET studies: a comparative analysis. *J Nucl Med.* 2005;46(12):1959-1972.

213. Gousias IS, Rueckert D, Heckemann RA, et al. Automatic segmentation of brain MRIs of 2-year-olds into 83 regions of interest. *Neuroimage.* 2008;40(2):672-684.

214. Hammers A, Allom R, Koepp MJ, et al. Three-dimensional maximum probability atlas of the human brain, with particular reference to the temporal lobe. *Hum Brain Mapp.* 2003;19(4):224-247.

215. Hammers A, Koepp MJ, Free SL, et al. Implementation and application of a brain template for multiple volumes of interest. *Hum Brain Mapp.* 2002;15(3):165-174.

216. Hammers A, Chen CH, Lemieux L, et al. Statistical neuroanatomy of the human inferior frontal gyrus and probabilistic atlas in a standard stereotaxic space. *Hum Brain Mapp.* 2007;28(1):34-48.

217. Aston JA, Cunningham VJ, Asselin MC, Hammers A, Evans AC, Gunn RN. Positron emission tomography partial volume correction: estimation and algorithms. *J Cereb Blood Flow Metab.* 2002;22(8):1019-1034.

218. Rousset O, Rahmim A, Alavi A, Zaidi H. Partial Volume Correction Strategies in PET. *PET Clin.* 2007;2(2):235-249.

219. Muller-Gartner HW, Links JM, Prince JL, et al. Measurement of radiotracer concentration in brain gray matter using positron emission tomography: MRI-based correction for partial volume effects. *J Cereb Blood Flow Metab.* 1992;12(4):571-583.

220. Thomas BA, Erlandsson K, Modat M, et al. The importance of appropriate partial volume correction for PET quantification in Alzheimer's disease. *Eur J Nucl Med Mol Imaging.* 2011;38(6):1104-1119.

221. Su Y, Blazey TM, Snyder AZ, et al. Partial volume correction in quantitative amyloid imaging. *Neuroimage.* 2015;107:55-64.

222. Klunk WE, Engler H, Nordberg A, et al. Imaging brain amyloid in Alzheimer's disease with Pittsburgh Compound-B. *Ann Neurol.* 2004;55(3):306-319.

223. Jack CR, Jr., Barrio JR, Kepe V. Cerebral amyloid PET imaging in Alzheimer's disease. *Acta Neuropathol.* 2013;126(5):643-657.

224. Rowe CC, Pejoska S, Mulligan RS, et al. Head-to-head comparison of 11C-PiB and 18F-AZD4694 (NAV4694) for beta-amyloid imaging in aging and dementia. *J Nucl Med.* 2013;54(6):880-886.

225. Rowe CC, Ng S, Ackermann U, et al. Imaging beta-amyloid burden in aging and dementia. *Neurology.* 2007;68(20):1718-1725.

226. Wong DF, Rosenberg PB, Zhou Y, et al. In vivo imaging of amyloid deposition in Alzheimer disease using the radioligand 18F-AV-45 (florbetapir [corrected] F 18). *J Nucl Med.* 2010;51(6):913-920.

227. Nelissen N, Van Laere K, Thurfjell L, et al. Phase 1 study of the Pittsburgh compound B derivative 18F-flutemetamol in healthy volunteers and patients with probable Alzheimer disease. *J Nucl Med.* 2009;50(8):1251-1259.

228. Ikonomovic MD, Klunk WE, Abrahamson EE, et al. Post-mortem correlates of in vivo PiB-PET amyloid imaging in a typical case of Alzheimer's disease. *Brain.* 2008;131(Pt 6):1630-1645.

229. Lowe VJ, Kemp BJ, Jack CR, Jr., et al. Comparison of 18F-FDG and PiB PET in cognitive impairment. *J Nucl Med.* 2009;50(6):878-886.

230. Kemppainen NM, Aalto S, Wilson IA, et al. Voxel-based analysis of PET amyloid ligand [11C]PIB uptake in Alzheimer disease. *Neurology.* 2006;67(9):1575-1580.

231. Rabinovici GD, Furst AJ, Alkalay A, et al. Increased metabolic vulnerability in early-onset Alzheimer's disease is not related to amyloid burden. *Brain.* 2010;133(Pt 2):512-528.

232. Mintun MA, Larossa GN, Sheline YI, et al. [11C]PIB in a nondemented population: potential antecedent marker of Alzheimer disease. *Neurology.* 2006;67(3):446-452.

233. Rowe CC, Ellis KA, Rimajova M, et al. Amyloid imaging results from the Australian Imaging, Biomarkers and Lifestyle (AIBL) study of aging. *Neurobiol Aging.* 2010;31(8):1275-1283.

234. Forsberg A, Engler H, Almkvist O, et al. PET imaging of amyloid deposition in patients with mild cognitive impairment. *Neurobiol Aging.* 2008;29(10):1456-1465.

235. Jagust WJ, Bandy D, Chen K, et al. The Alzheimer's Disease Neuroimaging Initiative positron emission tomography core. *Alzheimers Dement.* 2010;6(3):221-229.

236. Koivunen J, Scheinin N, Virta JR, et al. Amyloid PET imaging in patients with mild cognitive impairment: a 2-year follow-up study. *Neurology.* 2011;76(12):1085-1090.

237. Okello A, Koivunen J, Edison P, et al. Conversion of amyloid positive and negative MCI to AD over 3 years: an 11C-PIB PET study. *Neurology.* 2009;73(10):754-760.

238. Braak H, Braak E. Frequency of stages of Alzheimer-related lesions in different age categories. *Neurobiol Aging.* 1997;18(4):351-357.

239. Knopman DS, Parisi JE, Salviati A, et al. Neuropathology of cognitively normal elderly. *J Neuropathol Exp Neurol.* 2003;62(11):1087-1095.

240. Price JL, McKeel DW, Jr., Buckles VD, et al. Neuropathology of nondemented aging: presumptive evidence for preclinical Alzheimer disease. *Neurobiol Aging.* 2009;30(7):1026-1036.

241. Jack CR, Jr., Lowe VJ, Weigand SD, et al. Serial PIB and MRI in normal, mild cognitive impairment and Alzheimer's disease: implications for sequence of pathological events in Alzheimer's disease. *Brain.* 2009;132(Pt 5):1355-1365.

242. Clark CM, Pontecorvo MJ, Beach TG, et al. Cerebral PET with florbetapir compared with neuropathology at autopsy for detection of neuritic amyloid-beta plaques: a prospective cohort study. *Lancet Neurol.* 2012;11(8):669-678.

243. Rabinovici GD, Jagust WJ. Amyloid imaging in aging and dementia: testing the amyloid hypothesis in vivo. *Behav Neurol.* 2009;21(1):117-128.

244. Mattsson N, Insel PS, Donohue M, et al. Independent information from cerebrospinal fluid amyloid-beta and florbetapir imaging in Alzheimer's disease. *Brain.* 2015;138(Pt 3):772-783.

245. Vlassenko AG, Mintun MA, Xiong C, et al. Amyloid-beta plaque growth in cognitively normal adults: longitudinal [11C]Pittsburgh compound B data. *Ann Neurol.* 2011;70(5):857-861.

246. Villemagne VL, Burnham S, Bourgeat P, et al. Amyloid beta deposition, neurodegeneration, and cognitive decline in sporadic Alzheimer's disease: a prospective cohort study. *Lancet Neurol.* 2013;12(4):357-367.

247. Jack CR, Jr., Wiste HJ, Lesnick TG, et al. Brain beta-amyloid load approaches a plateau. *Neurology.* 2013;80(10):890-896.

248. Villain N, Chetelat G, Grassiot B, et al. Regional dynamics of amyloid-beta deposition in healthy elderly, mild cognitive impairment and Alzheimer's disease: a voxelwise PiB-PET longitudinal study. *Brain.* 2012;135(Pt 7):2126-2139.

249. Hardy J, De Strooper B. Alzheimer's disease: where next for anti-amyloid therapies? *Brain.* 2017;140(4):853-855.

250. Rowe CC, Ackerman U, Browne W, et al. Imaging of amyloid beta in Alzheimer's disease with 18F-BAY94-9172, a novel PET tracer: proof of mechanism. *Lancet Neurol.* 2008;7(2):129-135.

251. Buckley CJ, Sherwin PF, Smith AP, Wolber J, Weick SM, Brooks DJ. Validation of an electronic image reader training programme for interpretation of [18F]flutemetamol beta-amyloid PET brain images. *Nucl Med Commun.* 2017;38(3):234-241.

252. Seibyl J, Catafau AM, Barthel H, et al. Impact of Training Method on the Robustness of the Visual Assessment of 18F-Florbetaben PET Scans: Results from a Phase-3 Study. *J Nucl Med.* 2016;57(6):900-906.

253. Boccardi M, Altomare D, Ferrari C, et al. Assessment of the Incremental Diagnostic Value of Florbetapir F 18 Imaging in Patients With Cognitive Impairment: The Incremental Diagnostic Value of Amyloid PET With [18F]-Florbetapir (INDIA-FBP) Study. *JAMA Neurol.* 2016;73(12):1417-1424.

254. Ceccaldi M, Jonveaux T, Verger A, et al. Added value of (18)F-florbetaben amyloid PET in the diagnostic workup of most complex patients with dementia in France: A naturalistic study. *Alzheimers Dement.* 2017.

255. de Wilde A, van Maurik IS, Kunneman M, et al. Alzheimer's biomarkers in daily practice (ABIDE) project: Rationale and design. *Alzheimers Dement (Amst).* 2017;6:143-151.

256. Frisoni GB, Boccardi M, Barkhof F, et al. Strategic roadmap for an early diagnosis of Alzheimer's disease based on biomarkers. *Lancet Neurol.* 2017;16(8):661-676.

257. Johnson KA, Minoshima S, Bohnen NI, et al. Appropriate use criteria for amyloid PET: a report of the Amyloid Imaging Task Force, the Society of Nuclear Medicine and Molecular Imaging, and the Alzheimer's Association. *Alzheimers Dement.* 2013;9(1):e-1-16.

258. Johnson KA, Minoshima S, Bohnen NI, et al. Update on appropriate use criteria for amyloid PET imaging: dementia experts, mild cognitive impairment, and education. *J Nucl Med.* 2013;54(7):1011-1013.

259. McKhann GM, Knopman DS, Chertkow H, et al. The diagnosis of dementia due to Alzheimer's disease: recommendations from the National Institute on Aging-Alzheimer's Association workgroups on diagnostic guidelines for Alzheimer's disease. *Alzheimers Dement.* 2011;7(3):263-269.

260. Laforce R, Rosa-Neto P, Soucy JP, Rabinovici GD, Dubois B, Gauthier S. Canadian Consensus Guidelines on Use of Amyloid Imaging in Canada: Update and Future Directions from the Specialized Task Force on Amyloid imaging in Canada. *Can J Neurol Sci.* 2016;43(4):503-512.

261. Minoshima S, Drzezga AE, Barthel H, et al. SNMMI Procedure Standard/EANM Practice Guideline for Amyloid PET Imaging of the Brain 1.0. *J Nucl Med.* 2016;57(8):1316-1322.

262. Villemagne VL, Fodero-Tavoletti MT, Masters CL, Rowe CC. Tau imaging: early progress and future directions. *Lancet Neurol.* 2015;14(1):114-124.

263. Martin L, Latypova X, Terro F. Post-translational modifications of tau protein: implications for Alzheimer's disease. *Neurochem Int.* 2011;58(4):458-471.

264. Rosen RF, Walker LC, Levine H, 3rd. PIB binding in aged primate brain: enrichment of high-affinity sites in humans with Alzheimer's disease. *Neurobiol Aging.* 2011;32(2):223-234.

265. Mukaetova-Ladinska EB, Harrington CR, Roth M, Wischik CM. Biochemical and anatomical redistribution of tau protein in Alzheimer's disease. *Am J Pathol.* 1993;143(2):565-578.

266. Naslund J, Haroutunian V, Mohs R, et al. Correlation between elevated levels of amyloid beta-peptide in the brain and cognitive decline. *JAMA.* 2000;283(12):1571-1577.

267. Chien DT, Bahri S, Szardenings AK, et al. Early clinical PET imaging results with the novel PHF-tau radioligand [F-18]-T807. *J Alzheimers Dis.* 2013;34(2):457-468.

268. Maruyama M, Shimada H, Suhara T, et al. Imaging of tau pathology in a tauopathy mouse model and in Alzheimer patients compared to normal controls. *Neuron.* 2013;79(6):1094-1108.

269. Okamura N, Furumoto S, Harada R, et al. Novel 18F-labeled arylquinoline derivatives for noninvasive imaging of tau pathology in Alzheimer disease. *J Nucl Med.* 2013;54(8):1420-1427.

270. Harada R, Okamura N, Furumoto S, et al. 18F-THK5351: A Novel PET Radiotracer for Imaging Neurofibrillary Pathology in Alzheimer Disease. *J Nucl Med.* 2016;57(2):208-214.

271. Xia CF, Arteaga J, Chen G, et al. [(18)F]T807, a novel tau positron emission tomography imaging agent for Alzheimer's disease. *Alzheimers Dement.* 2013;9(6):666-676.

272. Declercq L, Rombouts F, Koole M, et al. Preclinical Evaluation of (18)F-JNJ64349311, a Novel PET Tracer for Tau Imaging. *J Nucl Med.* 2017;58(6):975-981.

273. Gobbi LC, Knust H, Korner M, et al. Identification of Three Novel Radiotracers for Imaging Aggregated Tau in Alzheimer's Disease with Positron Emission Tomography. *J Med Chem.* 2017;60(17):7350-7370.

274. Walji AM, Hostetler ED, Selnick H, et al. Discovery of 6-(Fluoro-(18)F)-3-(1H-pyrrolo[2,3-c]pyridin-1-yl)isoquinolin-5-amine ([(18)F]-MK-6240): A Positron Emission Tomography (PET) Imaging Agent for Quantification of Neurofibrillary Tangles (NFTs). *J Med Chem.* 2016;59(10):4778-4789.

275. Mueller A, Kroth H, Berndt M, et al. Characterization of the novel PET Tracer PI-2620 for the assessment of Tau pathology in Alzheimer's disease and other tauopathies. *J Nucl Med* 2017;58:847.

276. Villemagne VL, Dore V, Burnham SC, Masters CL, Rowe CC. Imaging tau and amyloid-beta proteinopathies in Alzheimer disease and other conditions. *Nat Rev Neurol.* 2018.

277. Marquie M, Normandin MD, Vanderburg CR, et al. Validating novel tau positron emission tomography tracer [F-18]-AV-1451 (T807) on postmortem brain tissue. *Ann Neurol.* 2015;78(5):787-800.

278. Lemoine L, Saint-Aubert L, Marutle A, et al. Visualization of regional tau deposits using (3)H-THK5117 in Alzheimer brain tissue. *Acta Neuropathol Commun.* 2015;3:40.

279. Johnson KA, Schultz A, Betensky RA, et al. Tau positron emission tomographic imaging in aging and early Alzheimer disease. *Ann Neurol.* 2016;79(1):110-119.

280. Chiotis K, Saint-Aubert L, Savitcheva I, et al. Imaging in-vivo tau pathology in Alzheimer's disease with THK5317 PET in a multimodal paradigm. *Eur J Nucl Med Mol Imaging.* 2016;43(9):1686-1699.

281. Cho H, Choi JY, Hwang MS, et al. Tau PET in Alzheimer disease and mild cognitive impairment. *Neurology.* 2016;87(4):375-383.

282. van Eimeren T, Bischof GN, Drzezga A. Is Tau Imaging More Than Just Upside-Down (18)F-FDG Imaging? *J Nucl Med.* 2017;58(9):1357-1359.

283. Kang JM, Lee SY, Seo S, et al. Tau positron emission tomography using [(18) F]THK5351 and cerebral glucose hypometabolism in Alzheimer's disease. *Neurobiol Aging.* 2017;59:210-219.

284. Pontecorvo MJ, Devous MD, Sr., Navitsky M, et al. Relationships between flortaucipir PET tau binding and amyloid burden, clinical diagnosis, age and cognition. *Brain.* 2017;140(3):748-763.

285. Brier MR, Gordon B, Friedrichsen K, et al. Tau and Abeta imaging, CSF measures, and cognition in Alzheimer's disease. *Sci Transl Med.* 2016;8(338):338ra366.

286. Blennow K, Hampel H. CSF markers for incipient Alzheimer's disease. *Lancet Neurol.* 2003;2(10):605-613.

287. Chiotis K, Saint-Aubert L, Rodriguez-Vieitez E, et al. Longitudinal changes of tau PET imaging in relation to hypometabolism in prodromal and Alzheimer's disease dementia. *Mol Psychiatry.* 2017.

288. Lohith TG, Bennacef I, Vandenberghe R, et al. First-in-human brain imaging of Alzheimer dementia patients and elderly controls with (18)F-MK-6240, a PET tracer targeting neurofibrillary tangle pathology. *J Nucl Med.* 2018.

289. Betthauser TJ, Cody KA, Zammit MD, et al. In vivo characterization and quantification of neurofibrillary tau PET radioligand [(18)F]MK-6240 in humans from Alzheimer's disease dementia to young controls. *J Nucl Med.* 2018.

290. Wong DF, Comley R, Kuwabara H, et al. First in-human PET study of 3 novel tau radiopharmaceuticals: [(11)C]RO6924963, [(11)C]RO6931643, and [(18)F] RO6958948. *J Nucl Med.* 2018.

291. Kikuchi A, Okamura N, Hasegawa T, et al. In vivo visualization of tau deposits in corticobasal syndrome by 18F-THK5351 PET. *Neurology.* 2016;87(22):2309-2316.

292. Cho H, Baek MS, Choi JY, et al. (18)F-AV-1451 binds to motor-related subcortical gray and white matter in corticobasal syndrome. *Neurology.* 2017;89(11):1170-1178.

293. Smith R, Scholl M, Widner H, et al. In vivo retention of (18)F-AV-1451 in corticobasal syndrome. *Neurology.* 2017;89(8):845-853.

294. Passamonti L, Vazquez Rodriguez P, Hong YT, et al. 18F-AV-1451 positron emission tomography in Alzheimer's disease and progressive supranuclear palsy. *Brain.* 2017;140(3):781-791.

295. Ishiki A, Harada R, Okamura N, et al. Tau imaging with [(18) F]THK-5351 in progressive supranuclear palsy. *Eur J Neurol.* 2017;24(1):130-136.

296. Perez-Soriano A, Stoessl AJ. Tau imaging in progressive supranuclear palsy. *Mov Disord.* 2017;32(1):91-93.

297. Schonhaut DR, McMillan CT, Spina S, et al. (18) F-flortaucipir tau positron emission tomography distinguishes established progressive supranuclear palsy from controls and Parkinson disease: A multicenter study. *Ann Neurol.* 2017;82(4):622-634.

298. Coakeley S, Cho SS, Koshimori Y, et al. Positron emission tomography imaging of tau pathology in progressive supranuclear palsy. *J Cereb Blood Flow Metab.* 2017;37(9):3150-3160.

299. Marquie M, Normandin MD, Meltzer AC, et al. Pathological correlations of [F-18]-AV-1451 imaging in non-alzheimer tauopathies. *Ann Neurol.* 2017;81(1):117-128.

300. Marquie M, Siao Tick Chong M, Anton-Fernandez A, et al. [F-18]-AV-1451 binding correlates with postmortem neurofibrillary tangle Braak staging. *Acta Neuropathol.* 2017;134(4):619-628.

301. Chiotis K, Stenkrona P, Almkvist O, et al. Head-to-Head In Vivo Comparison of Tau-Specific PET Tracers in Alzheimer's Disease: [11C]THK5351 Vs [11C] PBB3 PET Imaging. Paper presented at: Alzheimer's Association International ConferenceAlzheimer's Association International Conference; London, U.K.

302. Jang YK, Lyoo CH, Park S, et al. Head to head comparison of [(18)F] AV-1451 and [(18)F] THK5351 for tau imaging in Alzheimer's disease and frontotemporal dementia. *Eur J Nucl Med Mol Imaging.* 2018;45(3):432-442.

303. Barrio JR. The Irony of PET Tau Probe Specificity. *J Nucl Med.* 2018;59(1):115-116.

304. Ng KP, Pascoal TA, Mathotaarachchi S, et al. Monoamine oxidase B inhibitor, selegiline, reduces 18F-THK5351 uptake in the human brain. *Alzheimers Res Ther.* 2017;9(1):25.

305. Vermeiren C, Motte P, Viot D, et al. The tau positron-emission tomography tracer AV-1451 binds with similar affinities to tau fibrils and monoamine oxidases. *Mov Disord.* 2018;33(2):273-281.

306. Lemoine L, Leuzy A, Chiotis K, Rodriguez-Vieitez E, Nordberg A. Tau positron emission tomography imaging in tauopathies: The added hurdle of off-target binding. *Alzheimers Dement (Amst).* 2018;10:232-236.

307. Kasischke KA, Vishwasrao HD, Fisher PJ, Zipfel WR, Webb WW. Neural activity triggers neuronal oxidative metabolism followed by astrocytic glycolysis. *Science.* 2004;305(5680):99-103.

308. Zimmer ER, Parent MJ, Souza DG, et al. [18F]FDG PET signal is driven by astroglial glutamate transport. *Nat Neurosci.* 2017;20(3):393-395.

309. Attwell D, Laughlin SB. An energy budget for signaling in the grey matter of the brain. *J Cereb Blood Flow Metab.* 2001;21(10):1133-1145.

310. Schwartz WJ, Smith CB, Davidsen L, et al. Metabolic mapping of functional activity in the hypothalamo-neurohypophysial system of the rat. *Science.* 1979;205(4407):723-725.

311. Sokoloff L, Reivich M, Kennedy C, et al. The [14C]deoxyglucose method for the measurement of local cerebral glucose utilization: theory, procedure, and normal values in the conscious and anesthetized albino rat. *J Neurochem.* 1977;28(5):897-916.

312. Reivich M, Kuhl D, Wolf A, et al. The [18F]fluorodeoxyglucose method for the measurement of local cerebral glucose utilization in man. *Circ Res.* 1979;44(1):127-137.

313. Vannucci SJ, Maher F, Simpson IA. Glucose transporter proteins in brain: delivery of glucose to neurons and glia. *Glia.* 1997;21(1):2-21.

314. De Santi S, de Leon MJ, Rusinek H, et al. Hippocampal formation glucose metabolism and volume losses in MCI and AD. *Neurobiol Aging.* 2001;22(4):529-539.

315. Foster NL, Chase TN, Fedio P, Patronas NJ, Brooks RA, Di Chiro G. Alzheimer's disease: focal cortical changes shown by positron emission tomography. *Neurology.* 1983;33(8):961-965.

316. Reiman EM, Caselli RJ, Yun LS, et al. Preclinical evidence of Alzheimer's disease in persons homozygous for the epsilon 4 allele for apolipoprotein E. *N Engl J Med.* 1996;334(12):752-758.

317. Silverman DH, Small GW, Chang CY, et al. Positron emission tomography in evaluation of dementia: Regional brain metabolism and long-term outcome. *JAMA.* 2001;286(17):2120-2127.

318. Chetelat G, Desgranges B, de la Sayette V, Viader F, Eustache F, Baron JC. Mild cognitive impairment: Can FDG-PET predict who is to rapidly convert to Alzheimer's disease? *Neurology.* 2003;60(8):1374-1377.

319. Caselli RJ, Chen K, Lee W, Alexander GE, Reiman EM. Correlating cerebral hypometabolism with future memory decline in subsequent converters to amnestic pre-mild cognitive impairment. *Arch Neurol.* 2008;65(9):1231-1236.

320. Landau SM, Harvey D, Madison CM, et al. Comparing predictors of conversion and decline in mild cognitive impairment. *Neurology.* 2010;75(3):230-238.

321. Furst AJ, Rabinovici GD, Rostomian AH, et al. Cognition, glucose metabolism and amyloid burden in Alzheimer's disease. *Neurobiol Aging.* 2012;33(2):215-225.

322. Minoshima S, Giordani B, Berent S, Frey KA, Foster NL, Kuhl DE. Metabolic reduction in the posterior cingulate cortex in very early Alzheimer's disease. *Ann Neurol.* 1997;42(1):85-94.

323. Ewers M, Brendel M, Rizk-Jackson A, et al. Reduced FDG-PET brain metabolism and executive function predict clinical progression in elderly healthy subjects. *Neuroimage Clin.* 2014;4:45-52.

324. Rizk-Jackson A, Insel P, Petersen R, Aisen P, Jack C, Weiner M. Early indications of future cognitive decline: stable versus declining controls. *PLoS One.* 2013;8(9):e74062.

325. Hoffman JM, Welsh-Bohmer KA, Hanson M, et al. FDG PET imaging in patients with pathologically verified dementia. *J Nucl Med.* 2000;41(11):1920-1928.

326. Jagust W, Reed B, Mungas D, Ellis W, Decarli C. What does fluorodeoxyglucose PET imaging add to a clinical diagnosis of dementia? *Neurology.* 2007;69(9):871-877.

327. Woodward MC, Rowe CC, Jones G, Villemagne VL, Varos TA. Differentiating the frontal presentation of Alzheimer's disease with FDG-PET. *J Alzheimers Dis.* 2015;44(1):233-242.

328. Singh TD, Josephs KA, Machulda MM, et al. Clinical, FDG and amyloid PET imaging in posterior cortical atrophy. *J Neurol.* 2015;262(6):1483-1492.

329. Teune LK, Bartels AL, de Jong BM, et al. Typical cerebral metabolic patterns in neurodegenerative brain diseases. *Mov Disord.* 2010;25(14):2395-2404.

330. Jones SC, Greenberg JH, Dann R, et al. Cerebral blood flow with the continuous infusion of oxygen-15-labeled water. *J Cereb Blood Flow Metab.* 1985;5(4):566-575.

331. Kanno I, Iida H, Miura S, et al. A system for cerebral blood flow measurement using an H215O autoradiographic method and positron emission tomography. *J Cereb Blood Flow Metab.* 1987;7(2):143-153.

332. Raichle ME, Martin WR, Herscovitch P, Mintun MA, Markham J. Brain blood flow measured with intravenous H2(15)O. II. Implementation and validation. *J Nucl Med.* 1983;24(9):790-798.

333. Zhou Y, Resnick SM, Ye W, et al. Using a reference tissue model with spatial constraint to quantify [11C]Pittsburgh compound B PET for early diagnosis of Alzheimer's disease. *Neuroimage.* 2007;36(2):298-312.

334. Wu Y, Carson RE. Noise reduction in the simplified reference tissue model for neuroreceptor functional imaging. *J Cereb Blood Flow Metab.* 2002;22(12):1440-1452.

335. Chen YJ, Rosario BL, Mowrey W, et al. Relative 11C-PiB Delivery as a Proxy of Relative CBF: Quantitative Evaluation Using Single-Session 15O-Water and 11C-PiB PET. *J Nucl Med.* 2015;56(8):1199-1205.

336. Rostomian AH, Madison C, Rabinovici GD, Jagust WJ. Early 11C-PIB frames and 18F-FDG PET measures are comparable: a study validated in a cohort of AD and FTLD patients. *J Nucl Med.* 2011;52(2):173-179.

337. Koeppe RA, Gilman S, Joshi A, et al. 11C-DTBZ and 18F-FDG PET measures in differentiating dementias. *J Nucl Med.* 2005;46(6):936-944.

338. Paulson OB, Hasselbalch SG, Rostrup E, Knudsen GM, Pelligrino D. Cerebral blood flow response to functional activation. *J Cereb Blood Flow Metab.* 2010;30(1):2-14.

339. Nihashi T, Yatsuya H, Hayasaka K, et al. Direct comparison study between FDG-PET and IMP-SPECT for diagnosing Alzheimer's disease using 3D-SSP analysis in the same patients. *Radiat Med.* 2007;25(6):255-262.

340. Rodriguez-Vieitez E, Leuzy A, Chiotis K, Saint-Aubert L, Wall A, Nordberg A. Comparability of [(18)F]THK5317 and [(11)C]PIB blood flow proxy images with [(18)F]FDG positron emission tomography in Alzheimer's disease. *J Cereb Blood Flow Metab*. 2017;37(2):740-749.

341. Meyer PT, Hellwig S, Amtage F, et al. Dual-biomarker imaging of regional cerebral amyloid load and neuronal activity in dementia with PET and 11C-labeled Pittsburgh compound B. *J Nucl Med.* 2011;52(3):393-400.

342. Fu L, Liu L, Zhang J, Xu B, Fan Y, Tian J. Comparison of dual-biomarker PIB-PET and dual-tracer PET in AD diagnosis. *Eur Radiol.* 2014;24(11):2800-2809.

343. Forsberg A, Engler H, Blomquist G, Langstrom B, Nordberg A. The use of PIB-PET as a dual pathological and functional biomarker in AD. *Biochim Biophys Acta.* 2012;1822(3):380-385.

344. Appel L, Jonasson M, Danfors T, et al. Use of 11C-PE2I PET in differential diagnosis of parkinsonian disorders. *J Nucl Med.* 2015;56(2):234-242.

345. Hammes J, Leuwer I, Bischof GN, Drzezga A, van Eimeren T. Multimodal correlation of dynamic [(18)F]-AV-1451 perfusion PET and neuronal hypometabolism in [(18)F]-FDG PET. *Eur J Nucl Med Mol Imaging.* 2017;44(13):2249-2256.

346. Leuzy A, Rodriguez-Vieitez E, Saint-Aubert L, et al. Longitudinal uncoupling of cerebral perfusion, glucose metabolism, and tau deposition in Alzheimer's disease. *Alzheimers Dement*. 2018;14(5):652-663.

347. Tarantini S, Tran CH, Gordon GR, Ungvari Z, Csiszar A. Impaired neurovascular coupling in aging and Alzheimer's disease: Contribution of astrocyte dysfunction and endothelial impairment to cognitive decline. *Exp Gerontol.* 2016.

348. Pasqualetti G, Harris R, RInne J, et al. Does cerebral glucose metabolism and blood flow dissociate in early stages of Alzheimer's disease? Alzheimers Dement; July 12-17, 2014, 2014; Copenhagen, Denmark.

349. Fink GR, Pawlik G, Stefan H, Pietrzyk U, Wienhard K, Heiss WD. Temporal lobe epilepsy: evidence for interictal uncoupling of blood flow and glucose metabolism in temporomesial structures. *J Neurol Sci.* 1996;137(1):28-34.

350. Herman GT, Herman GT. *Fundamentals of computerized tomography : image reconstruction from projections.* 2nd ed. Dordrecht ; New York: Springer; 2009.

351. Schild HH. *MRI made easy.* Germany: Nationales Druckhaus Berlin; 1990.

352. Lehericy S, Baulac M, Chiras J, et al. Amygdalohippocampal MR volume measurements in the early stages of Alzheimer disease. *AJNR Am J Neuroradiol.* 1994;15(5):929-937.

353. Chan D, Fox NC, Scahill RI, et al. Patterns of temporal lobe atrophy in semantic dementia and Alzheimer's disease. *Ann Neurol.* 2001;49(4):433-442.

354. Dickerson BC, Goncharova I, Sullivan MP, et al. MRI-derived entorhinal and hippocampal atrophy in incipient and very mild Alzheimer's disease. *Neurobiol Aging.* 2001;22(5):747-754.

355. Killiany RJ, Hyman BT, Gomez-Isla T, et al. MRI measures of entorhinal cortex vs hippocampus in preclinical AD. *Neurology.* 2002;58(8):1188-1196.

356. Denihan A, Wilson G, Cunningham C, Coakley D, Lawlor BA. CT measurement of medial temporal lobe atrophy in Alzheimer's disease, vascular dementia, depression and paraphrenia. *Int J Geriatr Psychiatry.* 2000;15(4):306-312.

357. Baron JC, Chetelat G, Desgranges B, et al. In vivo mapping of gray matter loss with voxel-based morphometry in mild Alzheimer's disease. *Neuroimage.* 2001;14(2):298-309.

358. Frisoni GB, Testa C, Zorzan A, et al. Detection of grey matter loss in mild Alzheimer's disease with voxel based morphometry. *J Neurol Neurosurg Psychiatry.* 2002;73(6):657-664.

359. Scahill RI, Schott JM, Stevens JM, Rossor MN, Fox NC. Mapping the evolution of regional atrophy in Alzheimer's disease: unbiased analysis of fluid-registered serial MRI. *Proc Natl Acad Sci U S A.* 2002;99(7):4703-4707.

360. Arnold SE, Hyman BT, Flory J, Damasio AR, Van Hoesen GW. The topographical and neuroanatomical distribution of neurofibrillary tangles and neuritic plaques in the cerebral cortex of patients with Alzheimer's disease. *Cereb Cortex.* 1991;1(1):103-116.

361. Brun A, Gustafson L. Distribution of cerebral degeneration in Alzheimer's disease. A clinico-pathological study. *Arch Psychiatr Nervenkr (1970).* 1976;223(1):15-33.

362. Fox NC, Scahill RI, Crum WR, Rossor MN. Correlation between rates of brain atrophy and cognitive decline in AD. *Neurology.* 1999;52(8):1687-1689.

363. Frisoni GB, Fox NC, Jack CR, Jr., Scheltens P, Thompson PM. The clinical use of structural MRI in Alzheimer disease. *Nat Rev Neurol.* 2010;6(2):67-77.

364. Burton EJ, Barber R, Mukaetova-Ladinska EB, et al. Medial temporal lobe atrophy on MRI differentiates Alzheimer's disease from dementia with Lewy bodies and vascular cognitive impairment: a prospective study with pathological verification of diagnosis. *Brain.* 2009;132(Pt 1):195-203.

365. Duara R, Loewenstein DA, Potter E, et al. Medial temporal lobe atrophy on MRI scans and the diagnosis of Alzheimer disease. *Neurology.* 2008;71(24):1986-1992.

366. Scheltens P, Leys D, Barkhof F, et al. Atrophy of medial temporal lobes on MRI in "probable" Alzheimer's disease and normal ageing: diagnostic value and neuropsychological correlates. *J Neurol Neurosurg Psychiatry.* 1992;55(10):967-972.

367. DeCarli C, Frisoni GB, Clark CM, et al. Qualitative estimates of medial temporal atrophy as a predictor of progression from mild cognitive impairment to dementia. *Arch Neurol.* 2007;64(1):108-115.

368. Korf ES, Wahlund LO, Visser PJ, Scheltens P. Medial temporal lobe atrophy on MRI predicts dementia in patients with mild cognitive impairment. *Neurology.* 2004;63(1):94-100.

369. Scheltens P, Fox N, Barkhof F, De Carli C. Structural magnetic resonance imaging in the practical assessment of dementia: beyond exclusion. *Lancet Neurol.* 2002;1(1):13-21.

370. Likeman M, Anderson VM, Stevens JM, et al. Visual assessment of atrophy on magnetic resonance imaging in the diagnosis of pathologically confirmed young-onset dementias. *Arch Neurol.* 2005;62(9):1410-1415.

371. Whitwell JL, Dickson DW, Murray ME, et al. Neuroimaging correlates of pathologically defined subtypes of Alzheimer's disease: a case-control study. *Lancet Neurol.* 2012;11(10):868-877.

372. Ferreira D, Verhagen C, Hernandez-Cabrera JA, et al. Distinct subtypes of Alzheimer's disease based on patterns of brain atrophy: longitudinal trajectories and clinical applications. *Sci Rep.* 2017;7:46263.

373. Wattjes MP, Henneman WJ, van der Flier WM, et al. Diagnostic imaging of patients in a memory clinic: comparison of MR imaging and 64-detector row CT. *Radiology.* 2009;253(1):174-183.

374. Pasi M, Poggesi A, Pantoni L. The use of CT in dementia. *Int Psychogeriatr.* 2011;23 Suppl 2:S6-12.

375. Cordonnier C, van der Flier WM. Brain microbleeds and Alzheimer's disease: innocent observation or key player? *Brain.* 2011;134(Pt 2):335-344.

376. Soucy JP, Bartha R, Bocti C, et al. Clinical applications of neuroimaging in patients with Alzheimer's disease: a review from the Fourth Canadian Consensus Conference on the Diagnosis and Treatment of Dementia 2012. *Alzheimers Res Ther.* 2013;5(Suppl 1):S3.

377. Ten Kate M, Barkhof F, Boccardi M, et al. Clinical validity of medial temporal atrophy as a biomarker for Alzheimer's disease in the context of a structured 5-phase development framework. *Neurobiol Aging.* 2017;52:167-182 e161.

378. Wolk DA, Detre JA. Arterial spin labeling MRI: an emerging biomarker for Alzheimer's disease and other neurodegenerative conditions. *Curr Opin Neurol.* 2012;25(4):421-428.

379. Kantarci K, Murray ME, Schwarz CG, et al. White-matter integrity on DTI and the pathologic staging of Alzheimer's disease. *Neurobiol Aging.* 2017;56:172-179.

380. Sperling R. Potential of functional MRI as a biomarker in early Alzheimer's disease. *Neurobiol Aging.* 2011;32 Suppl 1:S37-43.

381. Voevodskaya O, Sundgren PC, Strandberg O, et al. Myo-inositol changes precede amyloid pathology and relate to APOE genotype in Alzheimer disease. *Neurology.* 2016;86(19):1754-1761.

382. Jack CR, Jr., Barnes J, Bernstein MA, et al. Magnetic resonance imaging in Alzheimer's Disease Neuroimaging Initiative 2. *Alzheimers Dement.* 2015;11(7):740-756.

383. Morrison BM. Physiology of Cerebrospinal Fluid, Secretion, Recirculation, and Resorption. In: Irani DN, ed. *Cerebrospinal fluid in clinical practice*. Philadelphia, PA: Elsevier; 2009.

384. Abbott NJ. Evidence for bulk flow of brain interstitial fluid: significance for physiology and pathology. *Neurochem Int.* 2004;45(4):545-552.

385. Matsumae M, Kikinis R, Morocz IA, et al. Age-related changes in intracranial compartment volumes in normal adults assessed by magnetic resonance imaging. *J Neurosurg.* 1996;84(6):982-991.

386. Nilsson C, Stahlberg F, Thomsen C, Henriksen O, Herning M, Owman C. Circadian variation in human cerebrospinal fluid production measured by magnetic resonance imaging. *Am J Physiol.* 1992;262(1 Pt 2):R20-24.

387. Redzic ZB, Segal MB. The structure of the choroid plexus and the physiology of the choroid plexus epithelium. *Adv Drug Deliv Rev.* 2004;56(12):1695-1716.

388. Hampel H, Lista S, Khachaturian ZS. Development of biomarkers to chart all Alzheimer's disease stages: the royal road to cutting the therapeutic Gordian Knot. *Alzheimers Dement.* 2012;8(4):312-336.

389. Blennow K, Wallin A, Hager O. Low frequency of post-lumbar puncture headache in demented patients. *Acta Neurol Scand.* 1993;88(3):221-223.

390. Peskind E, Nordberg A, Darreh-Shori T, Soininen H. Safety of lumbar puncture procedures in patients with Alzheimer's disease. *Curr Alzheimer Res.* 2009;6(3):290-292.

391. Peskind ER, Riekse R, Quinn JF, et al. Safety and acceptability of the research lumbar puncture. *Alzheimer Dis Assoc Disord.* 2005;19(4):220-225.

392. Zetterberg H, Tullhog K, Hansson O, Minthon L, Londos E, Blennow K. Low incidence of post-lumbar puncture headache in 1,089 consecutive memory clinic patients. *Eur Neurol.* 2010;63(6):326-330.

393. Engvall E, Perlmann P. Enzyme-linked immunosorbent assay (ELISA). Quantitative assay of immunoglobulin G. *Immunochemistry.* 1971;8(9):871-874.

394. Van Weemen BK, Schuurs AH. Immunoassay using antigen-enzyme conjugates. *FEBS Lett.* 1971;15(3):232-236.

395. Kohler G, Milstein C. Continuous cultures of fused cells secreting antibody of predefined specificity. 1975. *J Immunol.* 2005;174(5):2453-2455.

396. Avrameas S. Coupling of enzymes to proteins with glutaraldehyde. Use of the conjugates for the detection of antigens and antibodies. *Immunochemistry.* 1969;6(1):43-52.

397. Nakane PK, Pierce GB, Jr. Enzyme-labeled antibodies for the light and electron microscopic localization of tissue antigens. *J Cell Biol.* 1967;33(2):307-318.

398. Avrameas S, Uriel J. Méthode de marquage d'antigènes et d'anticorps avec des enzymes et son application en immunodiffusion. . *C R Acad Sci Hebd Seances Acad Sci D.* 1966;262:2543-2545.

399. You JS, Gelfanova V, Knierman MD, Witzmann FA, Wang M, Hale JE. The impact of blood contamination on the proteome of cerebrospinal fluid. *Proteomics.* 2005;5(1):290-296.

400. Blennow K, Zetterberg H. Understanding biomarkers of neurodegeneration: Ultrasensitive detection techniques pave the way for mechanistic understanding. *Nat Med.* 2015;21(3):217-219.

401. Olsson A, Vanderstichele H, Andreasen N, et al. Simultaneous measurement of beta-amyloid(1-42), total tau, and phosphorylated tau (Thr181) in cerebrospinal fluid by the xMAP technology. *Clin Chem.* 2005;51(2):336-345.

402. Kruse N, Schulz-Schaeffer WJ, Schlossmacher MG, Mollenhauer B. Development of electrochemiluminescence-based singleplex and multiplex assays for the quantification of alpha-synuclein and other proteins in cerebrospinal fluid. *Methods.* 2012;56(4):514-518.

403. Rondelez Y, Tresset G, Tabata KV, et al. Microfabricated arrays of femtoliter chambers allow single molecule enzymology. *Nat Biotechnol.* 2005;23(3):361-365.

404. Rissin DM, Kan CW, Campbell TG, et al. Single-molecule enzyme-linked immunosorbent assay detects serum proteins at subfemtomolar concentrations. *Nat Biotechnol.* 2010;28(6):595-599.

405. Rissin DM, Walt DR. Digital concentration readout of single enzyme molecules using femtoliter arrays and Poisson statistics. *Nano Lett.* 2006;6(3):520-523.

406. Cohen L, Walt DR. Single-Molecule Arrays for Protein and Nucleic Acid Analysis. *Annu Rev Anal Chem (Palo Alto Calif).* 2017;10(1):345-363.

407. Whitesides GM. The origins and the future of microfluidics. *Nature.* 2006;442(7101):368-373.

408. Price P. Standard definitions of terms relating to mass spectrometry : A report from the committee on measurements and standards of the American society for mass spectrometry. *J Am Soc Mass Spectrom.* 1991;2(4):336-348.

409. Mattsson N, Zegers I, Andreasson U, et al. Reference measurement procedures for Alzheimer's disease cerebrospinal fluid biomarkers: definitions and approaches with focus on amyloid beta42. *Biomark Med.* 2012;6(4):409-417.

410. ISO 17511. In Vitro Diagnostic Medical Devices – Measurement of Quantities in Biological Samples – Metrological Traceability of Values Assigned to Calibrators and Control Materials. International Organization for Standardization, Switzerland; 2003.

411. ISO 15193. In Vitro Diagnostic Medical Devices – Measurement of Quantities in Samples of Biological Origin – Presentation of Reference Measurement Procedures. International Organization for Standardization, Switzerland; 2002.

412. ISO Guide 30. Terms and Definitions Used In Connection With Reference Materials. International Organization for Standardization, Switzerland; 1992.

413. Joint Committee for Guides in Metrology. International Vocabulary of Metrology – Basic and General Concepts and Associated Terms (VIM), 3rd Edition, 2008 Version With Minor Corrections. Bureau international des Poids et Mesures, France; 2012.

414. Kitteringham NR, Jenkins RE, Lane CS, Elliott VL, Park BK. Multiple reaction monitoring for quantitative biomarker analysis in proteomics and metabolomics. *J Chromatogr B Analyt Technol Biomed Life Sci.* 2009;877(13):1229-1239.

415. Lame ME, Chambers EE, Blatnik M. Quantitation of amyloid beta peptides Abeta(1-38), Abeta(1-40), and Abeta(1-42) in human cerebrospinal fluid by ultra-performance liquid chromatography-tandem mass spectrometry. *Anal Biochem.* 2011;419(2):133-139.

416. Yost RA, Enke CG. Triple quadrupole mass spectrometry for direct mixture analysis and structure elucidation. *Anal Chem.* 1979;51(12):1251-1264.

417. Mattsson N, Andreasson U, Persson S, et al. The Alzheimer's Association external quality control program for cerebrospinal fluid biomarkers. *Alzheimers Dement.* 2011;7(4):386-395 e386.

418. Bjerke M, Portelius E, Minthon L, et al. Confounding factors influencing amyloid Beta concentration in cerebrospinal fluid. *Int J Alzheimers Dis.* 2010;2010.

419. Andreasen N, Hesse C, Davidsson P, et al. Cerebrospinal fluid beta-amyloid(1-42) in Alzheimer disease: differences between early- and late-onset Alzheimer disease and stability during the course of disease. *Arch Neurol.* 1999;56(6):673-680.

420. Bibl M, Esselmann H, Otto M, et al. Cerebrospinal fluid amyloid beta peptide patterns in Alzheimer's disease patients and nondemented controls depend on sample pretreatment: indication of carrier-mediated epitope masking of amyloid beta peptides. *Electrophoresis.* 2004;25(17):2912-2918.

421. Schoonenboom NS, Mulder C, Vanderstichele H, et al. Effects of processing and storage conditions on amyloid beta (1-42) and tau concentrations in cerebrospinal fluid: implications for use in clinical practice. *Clin Chem.* 2005;51(1):189-195.

422. Lewczuk P, Beck G, Esselmann H, et al. Effect of sample collection tubes on cerebrospinal fluid concentrations of tau proteins and amyloid beta peptides. *Clin Chem.* 2006;52(2):332-334.

423. Teunissen CE, Verwey NA, Kester MI, van Uffelen K, Blankenstein MA. Standardization of Assay Procedures for Analysis of the CSF Biomarkers Amyloid beta((1-42)), Tau, and Phosphorylated Tau in Alzheimer's Disease: Report of an International Workshop. *Int J Alzheimers Dis.* 2010;2010.

424. Blennow K, Dubois B, Fagan AM, Lewczuk P, de Leon MJ, Hampel H. Clinical utility of cerebrospinal fluid biomarkers in the diagnosis of early Alzheimer's disease. *Alzheimers Dement.* 2015;11(1):58-69.

425. Vos SJ, Visser PJ, Verhey F, et al. Variability of CSF Alzheimer's disease biomarkers: implications for clinical practice. *PLoS One.* 2014;9(6):e100784.

426. Carrillo MC, Blennow K, Soares H, et al. Global standardization measurement of cerebral spinal fluid for Alzheimer's disease: an update from the Alzheimer's Association Global Biomarkers Consortium. *Alzheimers Dement.* 2013;9(2):137-140.

427. Blennow K, Hampel H, Weiner M, Zetterberg H. Cerebrospinal fluid and plasma biomarkers in Alzheimer disease. *Nat Rev Neurol.* 2010;6(3):131-144.

428. Mattsson N, Andreasson U, Persson S, et al. CSF biomarker variability in the Alzheimer's Association quality control program. *Alzheimers Dement.* 2013;9(3):251-261.

429. Leinenbach A, Pannee J, Dulffer T, et al. Mass spectrometry-based candidate reference measurement procedure for quantification of amyloid-beta in cerebrospinal fluid. *Clin Chem.* 2014;60(7):987-994.

430. Haass C, Selkoe DJ. Cellular processing of beta-amyloid precursor protein and the genesis of amyloid beta-peptide. *Cell.* 1993;75(6):1039-1042.

431. Higgins LS, Murphy GM, Jr., Forno LS, Catalano R, Cordell B. P3 beta-amyloid peptide has a unique and potentially pathogenic immunohistochemical profile in Alzheimer's disease brain. *Am J Pathol.* 1996;149(2):585-596.

432. Wei W, Norton DD, Wang X, Kusiak JW. Abeta 17-42 in Alzheimer's disease activates JNK and caspase-8 leading to neuronal apoptosis. *Brain.* 2002;125(Pt 9):2036-2043.

433. Wiltfang J, Esselmann H, Bibl M, et al. Amyloid beta peptide ratio 42/40 but not A beta 42 correlates with phospho-Tau in patients with low- and high-CSF A beta 40 load. *J Neurochem.* 2007;101(4):1053-1059.

434. Van Nostrand WE, Wagner SL, Shankle WR, et al. Decreased levels of soluble amyloid beta-protein precursor in cerebrospinal fluid of live Alzheimer disease patients. *Proc Natl Acad Sci U S A.* 1992;89(7):2551-2555.

435. Farlow M, Ghetti B, Benson MD, Farrow JS, van Nostrand WE, Wagner SL. Low cerebrospinal-fluid concentrations of soluble amyloid beta-protein precursor in hereditary Alzheimer's disease. *Lancet.* 1992;340(8817):453-454.

436. Tabaton M, Nunzi MG, Xue R, Usiak M, Autilio-Gambetti L, Gambetti P. Soluble amyloid beta-protein is a marker of Alzheimer amyloid in brain but not in cerebrospinal fluid. *Biochem Biophys Res Commun.* 1994;200(3):1598-1603.

437. van Gool WA, Kuiper MA, Walstra GJ, Wolters EC, Bolhuis PA. Concentrations of amyloid beta protein in cerebrospinal fluid of patients with Alzheimer's disease. *Ann Neurol.* 1995;37(2):277-279.

438. Motter R, Vigo-Pelfrey C, Kholodenko D, et al. Reduction of beta-amyloid peptide42 in the cerebrospinal fluid of patients with Alzheimer's disease. *Ann Neurol.* 1995;38(4):643-648.

439. Southwick PC, Yamagata SK, Echols CL, Jr., et al. Assessment of amyloid beta protein in cerebrospinal fluid as an aid in the diagnosis of Alzheimer's disease. *J Neurochem.* 1996;66(1):259-265.

440. Jarrett JT, Berger EP, Lansbury PT, Jr. The carboxy terminus of the beta amyloid protein is critical for the seeding of amyloid formation: implications for the pathogenesis of Alzheimer's disease. *Biochemistry.* 1993;32(18):4693-4697.

441. Tamaoka A, Kondo T, Odaka A, et al. Biochemical evidence for the long-tail form (A beta 1-42/43) of amyloid beta protein as a seed molecule in cerebral deposits of Alzheimer's disease. *Biochem Biophys Res Commun.* 1994;205(1):834-842.

442. Iwatsubo T, Odaka A, Suzuki N, Mizusawa H, Nukina N, Ihara Y. Visualization of A beta 42(43) and A beta 40 in senile plaques with end-specific A beta monoclonals: evidence that an initially deposited species is A beta 42(43). *Neuron.* 1994;13(1):45-53.

443. Vanderstichele H, Blennow K, D'Heuvaert ND, et al. Progress in Alzheimer's and Parkinson's Diseases. In: Fisher A, Hanin S, Yoshiada M, eds. *Development of a Specific Diagnostic Test for Measurement of β-Amyloid (1-42) [βA4(l-42)] in CSF*. Boston, MA: Springer; 1998.

444. Blennow K, Vanmechelen E. CSF markers for pathogenic processes in Alzheimer's disease: diagnostic implications and use in clinical neurochemistry. *Brain Res Bull.* 2003;61(3):235-242.

445. Tapiola T, Alafuzoff I, Herukka SK, et al. Cerebrospinal fluid {beta}-amyloid 42 and tau proteins as biomarkers of Alzheimer-type pathologic changes in the brain. *Arch Neurol.* 2009;66(3):382-389.

446. Strozyk D, Blennow K, White LR, Launer LJ. CSF Abeta 42 levels correlate with amyloid-neuropathology in a population-based autopsy study. *Neurology.* 2003;60(4):652-656.

447. Seppala TT, Nerg O, Koivisto AM, et al. CSF biomarkers for Alzheimer disease correlate with cortical brain biopsy findings. *Neurology.* 2012;78(20):1568-1575.

448. Kawarabayashi T, Younkin LH, Saido TC, Shoji M, Ashe KH, Younkin SG. Age-dependent changes in brain, CSF, and plasma amyloid (beta) protein in the Tg2576 transgenic mouse model of Alzheimer's disease. *J Neurosci.* 2001;21(2):372-381.

449. Desgranges B, Baron JC, Lalevee C, et al. The neural substrates of episodic memory impairment in Alzheimer's disease as revealed by FDG-PET: relationship to degree of deterioration. *Brain.* 2002;125(Pt 5):1116-1124.

450. Otto M, Esselmann H, Schulz-Shaeffer W, et al. Decreased beta-amyloid1-42 in cerebrospinal fluid of patients with Creutzfeldt-Jakob disease. *Neurology.* 2000;54(5):1099-1102.

451. Sjogren M, Davidsson P, Wallin A, et al. Decreased CSF-beta-amyloid 42 in Alzheimer's disease and amyotrophic lateral sclerosis may reflect mismetabolism of beta-amyloid induced by disparate mechanisms. *Dement Geriatr Cogn Disord.* 2002;13(2):112-118.

452. Portelius E, Westman-Brinkmalm A, Zetterberg H, Blennow K. Determination of beta-amyloid peptide signatures in cerebrospinal fluid using immunoprecipitation-mass spectrometry. *J Proteome Res.* 2006;5(4):1010-1016.

453. Vandersteen A, Hubin E, Sarroukh R, et al. A comparative analysis of the aggregation behavior of amyloid-beta peptide variants. *FEBS Lett.* 2012;586(23):4088-4093.

454. Lewczuk P, Lelental N, Spitzer P, Maler JM, Kornhuber J. Amyloid-beta 42/40 cerebrospinal fluid concentration ratio in the diagnostics of Alzheimer's disease: validation of two novel assays. *J Alzheimers Dis.* 2015;43(1):183-191.

455. Bibl M, Gallus M, Welge V, et al. Cerebrospinal fluid amyloid-beta 2-42 is decreased in Alzheimer's, but not in frontotemporal dementia. *J Neural Transm (Vienna).* 2012;119(7):805-813.

456. Struyfs H, Van Broeck B, Timmers M, et al. Diagnostic Accuracy of Cerebrospinal Fluid Amyloid-beta Isoforms for Early and Differential Dementia Diagnosis. *J Alzheimers Dis.* 2015;45(3):813-822.

457. Hansson O, Zetterberg H, Buchhave P, et al. Prediction of Alzheimer's disease using the CSF Abeta42/Abeta40 ratio in patients with mild cognitive impairment. *Dement Geriatr Cogn Disord.* 2007;23(5):316-320.

458. Glenner GG, Wong CW. Alzheimer's disease: initial report of the purification and characterization of a novel cerebrovascular amyloid protein. *Biochem Biophys Res Commun.* 1984;120(3):885-890.

459. Masters CL, Simms G, Weinman NA, Multhaup G, McDonald BL, Beyreuther K. Amyloid plaque core protein in Alzheimer disease and Down syndrome. *Proc Natl Acad Sci U S A.* 1985;82(12):4245-4249.

460. Portelius E, Hansson SF, Tran AJ, et al. Characterization of tau in cerebrospinal fluid using mass spectrometry. *J Proteome Res.* 2008;7(5):2114-2120.

461. Kohnken R, Buerger K, Zinkowski R, et al. Detection of tau phosphorylated at threonine 231 in cerebrospinal fluid of Alzheimer's disease patients. *Neurosci Lett.* 2000;287(3):187-190.

462. Vanmechelen E, Vanderstichele H, Davidsson P, et al. Quantification of tau phosphorylated at threonine 181 in human cerebrospinal fluid: a sandwich ELISA with a synthetic phosphopeptide for standardization. *Neurosci Lett.* 2000;285(1):49-52.

463. Blennow K. Cerebrospinal fluid protein biomarkers for Alzheimer's disease. *NeuroRx.* 2004;1(2):213-225.

464. Hampel H, Buerger K, Zinkowski R, et al. Measurement of phosphorylated tau epitopes in the differential diagnosis of Alzheimer disease: a comparative cerebrospinal fluid study. *Arch Gen Psychiatry.* 2004;61(1):95-102.

465. Blennow K, Wallin A, Agren H, Spenger C, Siegfried J, Vanmechelen E. Tau protein in cerebrospinal fluid: a biochemical marker for axonal degeneration in Alzheimer disease? *Mol Chem Neuropathol.* 1995;26(3):231-245.

466. Blennow K, Vanmechelen E, Hampel H. CSF total tau, Abeta42 and phosphorylated tau protein as biomarkers for Alzheimer's disease. *Mol Neurobiol.* 2001;24(1-3):87-97.

467. Mori H, Hosoda K, Matsubara E, et al. Tau in cerebrospinal fluids: establishment of the sandwich ELISA with antibody specific to the repeat sequence in tau. *Neurosci Lett.* 1995;186(2-3):181-183.

468. Vigo-Pelfrey C, Seubert P, Barbour R, et al. Elevation of microtubule-associated protein tau in the cerebrospinal fluid of patients with Alzheimer's disease. *Neurology.* 1995;45(4):788-793.

469. Hampel H, Burger K, Pruessner JC, et al. Correlation of cerebrospinal fluid levels of tau protein phosphorylated at threonine 231 with rates of hippocampal atrophy in Alzheimer disease. *Arch Neurol.* 2005;62(5):770-773.

470. Blom ES, Giedraitis V, Zetterberg H, et al. Rapid progression from mild cognitive impairment to Alzheimer's disease in subjects with elevated levels of tau in cerebrospinal fluid and the APOE epsilon4/epsilon4 genotype. *Dement Geriatr Cogn Disord.* 2009;27(5):458-464.

471. Samgard K, Zetterberg H, Blennow K, Hansson O, Minthon L, Londos E. Cerebrospinal fluid total tau as a marker of Alzheimer's disease intensity. *Int J Geriatr Psychiatry.* 2010;25(4):403-410.

472. Snider BJ, Fagan AM, Roe C, et al. Cerebrospinal fluid biomarkers and rate of cognitive decline in very mild dementia of the Alzheimer type. *Arch Neurol.* 2009;66(5):638-645.

473. Wallin AK, Hansson O, Blennow K, Londos E, Minthon L. Can CSF biomarkers or pre-treatment progression rate predict response to cholinesterase inhibitor treatment in Alzheimer's disease? *Int J Geriatr Psychiatry.* 2009;24(6):638-647.

474. Buerger K, Ewers M, Pirttila T, et al. CSF phosphorylated tau protein correlates with neocortical neurofibrillary pathology in Alzheimer's disease. *Brain.* 2006;129(Pt 11):3035-3041.

475. Buerger K, Alafuzoff I, Ewers M, Pirttila T, Zinkowski R, Hampel H. No correlation between CSF tau protein phosphorylated at threonine 181 with neocortical neurofibrillary pathology in Alzheimer's disease. *Brain.* 2007;130(Pt 10):e82.

476. Engelborghs S, Sleegers K, Cras P, et al. No association of CSF biomarkers with APOEepsilon4, plaque and tangle burden in definite Alzheimer's disease. *Brain.* 2007;130(Pt 9):2320-2326.

477. Tapiola T, Overmyer M, Lehtovirta M, et al. The level of cerebrospinal fluid tau correlates with neurofibrillary tangles in Alzheimer's disease. *Neuroreport.* 1997;8(18):3961-3963.

478. Vincent I, Zheng JH, Dickson DW, Kress Y, Davies P. Mitotic phosphoepitopes precede paired helical filaments in Alzheimer's disease. *Neurobiol Aging.* 1998;19(4):287-296.

479. Hesse C, Rosengren L, Andreasen N, et al. Transient increase in total tau but not phospho-tau in human cerebrospinal fluid after acute stroke. *Neurosci Lett.* 2001;297(3):187-190.

480. Ost M, Nylen K, Csajbok L, et al. Initial CSF total tau correlates with 1-year outcome in patients with traumatic brain injury. *Neurology.* 2006;67(9):1600-1604.

481. Zetterberg H, Hietala MA, Jonsson M, et al. Neurochemical aftermath of amateur boxing. *Arch Neurol.* 2006;63(9):1277-1280.

482. Otto M, Wiltfang J, Tumani H, et al. Elevated levels of tau-protein in cerebrospinal fluid of patients with Creutzfeldt-Jakob disease. *Neurosci Lett.* 1997;225(3):210-212.

483. Jack CR, Jr., Bennett DA, Blennow K, et al. NIA-AA Research Framework: Toward a biological definition of Alzheimer's disease. *Alzheimers Dement.* 2018;14(4):535-562.

484. Jack CR, Jr., Bennett DA, Blennow K, et al. A/T/N: An unbiased descriptive classification scheme for Alzheimer disease biomarkers. *Neurology.* 2016;87(5):539-547.

485. DeKosky ST, Scheff SW. Synapse loss in frontal cortex biopsies in Alzheimer's disease: correlation with cognitive severity. *Ann Neurol.* 1990;27(5):457-464.

486. Davidsson P, Puchades M, Blennow K. Identification of synaptic vesicle, pre- and postsynaptic proteins in human cerebrospinal fluid using liquid-phase isoelectric focusing. *Electrophoresis.* 1999;20(3):431-437.

487. Guadano-Ferraz A, Vinuela A, Oeding G, Bernal J, Rausell E. RC3/neurogranin is expressed in pyramidal neurons of motor and somatosensory cortex in normal and denervated monkeys. *J Comp Neurol.* 2005;493(4):554-570.

488. Represa A, Deloulme JC, Sensenbrenner M, Ben-Ari Y, Baudier J. Neurogranin: immunocytochemical localization of a brain-specific protein kinase C substrate. *J Neurosci.* 1990;10(12):3782-3792.

489. Chen SJ, Sweatt JD, Klann E. Enhanced phosphorylation of the postsynaptic protein kinase C substrate RC3/neurogranin during long-term potentiation. *Brain Res.* 1997;749(2):181-187.

490. Fedorov NB, Pasinelli P, Oestreicher AB, DeGraan PN, Reymann KG. Antibodies to postsynaptic PKC substrate neurogranin prevent long-term potentiation in hippocampal CA1 neurons. *Eur J Neurosci.* 1995;7(4):819-822.

491. Thorsell A, Bjerke M, Gobom J, et al. Neurogranin in cerebrospinal fluid as a marker of synaptic degeneration in Alzheimer's disease. *Brain Res.* 2010;1362:13-22.

492. Hellwig K, Kvartsberg H, Portelius E, et al. Neurogranin and YKL-40: independent markers of synaptic degeneration and neuroinflammation in Alzheimer's disease. *Alzheimers Res Ther.* 2015;7:74.

493. Kvartsberg H, Duits FH, Ingelsson M, et al. Cerebrospinal fluid levels of the synaptic protein neurogranin correlates with cognitive decline in prodromal Alzheimer's disease. *Alzheimers Dement.* 2015;11(10):1180-1190.

494. Kvartsberg H, Portelius E, Andreasson U, et al. Characterization of the postsynaptic protein neurogranin in paired cerebrospinal fluid and plasma samples from Alzheimer's disease patients and healthy controls. *Alzheimers Res Ther.* 2015;7(1):40.

495. Portelius E, Zetterberg H, Skillback T, et al. Cerebrospinal fluid neurogranin: relation to cognition and neurodegeneration in Alzheimer's disease. *Brain.* 2015;138(Pt 11):3373-3385.

496. Wellington H, Paterson RW, Portelius E, et al. Increased CSF neurogranin concentration is specific to Alzheimer disease. *Neurology.* 2016;86(9):829-835.

497. Zetterberg H, Skillback T, Mattsson N, et al. Association of Cerebrospinal Fluid Neurofilament Light Concentration With Alzheimer Disease Progression. *JAMA Neurol.* 2016;73(1):60-67.

498. Fagan AM, Mintun MA, Mach RH, et al. Inverse relation between in vivo amyloid imaging load and cerebrospinal fluid Abeta42 in humans. *Ann Neurol.* 2006;59(3):512-519.

499. Fagan AM, Mintun MA, Shah AR, et al. Cerebrospinal fluid tau and ptau(181) increase with cortical amyloid deposition in cognitively normal individuals: implications for future clinical trials of Alzheimer's disease. *EMBO Mol Med.* 2009;1(8-9):371-380.

500. Fagan AM, Roe CM, Xiong C, Mintun MA, Morris JC, Holtzman DM. Cerebrospinal fluid tau/beta-amyloid(42) ratio as a prediction of cognitive decline in nondemented older adults. *Arch Neurol.* 2007;64(3):343-349.

501. Landau SM, Lu M, Joshi AD, et al. Comparing positron emission tomography imaging and cerebrospinal fluid measurements of beta-amyloid. *Ann Neurol.* 2013;74(6):826-836.

502. Palmqvist S, Zetterberg H, Blennow K, et al. Accuracy of brain amyloid detection in clinical practice using cerebrospinal fluid beta-amyloid 42: a cross-validation study against amyloid positron emission tomography. *JAMA Neurol.* 2014;71(10):1282-1289.

503. Zwan MD, Rinne JO, Hasselbalch SG, et al. Use of amyloid-PET to determine cutpoints for CSF markers: A multicenter study. *Neurology.* 2016;86(1):50-58.

504. Leuzy A, Carter SF, Chiotis K, Almkvist O, Wall A, Nordberg A. Concordance and Diagnostic Accuracy of [11C]PIB PET and Cerebrospinal Fluid Biomarkers in a Sample of Patients with Mild Cognitive Impairment and Alzheimer's Disease. *J Alzheimers Dis.* 2015;45(4):1077-1088.

505. Blennow K, Mattsson N, Scholl M, Hansson O, Zetterberg H. Amyloid biomarkers in Alzheimer's disease. *Trends Pharmacol Sci.* 2015;36(5):297-309.

506. Chhatwal JP, Schultz AP, Marshall GA, et al. Temporal T807 binding correlates with CSF tau and phospho-tau in normal elderly. *Neurology.* 2016;87(9):920-926.

507. Gordon BA, Friedrichsen K, Brier M, et al. The relationship between cerebrospinal fluid markers of Alzheimer pathology and positron emission tomography tau imaging. *Brain.* 2016;139(Pt 8):2249-2260.

508. Mattsson N, Scholl M, Strandberg O, et al. 18F-AV-1451 and CSF T-tau and P-tau as biomarkers in Alzheimer's disease. *EMBO Mol Med.* 2017.

509. La Joie R, Bejanin A, Fagan AM, et al. Associations between [(18)F]AV1451 tau PET and CSF measures of tau pathology in a clinical sample. *Neurology.* 2017.

510. Mattsson N, Smith R, Strandberg O, et al. Comparing (18)F-AV-1451 with CSF t-tau and p-tau for diagnosis of Alzheimer disease. *Neurology.* 2018;90(5):e388-e395.

511. Andreasen N, Minthon L, Clarberg A, et al. Sensitivity, specificity, and stability of CSF-tau in AD in a community-based patient sample. *Neurology.* 1999;53(7):1488-1494.

512. Blennow K, Zetterberg H, Minthon L, et al. Longitudinal stability of CSF biomarkers in Alzheimer's disease. *Neurosci Lett.* 2007;419(1):18-22.

513. Zetterberg H, Pedersen M, Lind K, et al. Intra-individual stability of CSF biomarkers for Alzheimer's disease over two years. *J Alzheimers Dis.* 2007;12(3):255-260.

514. Mattsson N, Scholl M, Strandberg O, et al. (18)F-AV-1451 and CSF T-tau and P-tau as biomarkers in Alzheimer's disease. *EMBO Mol Med.* 2017;9(9):1212-1223.

515. Meredith JE, Jr., Sankaranarayanan S, Guss V, et al. Characterization of novel CSF Tau and ptau biomarkers for Alzheimer's disease. *PLoS One.* 2013;8(10):e76523.

516. Sato C, Barthelemy NR, Mawuenyega KG, et al. Tau Kinetics in Neurons and the Human Central Nervous System. *Neuron.* 2018;97(6):1284-1298 e1287.

517. Wildsmith K, Barthélemy N, Bohorquez SS, et al. Tau Burden Measued using [18F]TGP1 Correlates With CSF Tau Phosphorylation At Sites T217 and T205 More Closely Than T181. Alzheimer's Association International Conference; 2018; Chicago, USA.

518. Jagust WJ, Landau SM, Shaw LM, et al. Relationships between biomarkers in aging and dementia. *Neurology.* 2009;73(15):1193-1199.

519. Mosconi L, De Santi S, Brys M, et al. Hypometabolism and altered cerebrospinal fluid markers in normal apolipoprotein E E4 carriers with subjective memory complaints. *Biol Psychiatry.* 2008;63(6):609-618.

520. Haense C, Buerger K, Kalbe E, et al. CSF total and phosphorylated tau protein, regional glucose metabolism and dementia severity in Alzheimer's disease. *Eur J Neurol.* 2008;15(11):1155-1162.

521. Ceravolo R, Borghetti D, Kiferle L, et al. CSF phosporylated TAU protein levels correlate with cerebral glucose metabolism assessed with PET in Alzheimer's disease. *Brain Res Bull.* 2008;76(1-2):80-84.

522. Fellgiebel A, Siessmeier T, Scheurich A, et al. Association of elevated phospho-tau levels with Alzheimer-typical 18F-fluoro-2-deoxy-D-glucose positron emission tomography findings in patients with mild cognitive impairment. *Biol Psychiatry.* 2004;56(4):279-283.

523. Herukka SK, Simonsen AH, Andreasen N, et al. Recommendations for cerebrospinal fluid Alzheimer's disease biomarkers in the diagnostic evaluation of mild cognitive impairment. *Alzheimers Dement.* 2017;13(3):285-295.

524. Simonsen AH, Herukka SK, Andreasen N, et al. Recommendations for CSF AD biomarkers in the diagnostic evaluation of dementia. *Alzheimers Dement.* 2017;13(3):274-284.

525. Rosen C, Farahmand B, Skillback T, et al. Benchmarking biomarker-based criteria for Alzheimer's disease: Data from the Swedish Dementia Registry, SveDem. *Alzheimers Dement.* 2015;11(12):1470-1479.

526. Bittner T, Zetterberg H, Teunissen CE, et al. Technical performance of a novel, fully automated electrochemiluminescence immunoassay for the quantitation of beta-amyloid (1-42) in human cerebrospinal fluid. *Alzheimers Dement.* 2016;12(5):517-526.

527. Ngo J, Holroyd-Leduc JM. Systematic review of recent dementia practice guidelines. *Age Ageing.* 2015;44(1):25-33.

528. Institute of Medicine (U.S.). Committee on Standards for Developing Trustworthy Clinical Practice Guidelines., Graham R. *Clinical practice guidelines we can trust.* Washington, DC: National Academies Press; 2011.

529. *Nationella riktlinjer för vård och omsorg vid demenssjukdom.* Swedish National Board of Health and Welfare - Socialstyrelsens;2016.

530. Folstein MF, Folstein SE, McHugh PR. "Mini-mental state". A practical method for grading the cognitive state of patients for the clinician. *J Psychiatr Res.* 1975;12(3):189-198.

531. Agrell B, Dehlin O. The clock-drawing test. 1998. *Age Ageing.* 2012;41 Suppl 3:iii41-45.

532. Mlinac ME, Feng MC. Assessment of Activities of Daily Living, Self-Care, and Independence. *Arch Clin Neuropsychol.* 2016;31(6):506-516.

533. Dubois B, Hampel H, Feldman HH, et al. Preclinical Alzheimer's disease: Definition, natural history, and diagnostic criteria. *Alzheimers Dement.* 2016;12(3):292-323.

534. Sperling RA, Aisen PS, Beckett LA, et al. Toward defining the preclinical stages of Alzheimer's disease: recommendations from the National Institute on Aging-Alzheimer's Association workgroups on diagnostic guidelines for Alzheimer's disease. *Alzheimers Dement.* 2011;7(3):280-292.

535. Alladi S, Xuereb J, Bak T, et al. Focal cortical presentations of Alzheimer's disease. *Brain.* 2007;130(Pt 10):2636-2645.

536. Rabinovici GD, Jagust WJ, Furst AJ, et al. Abeta amyloid and glucose metabolism in three variants of primary progressive aphasia. *Ann Neurol.* 2008;64(4):388-401.

537. Murray ME, Graff-Radford NR, Ross OA, Petersen RC, Duara R, Dickson DW. Neuropathologically defined subtypes of Alzheimer's disease with distinct clinical characteristics: a retrospective study. *Lancet Neurol.* 2011;10(9):785-796.

538. Visser PJ, Vos S, van Rossum I, Scheltens P. Comparison of International Working Group criteria and National Institute on Aging-Alzheimer's Association criteria for Alzheimer's disease. *Alzheimers Dement.* 2012;8(6):560-563.

539. Vos SJ, Verhey F, Frolich L, et al. Prevalence and prognosis of Alzheimer's disease at the mild cognitive impairment stage. *Brain.* 2015;138(Pt 5):1327-1338.

540. Schott JM, Petersen RC. New criteria for Alzheimer's disease: which, when and why? *Brain.* 2015;138(Pt 5):1134-1137.

541. Jack CR, Jr., Knopman DS, Jagust WJ, et al. Hypothetical model of dynamic biomarkers of the Alzheimer's pathological cascade. *Lancet Neurol.* 2010;9(1):119-128.

542. Hyman BT. Amyloid-dependent and amyloid-independent stages of Alzheimer disease. *Arch Neurol.* 2011;68(8):1062-1064.

543. Jack CR, Jr., Petersen RC, Xu Y, et al. Rates of hippocampal atrophy correlate with change in clinical status in aging and AD. *Neurology.* 2000;55(4):484-489.

544. Ridha BH, Barnes J, Bartlett JW, et al. Tracking atrophy progression in familial Alzheimer's disease: a serial MRI study. *Lancet Neurol.* 2006;5(10):828-834.

545. Jack CR, Jr., Weigand SD, Shiung MM, et al. Atrophy rates accelerate in amnestic mild cognitive impairment. *Neurology.* 2008;70(19 Pt 2):1740-1752.

546. Jack CR, Jr., Knopman DS, Jagust WJ, et al. Tracking pathophysiological processes in Alzheimer's disease: an updated hypothetical model of dynamic biomarkers. *Lancet Neurol.* 2013;12(2):207-216.

547. Musiek ES, Holtzman DM. Origins of Alzheimer's disease: reconciling cerebrospinal fluid biomarker and neuropathology data regarding the temporal sequence of amyloid-beta and tau involvement. *Curr Opin Neurol.* 2012;25(6):715-720.

548. Nordberg A. Molecular imaging in Alzheimer's disease: new perspectives on biomarkers for early diagnosis and drug development. *Alzheimers Res Ther.* 2011;3(6):34.

549. Petersen RC. Alzheimer's disease: progress in prediction. *Lancet Neurol.* 2010;9(1):4-5.

550. Fan Z, Brooks DJ, Okello A, Edison P. An early and late peak in microglial activation in Alzheimer's disease trajectory. *Brain.* 2017;140(3):792-803.

551. McDade E, Bateman RJ. Tau Positron Emission Tomography in Autosomal Dominant Alzheimer Disease: Small Windows, Big Picture. *JAMA Neurol.* 2018.

552. Bateman RJ, Xiong C, Benzinger TL, et al. Clinical and biomarker changes in dominantly inherited Alzheimer's disease. *N Engl J Med.* 2012;367(9):795-804.

553. Palmqvist S, Mattsson N, Hansson O, Alzheimer's Disease Neuroimaging I. Cerebrospinal fluid analysis detects cerebral amyloid-beta accumulation earlier than positron emission tomography. *Brain.* 2016;139(Pt 4):1226-1236.

554. EU Joint Programme – Neurodegenerative Disease Research (JPND). Biomarkers for Alzheimer's and Parkinson's Disease (BIOMARKAPD). JPND; 2017. http://www.neurodegenerationresearch.eu/publication/biomarkapd. Accessed May 25, 2018.

555. Roman GC, Tatemichi TK, Erkinjuntti T, et al. Vascular dementia: diagnostic criteria for research studies. Report of the NINDS-AIREN International Workshop. *Neurology.* 1993;43(2):250-260.

556. Neary D, Snowden JS, Gustafson L, et al. Frontotemporal lobar degeneration: a consensus on clinical diagnostic criteria. *Neurology.* 1998;51(6):1546-1554.

557. Wahlund LO, Pihlstrand E, Jonhagen ME. Mild cognitive impairment: experience from a memory clinic. *Acta Neurol Scand Suppl.* 2003;179:21-24.

558. McKeith IG, Galasko D, Kosaka K, et al. Consensus guidelines for the clinical and pathologic diagnosis of dementia with Lewy bodies (DLB): report of the consortium on DLB international workshop. *Neurology.* 1996;47(5):1113-1124.

559. Anderson JL. A rapid and accurate method to realign PET scans utilizing image edge information. *J Nucl Med.* 1995;36(4):657-669.

560. Nordberg A, Carter SF, Rinne J, et al. A European multicentre PET study of fibrillar amyloid in Alzheimer's disease. *Eur J Nucl Med Mol Imaging.* 2013;40(1):104-114.

561. Lilja J, Leuzy A, Chiotis K, Savitcheva I, Sorensen J, Nordberg A. Spatial normalization of [(18)F]flutemetamol PET images utilizing an adaptive principal components template. *J Nucl Med.* 2018.

562. ICBM-152 template. http://packages.bic.mni.mcgill.ca/tgz/mni-models_icbm152-lin-1.0.tar.gz.

563. Erlandsson K, Buvat I, Pretorius PH, Thomas BA, Hutton BF. A review of partial volume correction techniques for emission tomography and their applications in neurology, cardiology and oncology. *Phys Med Biol.* 2012;57(21):R119-159.

564. Maass A, Landau S, Baker SL, et al. Comparison of multiple tau-PET measures as biomarkers in aging and Alzheimer's disease. *Neuroimage.* 2017;157:448-463.

565. Klunk WE, Koeppe RA, Price JC, et al. The Centiloid Project: standardizing quantitative amyloid plaque estimation by PET. *Alzheimers Dement.* 2015;11(1):1-15 e11-14.

566. Rodriguez-Vieitez E, Carter SF, Chiotis K, et al. Comparison of Early-Phase 11C-Deuterium-l-Deprenyl and 11C-Pittsburgh Compound B PET for Assessing Brain Perfusion in Alzheimer Disease. *J Nucl Med.* 2016;57(7):1071-1077.

567. Wang LS, Leung YY, Chang SK, et al. Comparison of xMAP and ELISA assays for detecting cerebrospinal fluid biomarkers of Alzheimer's disease. *J Alzheimers Dis.* 2012;31(2):439-445.

568. Toombs J, Paterson RW, Schott JM, Zetterberg H. Amyloid-beta 42 adsorption following serial tube transfer. *Alzheimers Res Ther.* 2014;6(1):5.

569. Dillen L, Cools W, Vereyken L, Timmerman P. A screening UHPLC-MS/MS method for the analysis of amyloid peptides in cerebrospinal fluid of preclinical species. *Bioanalysis.* 2011;3(1):45-55.

570. Zhang Z, Song M, Liu X, et al. Cleavage of tau by asparagine endopeptidase mediates the neurofibrillary pathology in Alzheimer's disease. *Nat Med.* 2014;20(11):1254-1262.

571. Youden WJ. Index for rating diagnostic tests. *Cancer.* 1950;3(1):32-35.

572. Benaglia T, Chaveau D, Hunter DR, Young DS. mixtools: An R Package for Analyzing Finite Mixture Models. *J Stat Softw.* 2009;32(6):1-29.

573. Vandenberghe R, Van Laere K, Ivanoiu A, et al. 18F-flutemetamol amyloid imaging in Alzheimer disease and mild cognitive impairment: a phase 2 trial. *Ann Neurol.* 2010;68(3):319-329.

574. Tolboom N, van der Flier WM, Yaqub M, et al. Relationship of cerebrospinal fluid markers to 11C-PiB and 18F-FDDNP binding. *J Nucl Med.* 2009;50(9):1464-1470.

575. Degerman Gunnarsson M, Lindau M, Wall A, et al. Pittsburgh compound-B and Alzheimer's disease biomarkers in CSF, plasma and urine: An exploratory study. *Dement Geriatr Cogn Disord.* 2010;29(3):204-212.

576. Weigand SD, Vemuri P, Wiste HJ, et al. Transforming cerebrospinal fluid Abeta42 measures into calculated Pittsburgh Compound B units of brain Abeta amyloid. *Alzheimers Dement.* 2011;7(2):133-141.

577. Zwan M, van Harten A, Ossenkoppele R, et al. Concordance between cerebrospinal fluid biomarkers and [11C]PIB PET in a memory clinic cohort. *J Alzheimers Dis.* 2014;41(3):801-807.

578. Whitwell JL, Wiste HJ, Weigand SD, et al. Comparison of imaging biomarkers in the Alzheimer Disease Neuroimaging Initiative and the Mayo Clinic Study of Aging. *Arch Neurol.* 2012;69(5):614-622.

579. Leuzy A, Chiotis K, Hasselbalch SG, et al. Pittsburgh compound B imaging and cerebrospinal fluid amyloid-beta in a multicentre European memory clinic study. *Brain*. 2016;139(Pt 9):2540-2553.

580. Skillback T, Farahmand BY, Rosen C, et al. Cerebrospinal fluid tau and amyloid-beta1-42 in patients with dementia. *Brain.* 2015;138(Pt 9):2716-2731.

581. Janelidze S, Zetterberg H, Mattsson N, et al. CSF Abeta42/Abeta40 and Abeta42/Abeta38 ratios: better diagnostic markers of Alzheimer disease. *Ann Clin Transl Neurol.* 2016;3(3):154-165.

582. van Westen D, Lindqvist D, Blennow K, et al. Cerebral white matter lesions – associations with Abeta isoforms and amyloid PET. *Sci Rep.* 2016;6:20709.

583. Jack CR, Jr., Wiste HJ, Weigand SD, et al. Defining imaging biomarker cut points for brain aging and Alzheimer's disease. *Alzheimers Dement.* 2017;13(3):205-216.

584. Villeneuve S, Rabinovici GD, Cohn-Sheehy BI, et al. Existing Pittsburgh Compound-B positron emission tomography thresholds are too high: statistical and pathological evaluation. *Brain.* 2015;138(Pt 7):2020-2033.

585. Mormino EC, Brandel MG, Madison CM, et al. Not quite PIB-positive, not quite PIB-negative: slight PIB elevations in elderly normal control subjects are biologically relevant. *Neuroimage.* 2012;59(2):1152-1160.

586. Landau SM, Horng A, Jagust WJ, Alzheimer's Disease Neuroimaging I. Memory decline accompanies subthreshold amyloid accumulation. *Neurology.* 2018;90(17):e1452-e1460.

587. Ossenkoppele R, Jansen WJ, Rabinovici GD, et al. Prevalence of amyloid PET positivity in dementia syndromes: a meta-analysis. *JAMA.* 2015;313(19):1939-1949.

588. Paterson RW, Toombs J, Slattery CF, et al. Dissecting IWG-2 typical and atypical Alzheimer's disease: insights from cerebrospinal fluid analysis. *J Neurol.* 2015;262(12):2722-2730.

589. Lowe VJ, Wiste HJ, Senjem ML, et al. Widespread brain tau and its association with ageing, Braak stage and Alzheimer's dementia. *Brain.* 2018;141(1):271-287.

590. Chiotis K, Stenkrona P, Almkvist O, et al. Dual tracer tau PET imaging reveals different molecular targets for (11)C-THK5351 and (11)C-PBB3 in the Alzheimer brain. *Eur J Nucl Med Mol Imaging.* 2018.

591. Seppala TT, Koivisto AM, Hartikainen P, Helisalmi S, Soininen H, Herukka SK. Longitudinal changes of CSF biomarkers in Alzheimer's disease. *J Alzheimers Dis.* 2011;25(4):583-594.

592. Fagan AM, Xiong C, Jasielec MS, et al. Longitudinal change in CSF biomarkers in autosomal-dominant Alzheimer's disease. *Sci Transl Med.* 2014;6(226):226ra230.

593. Toledo JB, Xie SX, Trojanowski JQ, Shaw LM. Longitudinal change in CSF Tau and Abeta biomarkers for up to 48 months in ADNI. *Acta Neuropathol.* 2013;126(5):659-670.

594. Sutphen CL, McCue L, Herries EM, et al. Longitudinal decreases in multiple cerebrospinal fluid biomarkers of neuronal injury in symptomatic late onset Alzheimer's disease. *Alzheimers Dement.* 2018.

595. Bouwman FH, van der Flier WM, Schoonenboom NS, et al. Longitudinal changes of CSF biomarkers in memory clinic patients. *Neurology.* 2007;69(10):1006-1011.

596. Kanai M, Matsubara E, Isoe K, et al. Longitudinal study of cerebrospinal fluid levels of tau, A beta1-40, and A beta1-42(43) in Alzheimer's disease: a study in Japan. *Ann Neurol.* 1998;44(1):17-26.

597. Buchhave P, Blennow K, Zetterberg H, et al. Longitudinal study of CSF biomarkers in patients with Alzheimer's disease. *PLoS One.* 2009;4(7):e6294.

598. Blomberg M, Jensen M, Basun H, Lannfelt L, Wahlund LO. Increasing cerebrospinal fluid tau levels in a subgroup of Alzheimer patients with apolipoprotein E allele epsilon 4 during 14 months follow-up. *Neurosci Lett.* 1996;214(2-3):163-166.

599. de Leon MJ, Segal S, Tarshish CY, et al. Longitudinal cerebrospinal fluid tau load increases in mild cognitive impairment. *Neurosci Lett.* 2002;333(3):183-186.

600. Andreasen N, Minthon L, Vanmechelen E, et al. Cerebrospinal fluid tau and Abeta42 as predictors of development of Alzheimer's disease in patients with mild cognitive impairment. *Neurosci Lett.* 1999;273(1):5-8.

601. de Leon MJ, DeSanti S, Zinkowski R, et al. Longitudinal CSF and MRI biomarkers improve the diagnosis of mild cognitive impairment. *Neurobiol Aging.* 2006;27(3):394-401.

602. Lo RY, Hubbard AE, Shaw LM, et al. Longitudinal change of biomarkers in cognitive decline. *Arch Neurol.* 2011;68(10):1257-1266.

603. Mollenhauer B, Bibl M, Trenkwalder C, et al. Follow-up investigations in cerebrospinal fluid of patients with dementia with Lewy bodies and Alzheimer's disease. *J Neural Transm (Vienna).* 2005;112(7):933-948.

604. Parnetti L, Chiasserini D, Andreasson U, et al. Changes in CSF acetyl- and butyrylcholinesterase activity after long-term treatment with AChE inhibitors in Alzheimer's disease. *Acta Neurol Scand.* 2011;124(2):122-129.

605. Huey ED, Mirza N, Putnam KT, et al. Stability of CSF beta-amyloid(1-42) and tau levels by APOE genotype in Alzheimer patients. *Dement Geriatr Cogn Disord.* 2006;22(1):48-53.

606. Andreasen N, Vanmechelen E, Van de Voorde A, et al. Cerebrospinal fluid tau protein as a biochemical marker for Alzheimer's disease: a community based follow up study. *J Neurol Neurosurg Psychiatry.* 1998;64(3):298-305.

607. Sunderland T, Wolozin B, Galasko D, et al. Longitudinal stability of CSF tau levels in Alzheimer patients. *Biol Psychiatry.* 1999;46(6):750-755.

608. Brys M, Pirraglia E, Rich K, et al. Prediction and longitudinal study of CSF biomarkers in mild cognitive impairment. *Neurobiol Aging.* 2009;30(5):682-690.

609. Ringman JM, Taylor K, Teng E, Coppola G, Gylys K. Longitudinal change in CSF biomarkers in a presymptomatic carrier of an APP mutation. *Neurology.* 2011;76(24):2124-2125.

610. Bateman RJ, Munsell LY, Morris JC, Swarm R, Yarasheski KE, Holtzman DM. Human amyloid-beta synthesis and clearance rates as measured in cerebrospinal fluid in vivo. *Nat Med.* 2006;12(7):856-861.

611. Braak H, Braak E. Staging of Alzheimer's disease-related neurofibrillary changes. *Neurobiol Aging.* 1995;16(3):271-278; discussion 278-284.

612. Vos SJB, Gordon BA, Su Y, et al. NIA-AA staging of preclinical Alzheimer disease: discordance and concordance of CSF and imaging biomarkers. *Neurobiol Aging.* 2016;44:1-8.

613. Alexopoulos P, Kriett L, Haller B, et al. Limited agreement between biomarkers of neuronal injury at different stages of Alzheimer's disease. *Alzheimers Dement.* 2014;10(6):684-689.

614. Buee L, Troquier L, Burnouf S, et al. From tau phosphorylation to tau aggregation: what about neuronal death? *Biochem Soc Trans.* 2010;38(4):967-972.

615. de Calignon A, Spires-Jones TL, Pitstick R, Carlson GA, Hyman BT. Tangle-bearing neurons survive despite disruption of membrane integrity in a mouse model of tauopathy. *J Neuropathol Exp Neurol.* 2009;68(7):757-761.

616. Morsch R, Simon W, Coleman PD. Neurons may live for decades with neurofibrillary tangles. *J Neuropathol Exp Neurol.* 1999;58(2):188-197.

617. Dronse J, Fliessbach K, Bischof GN, et al. In vivo Patterns of Tau Pathology, Amyloid-beta Burden, and Neuronal Dysfunction in Clinical Variants of Alzheimer's Disease. *J Alzheimers Dis.* 2017;55(2):465-471.

618. Bischof GN, Jessen F, Fliessbach K, et al. Impact of tau and amyloid burden on glucose metabolism in Alzheimer's disease. *Ann Clin Transl Neurol.* 2016;3(12):934-939.

619. Ossenkoppele R, Schonhaut DR, Scholl M, et al. Tau PET patterns mirror clinical and neuroanatomical variability in Alzheimer's disease. *Brain.* 2016;139(Pt 5):1551-1567.

620. Hanseeuw BJ, Betensky RA, Schultz AP, et al. Fluorodeoxyglucose metabolism associated with tau-amyloid interaction predicts memory decline. *Ann Neurol.* 2017;81(4):583-596.

621. Olsson B, Lautner R, Andreasson U, et al. CSF and blood biomarkers for the diagnosis of Alzheimer's disease: a systematic review and meta-analysis. *Lancet Neurol.* 2016;15(7):673-684.

622. Farid K, Hong YT, Aigbirhio FI, et al. Early-Phase 11C-PiB PET in Amyloid Angiopathy-Related Symptomatic Cerebral Hemorrhage: Potential Diagnostic Value? *PLoS One.* 2015;10(10):e0139926.

623. Hsiao IT, Huang CC, Hsieh CJ, et al. Correlation of early-phase 18F-florbetapir (AV-45/Amyvid) PET images to FDG images: preliminary studies. *Eur J Nucl Med Mol Imaging.* 2012;39(4):613-620.

624. Lin KJ, Hsiao IT, Hsu JL, et al. Imaging characteristic of dual-phase (18) F-florbetapir (AV-45/Amyvid) PET for the concomitant detection of perfusion deficits and beta-amyloid deposition in Alzheimer's disease and mild cognitive impairment. *Eur J Nucl Med Mol Imaging.* 2016;43(7):1304-1314.

625. Vandenberghe R, Adamczuk K, Dupont P, Laere KV, Chetelat G. Amyloid PET in clinical practice: Its place in the multidimensional space of Alzheimer's disease. *Neuroimage Clin.* 2013;2:497-511.

626. Devous MD, Sr., Joshi AD, Navitsky M, et al. Test-Retest Reproducibility for the Tau PET Imaging Agent Flortaucipir F 18. *J Nucl Med.* 2018;59(6):937-943.

627. Baumgartner R, Joshi A, Feng D, Zanderigo F, Ogden RT. Statistical evaluation of test-retest studies in PET brain imaging. *EJNMMI Res.* 2018;8(1):13.

628. Ashraf A, Fan Z, Brooks DJ, Edison P. Cortical hypermetabolism in MCI subjects: a compensatory mechanism? *Eur J Nucl Med Mol Imaging.* 2015;42(3):447-458.

629. Gur RC, Ragland JD, Reivich M, Greenberg JH, Alavi A, Gur RE. Regional differences in the coupling between resting cerebral blood flow and metabolism may indicate action preparedness as a default state. *Cereb Cortex.* 2009;19(2):375-382.

630. Salinas CA, Searle GE, Gunn RN. The simplified reference tissue model: model assumption violations and their impact on binding potential. *J Cereb Blood Flow Metab.* 2015;35(2):304-311.

631. Harada R, Ishiki A, Kai H, et al. Correlations of (18)F-THK5351 PET with Postmortem Burden of Tau and Astrogliosis in Alzheimer Disease. *J Nucl Med.* 2018;59(4):671-674.

632. Lemoine L, Gillberg PG, Svedberg M, et al. Comparative binding properties of the tau PET tracers THK5117, THK5351, PBB3, and T807 in postmortem Alzheimer brains. *Alzheimers Res Ther.* 2017;9(1):96.

633. Lemoine L, Saint-Aubert L, Nennesmo I, Gillberg PG, Nordberg A. Cortical laminar tau deposits and activated astrocytes in Alzheimer's disease visualised by 3H-THK5117 and 3H-deprenyl autoradiography. *Sci Rep.* 2017;7:45496.

634. Tong J, Meyer JH, Furukawa Y, et al. Distribution of monoamine oxidase proteins in human brain: implications for brain imaging studies. *J Cereb Blood Flow Metab.* 2013;33(6):863-871.

635. Rousset OG, Ma Y, Evans AC. Correction for partial volume effects in PET: principle and validation. *J Nucl Med.* 1998;39(5):904-911.

636. Bartlett JW, Frost C, Mattsson N, et al. Determining cut-points for Alzheimer's disease biomarkers: statistical issues, methods and challenges. *Biomark Med.* 2012;6(4):391-400.

637. De Meyer G, Shapiro F, Vanderstichele H, et al. Diagnosis-independent Alzheimer disease biomarker signature in cognitively normal elderly people. *Arch Neurol.* 2010;67(8):949-956.

638. Blennow K. A Review of Fluid Biomarkers for Alzheimer's Disease: Moving from CSF to Blood. *Neurol Ther.* 2017;6(Suppl 1):15-24.

639. Korecka M, Waligorska T, Figurski M, et al. Qualification of a surrogate matrix-based absolute quantification method for amyloid-beta(4)(2) in human cerebrospinal fluid using 2D UPLC-tandem mass spectrometry. *J Alzheimers Dis.* 2014;41(2):441-451.

640. Bjerke M, Andreasson U, Kuhlmann J, et al. Assessing the commutability of reference material formats for the harmonization of amyloid-beta measurements. *Clin Chem Lab Med.* 2016;54(7):1177-1191.

641. McAvoy T, Lassman ME, Spellman DS, et al. Quantification of tau in cerebrospinal fluid by immunoaffinity enrichment and tandem mass spectrometry. *Clin Chem.* 2014;60(4):683-689.

642. Hansson O, Seibyl J, Stomrud E, et al. CSF biomarkers of Alzheimer's disease concord with amyloid-beta PET and predict clinical progression: A study of fully automated immunoassays in BioFINDER and ADNI cohorts. *Alzheimers Dement.* 2018.

643. Schmidt ME, Chiao P, Klein G, et al. The influence of biological and technical factors on quantitative analysis of amyloid PET: Points to consider and recommendations for controlling variability in longitudinal data. *Alzheimers Dement.* 2015;11(9):1050-1068.

644. Nayate AP, Dubroff JG, Schmitt JE, et al. Use of Standardized Uptake Value Ratios Decreases Interreader Variability of [18F] Florbetapir PET Brain Scan Interpretation. *AJNR Am J Neuroradiol.* 2015;36(7):1237-1244.

645. Pontecorvo MJ, Arora AK, Devine M, et al. Quantitation of PET signal as an adjunct to visual interpretation of florbetapir imaging. *Eur J Nucl Med Mol Imaging.* 2017;44(5):825-837.

646. Su Y, Flores S, Hornbeck RC, et al. Utilizing the Centiloid scale in cross-sectional and longitudinal PiB PET studies. *Neuroimage Clin.* 2018;19:406-416.

647. Ayakta N, Lockhart S, O'Neill J, Ossenkoppele R, Reed B, Olichney J. Centiloid thresholds for amyloid positivity derived from autopsy-proven cases. Human Amyloid Imaging; 2016; Miami, USA.

648. Rinne JO, Brooks DJ, Rossor MN, et al. 11C-PiB PET assessment of change in fibrillar amyloid-beta load in patients with Alzheimer's disease treated with bapineuzumab: a phase 2, double-blind, placebo-controlled, ascending-dose study. *Lancet Neurol.* 2010;9(4):363-372.

649. Palmqvist S, Mattsson N, Hansson O. Reply: Do we still need positron emission tomography for early Alzheimer's disease diagnosis? *Brain.* 2016.

650. Whittington A, Sharp DJ, Gunn RN, Alzheimer's Disease Neuroimaging I. Spatiotemporal Distribution of beta-Amyloid in Alzheimer Disease Is the Result of Heterogeneous Regional Carrying Capacities. *J Nucl Med.* 2018;59(5):822-827.

Karolinska Institutet

Arkitektkopia AB, Bromma, 2018